The Role of 3D Printing in Biological Anthropology

by

Travis T Allard

A Thesis submitted to the Faculty of Graduate Studies of

The University of Manitoba

in partial fulfilment of the requirements of the degree of

MASTER OF ARTS

Department of Anthropology

University of Manitoba

Winnipeg

Table of Contents

Acknowledgements …..ii

Abstract …..iii

List of Tables …..iv

List of Figures …..v

Chapter I: Introduction …..1

Chapter II: Literature Review …..3
The Origin of 3D Printing …… 4
Anatomical Modeling ……..…. 12
Rapid Prototyping in Anthropology ……15
Methods of Data Acquisition ……... 19
X-Ray Computed Tomography Scanning ……. 20
3D Surface Scanning …… 29
Creating 3D Models from Virtual 3D Data …….. 33
The Role of 3D Printing in Biological Anthropology ... 40

Chapter III: Virtual Reconstruction …..44
Objectives ……... 45
Methods ……..… 45
Results ……..... 61
Discussion …….. 67
Conclusion ……. 69

Chapter IV: Skeletal Reproduction …..70
Objectives …….. 70
Materials ……..... 71
Methods ……...…….. 72
Results ……... 88
Discussion ……. 101
Conclusion ……...……. 105

Chapter V: Discussion …..107
The Role of 3D Printing in Biological Anthropology .. 107
From Real to Virtual and Real Again ……... 114

Chapter VI: Conclusion …..125

Work Cited …..128
Appendix I: List of Abbreviations …..133

Acknowledgements

This work would not have been possible without the support and dedication of many people. First, I would like to acknowledge the generous support by Z-Corp in donating printing consumables. Other financial support throughout the course of this research was provided by the Canada Research Chairs program and the University of Manitoba. To Myra Sitchon, Dr. Roland Sawatzky and the Mennonite Heritage Village (Steinbach, Manitoba, Canada), I extend my sincerest gratitude for their insight and innovation in organizing the skeletal reproduction for the New Life exhibit. I would also like to thank Dr. Deborah Merrett, the University of Winnipeg, Dr. Martin Reed and the Dept. of Radiology, Sick Children's Hospital for facilitating Case Study Two. Several figures in this thesis (2.1, 2.2, 2.3) illustrate aspects of CT data using the Bosma Collection (Shapiro and Richtsmeier 1997) which is now curated in the Dept. of Anthropology at the Pennsylvania State University.

I also want to thank the members of my committee, Dr. Mary Silcox and Patrick Harrop, for their contribution to this work. Both challenged me to think more clearly and recognize my biases. They have contributed immensely not only to this work but to my overall intellectual development as well. Thank you.

A very special recognition goes out to my advisor Dr. Robert D. Hoppa. Most of his student's know him as Rob, and he is the most inspiring mentor anyone could be blessed to work with. Rob has challenged me and given me great freedom to achieve far beyond what I could ever dream possible. It is Rob I thank for this passage into the next phase of my life with more strength and wisdom than I have ever had. My greatest gratitude to the best advisor ever, Dr. Robert D. Hoppa.

In every major achievement there are always struggles. The people that surround us have an impact on how such things work out. For this, I would like to thank Dr. Dave Stymeist and Dr. Greg Monks. I also want to thank Enza Pohl, Dr. Heather Gill-Robinson and Barb Hewitt for their support and insight. All of you add or have added greatly to the richness of character and vibrancy of the department and my experience there.

Lastly, I want to dedicate this work to my wife, Lyndsey Smith, for her strength, stability and patience throughout this time. The past three years have been a time of tremendous growth for both of us, and I am glad we could share in this together. Without you Lyndsey, this truly would have never been possible. I also dedicate this work to my family that has been there through thick and thin and even pulled me out of the thick from time to time. Thank you to Grandma "G", Dad and Joyce. A special thanks to Dad and Joyce for teaching me to follow through with what I started, and honour the commitments I make.

Abstract

The following work explores the role of 3D printing in biological anthropology. A case study approach is used to provide an understanding of two different applications for 3D printing and to identify a potential methodology for creating 3D models. Case study one looks at the application of 3D printing to reconstruction projects using a flowerpot to test the reconstruction methodology. The second case study uses both laser surface and CT scanning to create a replica of a human skeleton. The two methods of data acquisition are evaluated for advantages and limitations in creating the virtual model. This work shows that there is a role for 3D printing in biological anthropology, but that data acquisition and processing issues are the most significant limiting factors in producing skeletal replicas.

List of Tables

Chapter III:

Table 3.1: Original and Printed Pot Comparison ……..….. 61
Table 3.2: Unbroken and Reconstructed Differences …….…… 64

Chapter IV:

Table 4.1: Surface Scan Summary …….. 74
Table 4.2: Total Deviation Between Surface and CT Scan Data …… 89
Table 4.3: Skull and Sacrum Comparison of Virtual and Printed Models …….. 98

Chapter V:

Table 5.1: Numerical Results of Acquisition Method Comparison ……. 116

List of Figures

Chapter II:

Figure 2.1: Partial Volume Effect ……24
Figure 2.2: Beam Hardening ……25
Figure 2.3: Frozen Noise ……26
Figure 2.4: Non-Manifold Face ……37
Figure 2.5: Runaway Feature ……38
Figure 2.6: Z-406 Build Chamber ……42

Chapter III:

Figure 3.1: Original Flowerpot ……46
Figure 3.2 Scanning Diagram ……47
Figure 3.3: Camera and Laser Angle for Optimum Scanning ……48
Figure 3.4: Final Virtual Model of Unbroken Flowerpot ……50
Figure 3.5: Unbroken Flowerpot Post-processing Method Two ……51
Figure 3.6: Broken Flowerpot ……51
Figure 3.7: Shard Models ……52
Figure 3.8: Thin Shard to Thick Shard ……53
Figure 3.9: Reconstruction Using Volume Shards ……54
Figure 3.10: Thin-wall Registration ……55
Figure 3.11: After Hole Filling and Smoothing ……56
Figure 3.12: Final Virtual Model Using Reconstruction Method Two ……57
Figure 3.13: Virtual Models of Unbroken and Reconstructed Flowerpots ….58
Figure 3.14: Unbroken Model Using Post-Processing Method One ……59
Figure 3.15: Unbroken Model Using Post-Processing Method Two ……59
Figure 3.16: Reconstructed Model Using Method Two ……60
Figure 3.17: Reconstructed Model Three (Combined Methods) ……60
Figure 3.18: Side View of Flowerpot Inspection Results ……65
Figure 3.19: Top/Inside View of Flowerpot Inspection Results ……66
Figure 3.20: Colour Model of Flowerpot Differences ……68

Chapter IV:

Figure 4.1: General Scanning for Bones ……72
Figure 4.2: Registration Process Step One ……76
Figure 4.3: Result of Registration ……77
Figure 4.4: Simplification ……78
Figure 4.5: Model Detailing ……79
Figure 4.6: Series One ……80
Figure 4.7: Series Two ……81
Figure 4.8: Series Three ……81
Figure 4.9: Series Four ……82
Figure 4.10: Series Five ……82

List of Figures Continued

Figure 4.11: CT Position Error ……83
Figure 4.12: Working in Mimics ……..84
Figure 4.13: Segmented Elements ……85
Figure 4.14: Joining the Proximal and Distal Femurs ……..87
Figure 4.15: Completed Long Bone ……88
Figure 4.16: CT vs. Surface Scan for Left Clavicle ……90
Figure 4.17: Registered CT and Surface Scans of the Skull ……91
Figure 4.18: Innominate Inspection ……..92
Figure 4.19: Left Humerus Inspection ……..93
Figure 4.20: Left Scapula Inspection ……93
Figure 4.21: Right Clavicle Inspection ……94
Figure 4.22: Right Humerus Inspection ……95
Figure 4.23: Left Ulna Inspection ……96
Figure 4.24: Right Ulna Inspection ……...96
Figure 4.25: Skull Inspection ……97
Figure 4.26: New Life Exhibit ……..99
Figure 4.27: Skeletal Reproduction ……..100
Figure 4.28: CT and Surface Scan Comparison Models ……..104

Chapter V:

Figure 5.1: Seamless Long Bones ……113
Figure 5.2: Visual-Spatial Data Analysis Using 3D Object ……117
Figure 5.3: Colour Bone Density Model of Mandible ……..121

Chapter I: Introduction

The goal of this work is to investigate the role of 3D printing in biological anthropology. 3D printing is a method of producing physical models using computer-generated data. Weber (2001) discusses the increasing use of technology in anthropology and how, despite the conservative nature of anthropological research, new technologies are going to change the way in which we approach research in the future. 3D printing is one of those technologies waiting for regular use in biological anthropology. Before this more widespread use occurs, researchers need to understand how 3D printing can be used and exactly what it is. This work is intended to provide a basic understanding of how to use 3D printing in biological anthropology. This basic introduction to the advantages and limitations is necessary for a conceptual appreciation of the role of 3D printing for future projects.

Chapter II provides an introduction to the wider topic of rapid prototyping as it applies to the birth of 3D printing technology. This discussion describes the rationale for choosing the 3D printing approach to rapid prototyping over other approaches. An overview of anatomical modeling and the use of rapid prototyping in anthropology to date provides context for the later discussion of the role of 3D printing. The final section of this chapter outlines the objectives of the following work and the case studies used to explore the role of 3D printing in biological anthropology. Two case studies form the basis for this discussion and also provide a methodological guideline for future research.

Chapter III presents the first case study. Case study one is a look at the use of 3D printing for reconstruction projects in biological anthropology. A flowerpot is used as a

pilot for exploring a reconstruction method that involves 3D printing. The reconstruction efforts were not entirely successful. More research is needed into better reconstruction methods prior to using skeletal material. This case study does outline the use of 3D laser scanning and some principals for using 3D printing in reconstruction projects.

Chapter IV presents case study two, the creation of a skeletal replica using both 3D laser scanning and computed tomography scanning as data acquisition methods. This case study builds on some of the lessons learned in the previous case study and evaluates the differences between the two acquisition methods (laser surface scanning and computed tomography scanning). This case study also describes the use of the skeletal replica in a museum exhibit.

Chapter V explores the role of 3D printing in anthropology from a more conceptual viewpoint. The case studies are intended to give a methodological understanding of the ways in which 3D printing can be used and this chapter explores what the results mean to researchers in biological anthropology. In particular McLuhan's (1966) notion of the "medium is the message" is explored as it relates to 3D printing in biological anthropology.

Chapter VI concludes the discussion on the role of 3D printing in biological anthropology. This chapter summarizes the results of the exploration of methodology and the potential future role of 3D printing in biological anthropology. Future directions for this research are presented.

Chapter II: Literature Review

The term rapid prototyping (RP) refers to a process of manufacturing computer-generated models by adding consecutive layers of material to build a physical 3D object. There are many different adaptations of this approach that have resulted in a variety of devices each with their own unique features and types of building materials. In order to address the role of rapid prototyping in biological anthropology, it is important to understand the origins and impetus for the development of this technology. Understanding this history will facilitate a better grasp of the future directions and limitations for this technology in anthropology.

It is also necessary to review how data is gathered and used for the RP process in biological anthropology. Originally RP was developed for the manufacturing industry utilizing computer assisted design (CAD) data for the RP process. The CAD data represent the authors' computer-generated design concept and is validated using the physical object from the RP process. In contrast to this, studies in biological anthropology using RP first require making a digital replica of an item that already physically exists, such as a skull, and then reproducing it using the RP technology.. This process is known in the industrial world as reverse engineering. There are several different ways data can be acquired to produce the output for the RP process following a reverse engineering approach. Two of the most common methods for studies in biological anthropology are laser surface scanning and X-ray computed tomography (CT) scanning. A discussion of the types of data derived from these two processes is essential for understanding the role and limitations of RP in biological anthropology.

The Origin of 3D Printing

Rapid Prototyping (RP) is a generic term that was introduced with the release of the first device in the 1980s (Grimm 2004). This use of the term RP is linked to the marketing of the technology to the engineering and product-design industries. RP was intended to replace computer numerical control (CNC) manufacturing, a process that subtracts material from a larger block to yield a physical object from CAD data. CNC manufacturing was developed out of the merger between traditional lathing and computer programming and was the first computer automated manufacturing process.

CNC devices use a cutting tool controlled by a user-guided computer algorithm to carve the desired shape out of a larger block of material. Since CNC devices cut away material from a larger base, they are limited to producing models of external features. RP devices were introduced to overcome this barrier and are capable of producing internal structures as well, such as the internal sinuses in a skull. CNC manufacturing also has difficulty producing very complicated external features, especially deep holes and slots (Grimm and Wohlers 2003). The interface between the user and the device is also more complicated for CNC manufacturing, often requiring specialized training for the operator (Grimm 2004, Grimm and Wohlers 2003, Seely 2004). The proliferation of RP devices particularly in the educational environment is partially attributed to the ease of use of the technology over CNC manufacturing (Seely 2004). Grimm (2004) does note that both CNC and RP devices produce models relatively quickly. However, RP does not require extensive training to operate, meaning the overall process of design to model is faster than with CNC manufacturing (Grimm 2004).

CNC manufacturing still has a number of advantages over the more recent RP technology. RP devices are limited to a range in build chamber sizes (203 mm^3 to 610mm X 914mm X 508mm), where as CNC manufacturing is capable of handling items as large as aerospace parts (Grimm 2004). CNC is also more accurate, with results ranging from 0.03mm to 0.13mm, whereas RP is accurate to between 0.13mm and 0.76mm (Grimm 2004). Finally, RP devices are also limited in the range of materials that can be used and CNC devices are capable of accepting virtually any material (Grimm 2004, Grimm and Wohlers 2003). Both RP and CNC have advantages and disadvantages. The decision to use one or the other is related to the project (Grimm 2004, Grimm and Wohlers 2003).

CNC manufacturing was successfully used to produce the moulds for the creation of the tiles used to make the replica of the tomb of Seti I (Ahmon 2004). The CNC device used in this case was able to handle the manufacturing of the large blocks; the researchers were also reproducing only the visible surface that was ornate but not topographically complicated. There is currently no RP technology capable of producing models as large as the blocks used for the creation of the tomb. In the case of the recreation of the tomb of Seti I, CNC manufacturing was the most appropriate technology to use. For applications in biological anthropology RP is likely the best approach. Unlike the engineering and manufacturing disciplines, it is important to have a device that can be used with minimal investment in training. The size constraints are less of an issue in biological anthropology as well, where the focus is primarily on human bones. Most importantly, the ability to reproduce internal structures and complicated surfaces is

important to creating skeletal replicas. Skeletal elements are often morphologically complicated and have many canals and similar structures that are best produced using RP.

On March 11th, 1986, Charles Hull received patent number 4575330 "Apparatus for Production of Three-Dimensional Objects by Stereolithography" (Grimm 2004: 15). This patent was the beginning of the RP approach to physical model creation from CAD data. The construction of a 3D model from 2D layers successively organized on the Z-axis allows for the creation of both internal and external surfaces. In 1988, 3D Systems Incorporated released the first commercial stereolithography (SLA) device based on Hull's patent and termed the process "rapid prototyping". Since this first SLA device, a number of different technologies have been released based on a similar approach. These technologies are typically all grouped under the RP heading, although the term originated with SLA. The resulting technological approaches have spread to a variety of industries and most recently, academic research.

RP has now become a confusing blanket term to generically describe many different technologies, all of which are based on the same computer to model, additive-based approach to 3D object creation. Zollikofer and Ponce de Leon (2005: 209) discuss the term "real virtuality" as being synonymous with RP. In this instance, the focus is on the model as a facsimile of reality, thus they link 3D object creation to a method of making virtual reality tangible. Another term used to describe RP is 3D Printing (3DP). 3DP is sometimes used to refer to all RP technologies, and sometimes to specific approaches to RP (Grimm 2004). However, both rapid prototyping and 3D printing carry a specific meaning tied to its particular usage. As suggested by Grimm (2004), RP will be used in this work to describe the total range of additive-based production methods

from computer generated 3D models. This will ensure continuity with other available literature and help to establish consistency in terms. 3DP will refer to a specific technology marketed by Z-Corp, which falls under the RP umbrella. Real virtuality will be addressed during the discussion of the role of 3D printing in relation to the crossover of this technology from industry to academe in Chapter V.

The varieties of RP technologies are based on one of five key methods: curing, sheeting, dispensing, sintering or binding (Upcraft and Fletcher 2003). **Curing** involves solidifying photosensitive resins using a focused light source such as a laser. The SLA technology patented by Hull uses this approach. The only materials available for SLA are epoxy-based resins (Upcraft and Fletcher 2003). Having only one available material limits the range of possibilities in part quality and versatility. **Sheeting**, or Laminated Object Manufacturing (LOM) relies on the application of consecutive layers of material that are cut to shape as they are layered on the z-axis. The materials available are paper, polyester/polyethylene, ceramic coated paper and polycarbonate composites (Upcraft and Fletcher 2003). **Dispensing** utilizes a systematic discharge of a filament onto a specified area, the part is grown from the result of successive deposits. This process is also known as Fused Deposition Modeling (FDM). The materials available for this include thermoplastic (acrylonitrile butadiene styrene, or ABS), elastomer, wax and polycarbonate (Upcraft and Fletcher 2003). **Sintering** (Selective Laser Sintering) is similar to SLA, except that heat sensitive powders are solidified using a concentrated heat source, instead of photosensitive resins. Several different materials are available for this process such as carbon steel, nylon, polystyrene, polycarbonate, wax, ceramics, zirconium sand and flexible elastomere (Upcraft and Fletcher 2003). **Binding** (the

binder-jet process) also uses powders but with a gluing solution rather than a heat source to solidify the powder into the desired shape. This process uses either starch or plaster (Upcraft and Fletcher 2003: 326). The binder-jet process is often referred to as 3D Printing (3DP) because it uses print-head technology similar to a bubble-jet printer (Grimm 2004).

Each of the above-mentioned approaches has both strengths and weaknesses. Users choose a technique based on the desired printing medium, and part properties such as accuracy, durability, and production cost. In an effort to give new and prospective users a more objective overview of what to expect from RP systems than what is available from manufacturers, Grimm (2004) tested four of the leading machines. In this overview, the Viper si2 SLA, Vangaurd si2 SLS, Titan FDM and Z-406 3DP were assessed for part accuracy, stability, feature definition and speed. Grimm qualifies these results by stating that they cannot be analyzed statistically since they are based on a single trial of one part on just four machines. Neither inter-observer nor intra-observer error is reported for these tests since they are based on only one trial. The results however, do give potential users a base-line of what to expect from each method.

Grimm's assessment of accuracy is measured through average material shrinkage over a series of measurements. SLA and FDM are the best and 3DP the worst (Grimm 2004). Grimm reports average total deviation for each system as follows: SLA 0.8 percent, SLS 1.2 percent, FDM 0.5 percent and 3DP 1.4 percent. In contrast to the parts built using the other technologies, the 3DP part is built in a chamber of loose powder. The powder is used to support and suspend the object during the printing process. Unfortunately, the action of natural forces such as gravity can have a negative impact on

parts built using 3DP. Lee and colleagues (1995) suggest that layer displacement from the compaction of powder in the build chamber, may contribute to part inaccuracy for the 3DP process. The centre of the build chamber is the most volatile for both compression and layer displacement (Lee *et al.* 1995). Therefore parts built in the center of the chamber may be subjected to additional compression affecting overall accuracy.

Part accuracy is relative to the overall purpose of the part being printed. While SLA is more accurate than 3DP by a factor of 0.6 percent, it may not be as cost effective or as quick. For concept modeling (demonstrating product design ideas) this is an acceptable trade-off. The purpose of the final object is to convey a physical representation of a design idea that does not need to be highly accurate. In this case speed and cost efficiency are more beneficial traits. In applications involving a reverse engineering approach (such as with studies in biological anthropology), it is important to match the spatial resolution of the data acquisition device with the approach with the most appropriate accuracy potential. For example, the 1.4 percent difference in the original part and the part printed using the 3DP method corresponds to a difference in linear dimensions of –0.38mm for shrinkage and 0.64 mm for expansion. Some data sets are based on CT scans, and can range in spatial resolution from 2mm slices to 0.04mm slices. A user's understanding of the capabilities of a rapid prototyping method should be framed in the context of the application and data source being replicated.

Part stability, as measured by Grimm (2004) refers to the degree of change in size and shape of parts over time. This assessment is more closely related to the properties of the production mediums than the actual machine capabilities. Part stability can improve with advancements in consumable materials used by each technology.

Grimm reports that SLA is not stable over time and that a limitation of the photosensitive resins is their susceptibility to distortion from heat, moisture and chemical agents. Both SLS and FDM materials are stable when removed from the build chamber. 3DP parts are not stable when removed from the build chamber, but can be made stable through post-processing infiltration with wax, epoxy or cyanoacrylate (CA). When this is done the parts take on the material properties of the infiltration medium. This is because the bonds between plaster particles are far enough apart to allow for the infiltration medium to envelop the entire structure, encapsulating the bonded starch or plaster particles (personal communication, Z-Corp).

Feature definition refers to the smallest amount of detail that can be produced by each method. Grimm (2004) notes that the theoretical feature size capable of being built using any given approach is not necessarily equivalent to what will survive removal from the build chamber. The tested values Grimm reports are realistic to what the user can expect after removing the part from the build chamber. The minimum feature size for each system is as follows: SLA 0.51mm, SLS 0.64mm, FDM 0.41 to 0.61mm and 3DP 0.76 to 1.52mm. Grimm does not report these values in terms of 3D structures leading the reader to assume that the values presented correspond to the smallest feature cubed. These results relate to the material properties of the printing medium and the user's skill at retrieving items from the build chamber. Parts printed using the 3DP process are usually weakest in the initial few hours following print completion. This is known as "green strength" and is the most limiting factor of the 3DP method. Small features have a tendency to break when being excavated from the powder in the build chamber; this is a significant limitation of the 3DP technology. Recent advances in the Z-510 (Z-Corp's

replacement for the Z-406 in 2005), such as a heated build chamber and stronger material systems should change the minimum feature size capable of being produced with the 3DP technology. Similar to the discussion on accuracy, feature size limitations should also be considered with the resolution of the original data in mind. The printer will not be able to print features smaller than the resolution of the source data.

The SLA technology performs well on both the accuracy and feature definition categories of Grimm's assessment, while the 3DP technology comes up short next to SLA. Production speed is where the 3DP technology wins out over the other methods (SLA, SLS and FDM). The SLA technology performed the worst. The methods evaluated in Grimm's previous tests yielded the following time results for the same part (measuring 15.24 x10.16 x 1.91 cm): SLA 5.4 hours, SLS 1.5 hours, FDM 4.2 hours and 3DP 35 minutes. Faster machines for the SLA and FDM methods were also tested and included in Grimm's report on speed, but were not included in the other tests for accuracy and feature definition. It is therefore difficult to include the faster models in a fair comparison between the different methods.

Since the mid to late 1990's the number of different approaches to RP have increased the availability of this technology and allowed for the development of a range of technological options for consumers. An often-asked question is how RP can be used in specific industries (Carrion 1997, Grimm 2004, Kochan 2000). RP technologies are primarily used to communicate information about concept designs, analytical results and related visual and tactile information. Grimm (2004: 35) writes, "since rapid prototyping requires no manipulation or human interpretation of the design data, its direct output offers design verification". Discussing attributes about an object is potentially more

effective than discussing either a written description or photograph. Holding the physical object in question allows the interpreter to freely associate with the object, without complicating issues such as industry-specific discourse in a written account or photographic bias. Consider the difference between learning osteology from a textbook only versus actually holding the bones. The student gains a richer appreciation for subject material by handling the actual bones than simply reading about them or looking at pictures. The same is true for communicating design ideas to an audience of potential clients (especially when the clients are not from a design related field). The interpretation of the object is not filtered through someone else, as is the case with written descriptions or photographs, which represent the object as the writer or photographer viewed it. The most obvious use of RP is therefore in communicating complex design, shape or form concepts. In support of this, Zollikofer (2005) cautions that RP is not an analytical tool, but simply a tool used to share information.

Anatomical Modeling

RP technology was originally developed for the design and manufacturing industries. Recently, biomedical applications for RP have flourished beyond what was originally imagined for the technology. The majority of this usage is reported in case studies where RP has been used in novel ways to solve biomedical problems. Zollikofer and Ponce de Leon (2005) note that RP enhances surgical planning, custom implant design, case collection and teaching. The key breakthrough is the ability to non-invasively reproduce physical 3D models from 3D medical scan data of living or dead subjects. The advantages of using 3D models in a surgical context include more effective and accurate pre-operative planning and better surgeon to patient communication.

Powers (1998) reports that the use of 3D models in surgical planning reduces both the length of surgeries and the chance of mortality. Many of these studies have focused on using SLA technology and most examples focus on surgical applications (e.g. Anderl *et al.*, 1994; Borah *et al.*, 2001; Brown *et al.*, 2001 & 2003; Hieu *et al.* 2005; Perez-Arjona *et al.*, 2003).

The linear accuracy of SLA models is also well established in the biomedical literature (Barker *et al.*, 1994; Bouyssie *et al.*, 1997; Choi *et al.*, 2002; Ono *et al.*, 2000, Wulf *et al.* 2001). Barker and colleagues (1994) and Choi and colleagues (2002) examine the accuracy of SLA models by comparing deviation in linear measurements between dry skulls and their model analogues. Both studies utilized CT data for the creation of the virtual 3D models. Choi and colleagues also considered the accuracy of the CT data used to create the SLA model. They raise the important point that the model is only as good as the original data. Their CT scan was performed with 1mm slices, making maximum resolution limited by this margin of error. Choi and colleagues (2002) report the accuracy of their skull models over 16 landmark-based measurements to be within 0.62mm, +/- 0.35mm. They note that this is smaller than previously reported values by other researchers. The earlier study by Barker and colleagues reports an overall average difference of 0.85mm between the skulls and skull models. This is based on a comparison of four linear measurements of 11 skulls over five trials. Bouyssie and colleagues (1997) published a similar study investigating accuracy of SLA models from CT data using only mandibles instead of complete skulls. They state that there is no statistically significant difference between the original and the SLA replicas of 12 mandibles. Bouyssie and colleagues report an average difference in measurements

between the models and original mandibles as 0.12mm. This value was compared to the standard error of the mean (0.02mm) using a Student's t-test with an $\propto$ level of 0.005. According to this analysis, they conclude that there is no statistically significant difference between the original and model. The ability of SLA to reproduce almost exact RP replicas of original objects is fairly well documented by the literature to date. Accuracy-based assessments in the anatomical modeling literature consistently note that significant sources of error result from either observational biases, such as landmark replication, or data acquisition error (Barker *et al.*, 1994; Bouyssie *et al.*, 1997; Choi *et al.*, 2002; Clark *et al.* 2004; D'Urso *et al.* 2000; Hjalgrim *et al.* 1995; Ono *et al.*, 2000). The real test of RP technology is how it can be used to solve particular communication and visualization problems. Borah and colleagues (2001) find that models provide an independent evaluation of biological architecture through a material of known uniform properties. They use 3D models to represent microscopic structures such as trabecular bone. The model is then subjected to stress tests, which assess the geometric tolerance of the structure alone without the added complication of multiple substances and varying chemical composition. Borah and colleagues have been able to understand changes in bone strength relative to bone loss in patients suffering from osteoporosis using 3D models of real bones. Bibb and Sisias (2002) performed a similar study aimed at validating finite element analysis (FEA) results from μCT data of cancellous bone.

Another important application explored for SLA replicas is the ability to reproduce specific regions of interest for surgeons and allow more effective pre-operative planning (Hieu *et al.* 2005). Brown and colleagues (2003) examined this by looking at 117 patients with complicated fractures and using SLA models of those fractures to

improve surgical success rate. One such successful example they site is the use of the SLA models for planning the trajectory of screws used in the treatment of a spinal injury. Brown and colleagues (2001) reported similar success for the treatment of a hip fracture. Anderl and colleagues (1994) used SLA for planning a sensitive osteotomy (surgical removal of bone tissue) on an eight-month-old patient requiring extensive reconstructive craniofacial surgery. In these cases, SLA models allow surgeons to visualize tangible replicas of the patient's bodies and plan "what-if" scenarios, without having to make contact with the patient. Related to surgical applications are the medical-legal implications for RP technology in general. Dolz and colleagues (2000) present a case study in which an SLA model of a child's skull was presented during a child abuse trial. They argue that presenting the model of the fracture patterns is less inflammatory and more dignifying to the victim than presenting photographs.

Rapid Prototyping in Anthropology

While the biomedical community is making use of RP, less work has been done in anthropology to assess the usefulness of this technology. The most important possible advantage to using RP in anthropology is the ability to non-destructively create models of the past for further study. Hjalgrim and colleagues (1995) used CT scans to non-invasively create a 3D model of an ancient Egyptian mummy skull. This approach allowed the researchers to examine the skeletal structure of the individual without having to physically manipulate or unwrap the mummy. Ancient remains in particular are precious resources, and can often be associated with a need for cultural sensitivity. Hjalgrim and colleagues (1995) further noted that it was possible to perform traditional methods of anthropological analysis (such as sexing and estimating ancestry) on the

model without having to disturb the original specimen. D'Urso and colleagues (2000) contrast traditional approaches to anatomical modeling such as using casts with RP. Creating casts of specimens requires making contact and adhering molding compounds to the original item's surface. This approach has the potential to damage the surface of the object, and makes it difficult to capture detail such as internal cranial structures (D'Urso *et al.* 2000).

In anthropology, one of the first reports of 3D modeling is from the investigation of the Tyrolean Iceman found in the Alps (Weber, 2001b; zur Nedden, 1994). Every effort to preserve the original condition of this mummy was taken; therefore conservation focused on replicating the preservation environment. This meant that the iceman could not leave the freezer long enough to be studied. A full CT scan was performed in order to provide researchers with images of the skeleton and other associated artefacts. An SLA model of the Iceman's skull was made for further analysis and facial reconstruction. This proved to be a breakthrough in the limitations of working with limited and precious resources. The model of the Iceman's head could be shown and handled by researchers without disturbing the very delicate nature of the mummified individual. The SLA model effectively replicated the structural and anatomical anomalies such as the flattening of the face, which was not as clearly visible in the CT scans (zur Nedden *et al.* 1994). In this case, SLA was also used to create models to inform the public while the body was kept safely curated.

Zollikofer and Ponce de Leon (2005) outline that RP can be used in paleoanthropology for direct replication, replication of hidden structures (as in fossils encased in matrix), and for validating and reproducing virtual reconstructions. D'Urso

and colleagues (2000) and Clark *et al.* (2004) each used SLA to create replicas of a fossil still encased in matrix. Although both of these studies examine non-primate paleontological material, the same principals apply to using the imaging and RP methods on fossils of anthropological significance. When there is sufficient difference between the fossil and matrix, the outline of the fossil can be distinguished from the matrix by shape and density differences as observed in a CT scan. The fossil or object can then be segmented out and reproduced without the need to attempt further excavation. This is important because excavating fossils from dense matrix can be dangerous to the precious resources. The models can then be made permanently available, and internal structures never before seen can be reproduced and examined (Weber 2001). All of these examples of RP focus on using SLA technology.

While there are many different RP technologies available, researchers do not report why SLA was chosen over other approaches. SLA is one of the first and most broadly available RP technologies. In addition to this, some researchers note a knowledge, or communication gap between biomedical and engineering communities (Fontana *et al.* 2002, Hieu *et al.* 2005). A lack of awareness of the variety of RP methods available by biomedical and anthropological researchers may contribute to the bias towards using SLA technology. The novelty of the relatively recent uses of SLA may also over-shadow a more critical examination of the usefulness of the different RP approaches for specific projects.

Another significant barrier to the use of RP and in particular SLA is cost (Dolz *et al.* 2000, Hieu *et al.* 2005, Hjalgrim *et al.* 1995, Powers 1998). Dolz and colleagues (2000) give general figures for cost and speed of the SLA models for their purposes.

They estimate that a single case may range from $2000 to $3000 and if rushed will be ready within two to three days. Hjalgrim and colleagues (1995) go a step further and report the SLA model of an Egyptian skull they produced resulted in a total consumables cost of $2500 (US) and took 40 hours to build. The photosensitive resin is a very expensive material. The high cost of SLA consumables is a widely accepted and recognized drawback for the technology (Grimm 2004). The lack of widespread use of RP in research environments is likely due to the combination of SLA being both the most broadly available and the most expensive approach. Researchers will naturally tend to use RP for exceptional projects such as the reproduction of the skull of the Iceman by Hjalgrim and colleagues (1995). A more cost-friendly approach to RP may increase not only the use of RP in research environments, but also the overall availability and breadth of projects in which it can be used.

Ono and colleagues (2000) report that the 3DP method of printing models is able to overcome the cost barrier, which has prevented the use of RP in everyday research. In their study, Ono and colleagues (2000) compare the accuracy and viability of skulls printed using the binder-jet method and the standard SLA method. They find that the binder-jet method is not only more cost effective, but is also capable of producing better anatomical specimens. The plaster-based materials of the 3DP method are capable of reproducing complex structures without the support struts often needed for SLA models of the skull in orbits, sinuses and the cavities at the base of the skull (Ono *et al.* 2000: 532). As well, the binder-jet method is capable of reproducing finer surface detail such as pores and nerve cavities (Ono *et al.* 2000: 532). Irregularities in surface morphology

are important to anatomical modeling, especially for disciplines such as biological anthropology that focus on examining variation in biological form.

The transparency of the semi-translucent SLA material is an advantage for seeing structures under the surface morphology. While losing this benefit, the binder-jet method is capable of adding colour to objects. Gibson and Ming (2001) note that colour has been traditionally limited to the manufacturing and architectural industries to distinguish regions of parts, design iterations or artistic flare. In contrast to this, few researchers have experimented with the use of colour in anatomical modeling. The 3D printers marketed by Z-Corp offer potential to enhance anatomical modeling through the use of colour 3DP. Colour is also available in a limited fashion by LOM (Gibson and Ming 2001).

To date, there are few examples of anatomical modeling using 3DP technology. This is likely due to the point that the first 3DP platforms were only released in 1999 (Grimm 2004). The 3DP technology needs to be examined further to better understand its potential role in anatomical modeling.

Methods of Data Acquisition

The RP process is dependant upon a virtual model created using a variety of methods such as CAD, CT scanning or surface laser scanning to name a few. The following section will provide an overview of data acquisition as it applies to anatomical modeling in anthropology. The focus will be on the limitations and possibilities of using CT and surface scanning in biological anthropology. The final section of this review of data acquisition will examine some basic issues associated with the creation of virtual 3D models.

The literature discussed in this chapter cites the process of data acquisition as the most significant limiting factor for spatial resolution and accuracy of RP models (Barker *et al.*., 1994; Bouyssie *et al.*, 1997; Choi *et al.*, 2002; Clark *et al.* 2004; D'Urso *et al.* 2000; Hjalgrim *et al.* 1995; Ono *et al.*, 2000). These researchers utilized CT data for the creation of models. The following section will briefly examine some of the fundamental bases of CT scanning, and the emerging use of 3D laser scanning to produce both physical and virtual surface models and end with a brief discussion on file formats including some of the errors that can occur in the printing process from poorly prepared files.

X-Ray Computed Tomography Scanning

X-ray CT scanning has become a common and accepted method of data acquisition in biological anthropology (Spoor *et al.* 2000, Weber 2001a and 2001b, Zollikofer and Ponce de Leon 2005). While RP is still a relatively novel application in anthropology, the use of CT as a viable method of data acquisition has been well explored for non-invasive visualization in palaeoanthropology, palaeopathology and morphometric studies. Mehta (1997) concludes that CT scanning is an effective method of acquiring data allowing one to visualize 3D reconstructions of bone. This makes CT scanning ideal for most anthropological applications, where dose is not as great a concern for skeletal remains versus living patients for biomedicine. Lynnerup and colleagues (1997) highlight the non-invasive aspects of CT scanning archaeological material, one of the principal advantages of using this type of data acquisition. Wood (2000) also notes that CT scanning helps identify fossilized bone from matrix, avoiding potentially damaging cleaning methods. Perez and colleagues (2000) illustrate that the 3D structure

of hidden anatomy such as nasal cavities can be effectively studied using CT scanning. Ruhli and colleagues (2002a,b) show how CT scanning significantly enhanced diagnosis of palaeopathological lesions by more effectively visualizing structures. In particular, Ruhli and colleagues (2002a) demonstrate that the multi-detector CT approach used increased spatial resolution for more effective diagnosis of cranial lesions for three ancient cases. Multi-detector CT scanning utilizes several collection devices to simultaneously record multiple angles of the subject being scanned. Pasquier and colleagues (1999) use CT scans to create a more effective numerical scoring for age-at-death estimation using the Suchey-Brooks casts. The correlation coefficient they report for the comparison between virtually identified pubic symphyses and those identified from direct observation is 0.74. This result does show a relationship, but it is weak in the context of providing meaningful conclusions about age at death. Evolutionary analysis and morphometric studies also commonly use data obtained through CT scanning (eg., Brown and Wood 1999; Williams and Richtsmeier 2003, Zumpano and Richtsmeier 2003 to name a few such studies). The purpose of this section is not to explore CT scanning in biological anthropology *per se*, but to show that this method is well established as a valuable tool in anthropological studies and introduce the advantages and limitations. These advantages and limitations have a bearing on the use of CT scanning with RP applications. RP can be used to extend the advantages of non-invasive study to tangible and accurate replicas of scanned specimens.

The general process for using CT data requires 3 basic steps. The first is recording the object using a CT scanner. From the CT scanner, files are typically exported as raw or DICOM (Digital Imaging and Communications in Medicine) formats.

Both file formats are composed of a series of 2D images each representing a section of the imaged object. The images must then be imported and visualized using an imaging program where structures can be isolated as regions of interest and 3D rendering can take place if required. The potential for data problems exist at each stage of the CT process illustrated above. Understanding CT data acquisition and processing is integral to the effective use of this data in anatomical modeling and biological studies (Zollikofer and Ponce de Leon 2005). Lester and Olds (2001) emphasize that it is important to consider the nature of the data required before attempting any imaging study.

Like traditional radiography, CT uses the passage of X-rays through an object and records the resulting attenuation profile. For conventional radiography the attenuation profile is recorded on a film as an averaged sum. The varying shades reflect differences in the radiopacity of regions of the object under study, which reflect the attenuation profile of the x-ray beam. CT scanning uses a more focused X-ray beam, whose attenuation profile is recorded as a line integral by a data collector. The values from multiple line integrals from various angles are used to reconstruct the overall attenuation profile of a 3D object using the Radon theorem (Zollikofer and Ponce de Leon 2005). Conceptually, a radiograph is a 2D representation of a 3D object, but a CT scan is actually composed of a series of 1D projections approximating a 2D representation (Zollikofer and Ponce de Leon 2005). Thus, the 2D section of CT data is an approximation of the object based on the formulae used to compile the 2D image from the line integrals (Zollikofer and Ponce de Leon 2005).

The 2D “slice” of the object at this stage is considered “raw data” and simply reflects the attenuation profiles from multiple angles at a given point of the object. The

values throughout the object on a given line are estimated using the principal of back-projecting (Zollikofer and Ponce de Leon 2005). The profiles at any given points of attenuation are measured as Hounsefield (H) values (named after the founder of the CT in 1973) that range from –1000 to 4096 (Spoor *et al.* 2000). For reference, Spoor and colleagues (2000) write that air corresponds with an H value of –1000, water has an H value of 0 and dental enamel has an H value of 3095. At the raw data level, image quality is affected by hardware parameters such as detector calibration and amount of radiation used (duration and intensity; Zollikofer and Ponce de Leon 2005). The process of back-projecting favours low frequency attenuation values over high frequency values, requiring a filter to calibrate the data to an appropriate threshold (filters exist for hard and soft tissue identification; Zollikofer and Ponce de Leon 2005). The resulting image quality is dependant upon proper calibration of the actual CT device and appropriate raw data back-projection filters.

Some errors in CT data result from the imaging process itself and are difficult to control and can have a significant impact on model and image quality. **Partial volume effect** (PVE) is an artifact that looks like light coloured streaks through the border of an object (Zollikofer and Ponce de Leon 2005: 77). Figure 2.1 below from the Bosma Collection, (see Shapiro and Richtsmeier 1997), illustrates PVE by the streaks passing in line with the edges of the skull.

Figure 2.1: Partial Volume Effect

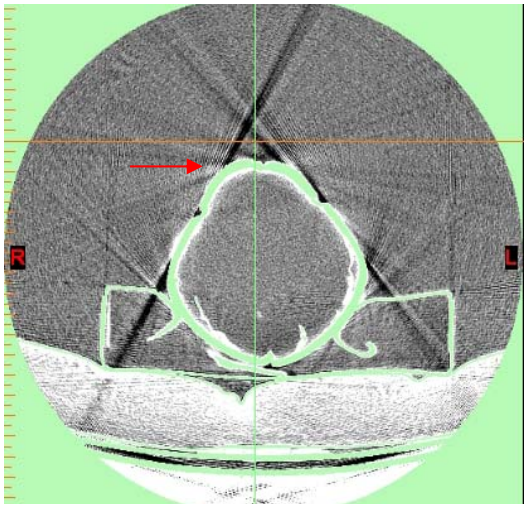

Figure 2.1: An image slice taken from one of the Bosma collection CT scans (Shapiro and Richtsmeier 1997). The red arrow identifies the artifact resulting from PVE.

This artifact is caused by a line integral passing only partially through the object, but being collected totally by the detector causing an error in the definition of the object's border. Souza and Udupa (2005) note that PVE can cause the creation of psuedostructures and obscure regions of interest when CT objects are volume rendered. Proper segmentation and thresholding is typically used at the image processing level to deal with PVE. Choi and colleagues (2002) discuss that compensating for PVE reduces the Z-axis accuracy of a 3D model through shrinking the objects' border using segmentation or thresholding techniques. **Beam-hardening** is an artifact that is characterized by dark bands appearing within an object due to variations in beam intensity (Zollikofer and Ponce de Leon 2005: 77-78). Beam hardening is apparent in the

dark and light variations in the support structures around the posterior margin of the same CT slice from the Bosma collection in Figure 2.2 below.

Figure 2.2: Beam Hardening

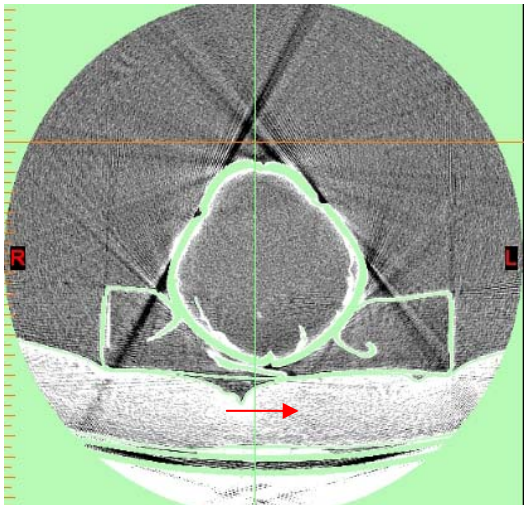

Figure 2.2: The same slice from the Bosma collection as Figure 2.1 above (Shapiro and Richtsmeier 1997). The red arrow illustrates beam hardening.

Since the process of back-projection favours low intensity attenuation profiles, high intensity values are filtered out causing the beam hardening affect, which can result in holes in the final model if not properly dealt with in the image processing software.

Frozen-noise are artifacts produced from detectors working at maximum sensitivity that are back-projected onto the final image (Zollikofer and Ponce de Leon 2005: 78). This artifact is sometimes more difficult to find. Figure 2.3 below from the same CT slice as the above figure may show a very small example of frozen noise as a small light object in the middle of the empty cranial vault.

Figure 2.3: Frozen Noise (marked with red circle)

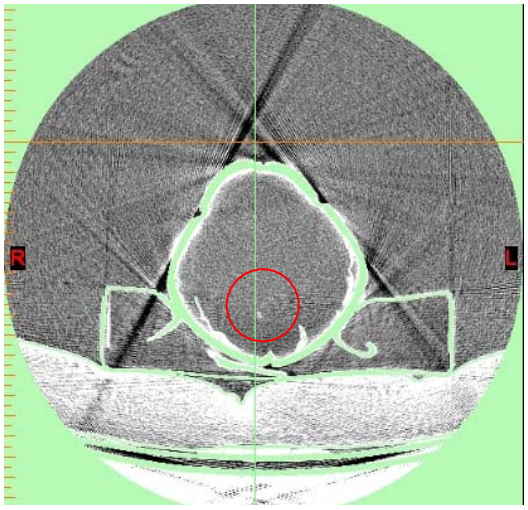

Figure 2.3: The same CT image slice as in Figure 2.1 (Shapiro and Richtsmeier 1997). The red circle indicates frozen noise. The skull depicted has an empty calvarium, suggesting the easily edited light spot is just noise.

In this case the detectors image tiny spots that do not really exist in the original object's profile. These items must also be segmented out using image-processing software.

Other potential problems with CT images relate to the display and user-level handling of the data. Individual slices of CT data are analogous to 2D images at a given X-Y point of the object scanned. The most basic unit of data is the pixel in these images, which is a calibrated square unit of data. For example, an image with a 1-millimeter pixel size is made up of 1-millimeter square units of data. The slices are organized as a stack making up the third dimension, or z-axis. When rendered, the pixels are converted into 3D units of data termed voxels. The data that makes up the image is therefore converted into a cubic measurement. The limitation of this rendering method concerns the resolution of the units of data. The shade of the pixel is an averaged value of the density of the object within the predetermined unit (in this case 1-millimeter). This

averaged value is exacerbated by adding the inferred slice distance to make the voxel. This phenomenon is called **Partial volume averaging** (Spoor *et al.* 2000: 64). Partial volume averaging can produce holes in the imaged structure of thin bones when the pixel values are averaged closer to the surrounding air or lower density tissues (Spoor *et al.* 2000). This can also lead to foramina and sutures becoming enlarged in the resulting 3D virtual model (Spoor *et al.* 2000:).

Another source of error unique to CT data is the "Dumb-bell effect" identified by Choi and colleagues (2002: 29). The dumb-bell effect results from the averaging of threshold values of the inner and outer surfaces of the object. In this case, isolating a structure based on threshold values leads the researcher to image more of either the outer or inner surface. The result is an inner surface that is proportionally greater than the outer, or vice versa. Measurements of either surface must be considered prior to using thresholding as a method of segmentation since one surface may be arbitrarily reduced during the thresholding process.

Image preparation and acquisition protocols can have an impact on the accuracy of CT data. Both Jung and colleagues (2002) and Kim and colleagues (2002) performed image accuracy assessments and found that image slice thickness is the most significant factor for spatial resolution. Spoor and colleagues (2000) also support this by noting that spatial resolution is primarily limited by slice thickness. The stepped appearance of 3D renderings of CT images is produced because CT slices are not infinitely thin. Each section of data has an inferred thickness that is layered on the z-axis. The difference between the actual thickness and the inferred thickness, results in the stepped appearance.

Stepping is usually smoothed by rendering software using a proprietary algorithm that can affect the surface quality of the visualization (Spoor *et al.* 2000).

The final aspect of error in CT data comes from observer error during image processing. Segmenting and thresholding are two methods of isolating tissues and regions of interest (ROIs). Thresholding identifies tissues based on Hounsefield values. Segmentation is a more user driven active isolation of a tissue using a variety of image editing tools from the software being used. Both of these techniques require user input to identify objects in the image. Bouyssie and colleagues (1997) and Spoor *et al.* (2000) report that thresholding and segmentation issues resulted in the imperfections in their SLA models of mandibles. One such problem resulted from partial volume averaging that produced holes in the model. User-based image processing is the final step in creating effective anatomical models using CT data and has the largest impact on model quality (Bouyssie *et al.*, 1997; Choi *et al.*, 2002; Clark *et al.* 2004; D'Urso *et al.* 2000; Gateno *et al.* 2003; Hjalgrim *et al.* 1995; Ono *et al.* 2000). Kang and colleagues (2004) attempt to create an automated segmentation algorithm, recognizing that segmentation is slow, tedious and subject to inter-observer error. Individual variation in tissue radiopacity, between datasets and between scans within a data set, makes the development of effective automated tools difficult. Various software packages offer varying tools and advantages for this stage of data manipulation. Once the data is acceptably processed it can be exported to one of several file formats accepted by the RP device, such as STL or VRML.

3D Surface Scanning

3D surface scanning is another common method for generating 3D models for printing. Unlike CT scanning, this method collects information only about the surface of an object allowing the user to create a virtual model in 3D-space. There are two principal approaches to surface scanning (Zollikofer and Ponce de Leon 2005). **Photogrammetry** uses multiple camera viewpoints and a grid to make 2D images three-dimensional. The grid of known proportions is projected onto the object. Spatial dimensions are based on the difference between the deformation of the grid and the original known values. **Laser range scanning** uses the reflection of focused light from an object's surface to estimate distance values that are used for creating a representation in 3-space. Feng and colleagues (2001) state that laser range scanning is only 1 order of magnitude less accurate than coordinate measuring machine (CMM) approaches to digitizing points. However, they do not account for all the different approaches to laser range scanning that may have variable accuracy and results. CMM devices record points in 3-space by actually making contact with the object using a sensor probe.

There are many different approaches to the optical triangulation approach to surface scanning and many of these methods are the product of ad hoc developments to solve specific scanning needs (Ahmon 2004, Fontana *et al.* 2002, Willems *et al.* 2005). For example, some range scanners use a radar-based approach that measures the time difference between outgoing and incoming laser light. These scanners are typically used for larger structures such as buildings (Zollikofer and Ponce de Leon 2005). This means that each approach needs to be evaluated on its own merits, and researchers need to consider their own needs prior to engaging in a scanning project.

Some researchers choose to build their own laser scanning systems for specific and highly specialized projects or to overcome issues encountered with other technology (Ahmon 2004, Fontana *et al.* 2002, Kofman and Knopf 2002). All optical triangulation systems are limited to recording only line of sight data. Complex geometry is therefore difficult to record accurately (Zollikofer and Ponce de Leon 2005). Kofman and Knopf (2002) offer a solution to this problem of acquiring complex geometry by proposing a scanning method that allows six degrees of freedom (unconstrained movement in 3D-space) without needing an external device for tracking the sensor-head position. This approach allows the users to have complete freedom when moving around an object capturing various hidden facets, independent of the limitations of tracking equipment. This approach to range scanning is termed "continuous unconstrained range sensing" (Kofman and Knopf 2002: 1496).

Error in the data captured results from either random variations in light, which are difficult to control for, or systematic problems that can be controlled (Feng *et al.* 2001). The optical triangulation method typically uses the diffuse (non-directional) light reflected off the object, therefore specular (highly directional) light can cause interference. Overly reflective objects increase the noise errors from specular light (Zollikofer and Ponce de Leon 2005). Conversely, flat-black objects absorb all the diffuse light and cannot be recorded using this method (Zollikofer and Ponce de Leon 2005). Adjusting laser intensity is one way of dealing with random error caused by too much specular noise or not enough diffuse light. Systematic error is caused by problems interpreting the data within the device, since the triangulation method depends on accurately assessing the incident angle of the light and projected angle from the depth of

field (Feng *et al.* 2001). Systematic errors can largely be corrected for through calibration of the device (Feng *et al.* 2001).

The range-scanning process results in data collected as points in a Cartesian x, y, z coordinate system, generating a mass of points representing an object called a point-cloud. Point-cloud data is often used for 3D morphometric analysis in anthropological studies (Zollikofer and Ponce de Leon 2005). Engineers also use such data to test the accuracy between a virtual object designed with CAD software against the physical prototype. The use of point-cloud data by either engineering or biological researchers usually involves working with the point-set in another software program that allows examination of shape deviation or other dimensional parameters.

Accuracy changes with the surface properties of the scanned object, operator skill and device calibration as mentioned earlier. Harrison and colleagues (2004) use a Polhemus Fastscan to evaluate facial swelling for patients recovering from tooth extraction. In their tests of a mannequin as control they determined overall repeated measurement error to have a standard deviation of 12.5 cm^3, or 4 percent. They conclude that the main source of error is due to repositioning of the head for comparative scans (before and after). While this study does not use the point-data for morphometric analysis, the scanning process was helpful for non-invasively assessing patient swelling after surgery. For example, Harrison and colleagues (2004) note that the ease of use, lack of radiation and relative low cost made the Fastscan range-scanner valuable in a clinical context.

3D scanning technology is also making an impact on the collection of anthropometric data. In very general terms anthropometry is the study of measurements,

which was used for understanding human shape variation and was traditionally accomplished by acquiring a series of physical measurements often using calipers. The CAESER project by the National Research Council of Canada uses 3D scanning technology to acquire a set of data points representing the shape of different individuals. This is a more comprehensive approach to anthropometrics resulting in data that can be used to understand shape, create animated characters, or design better products (Azouz *et al* 2005).

Scanning can also be used recreate objects, but the data used to create the 3D models often require extensive post-processing. There are many case studies of scanning for the preservation of culture heritage material (Ahmon 2004, Fontana *et al.* 2002, Fowles 2000, Godin *et al* 2002, Taylor *et al* 2002 and 2003, Willems 2005 etc). Godin and colleagues (2003) note that archaeology is a key market for 3D scanning technology. Fowles (2000) argues that scanning should be made part of a conservation strategy, especially when the material needs to be moved and/or restored. Virtual models can be an accurate record of the object before restoration and movement, and can be made into physical replicas for display using RP methods (Fowles 2000). For example, the digitization of frescoed walls in Italy allowed for closer study of the paintings while protecting the site from contamination by visitors (El-Hakim *et al* 2005). Fresco paintings are particularly sensitive to mold and other environmental pollutants and are often sealed from visitors (pers comm. Italian Tour Guide). Traditional methods of replicating objects using either artistic imitation or moulding methods are inappropriate for most precious cultural resources. Making moulds of objects for the casting process requires contact with the object and can lead to damage (Ahmon 2004, Fontana *et al.* 2002, Fowles 2000).

Additionally, accurate dimensional data is available in the form of point clouds from 3D scanning (Godin *et al* 2002).

While scanning and creating virtual replicas is a solution to non-contact accurate recording of objects, it certainly is not free of problems. The cost of hardware and software and the required time investment and knowledge are barriers to widespread use of surface scanning (Fontana *et al.* 2002). Creating a 3D virtual model usually involves scanning the object several times from different viewpoints so as to capture as much surface detail as possible (Ahmon 2004, Fontana *et al.* 2002, Fowles 2000). Following the physical scanning, extensive post-processing is required to generate a 3D surface model from the point data. There is no one correct way to prepare scan data, making post acquisition treatment of data the most subjective part of this method. For example, Fontana and colleagues (2002) report that the scanning of the Minerva of Arezzo involved the design of a scanner and the writing of software to solve specific data problems. Their post-processing sequence consisted of registering a series of scans, merging the scans (eliminating redundant data) and simplifying the overall mesh. The whole process took four weeks to create one virtual model (Fontana *et al.* 2002). Ahmon (2004) estimates that one-hour of scanning typically results in five hours of post-processing.

Creating Virtual Models from Virtual 3D Data

The creation of a surface model requires converting point-data into some type of surface representation. Surfaces can be created using either NURBS (non-uniform rational B-spline) surfaces or another meshing algorithm (Boehler *et al.* 2002). NURBS surfaces are used to define objects in CAD environments. A NURBS surface is a

mathematical representation of a surface curve. The NURBS approach results in smaller file sizes compared to surface meshes and better representation of smooth surfaces, since they are not composed of a series of points (Boehler *et al.* 2002). Meshed surfaces are composed of a series of triangles connecting the discrete points in a point-cloud. A number of algorithms can be used to generate a surface mesh (Lin and Liang 2002). A comprehensive examination of the strengths and weaknesses of each algorithm is outside the scope of this work (Lin and Liang 2002), however it is important to understand that there are different methods for generating surface meshes and they can have an impact on surface quality. The appropriate mesh algorithm is also dependant upon the type of data used, thus volume data from CT scans requires a different method than other, more simple data sets (Lin and Liang 2002).

The accuracy of the surface model is dependant upon the number of points of data, and areas of greater curvature require more data to be accurately represented (Wang *et al.* 1999). The catch is that increases in the amount of data representing an object also increase the chance of error when connecting the points to make a surface (Wang *et al.* 1999). When data is filtered and averaged, points are removed to assist in the meshing process (creating a polygon surface from point data). The necessary reduction in data means that the accuracy in representing the original shape of the object in 3D space is compromised.

Treatment of the point-cloud prior to the meshing process can also have an impact on mesh quality (Boehler *et al.* 2002). For example, Lin and Liang (2002: 294) note that the "adaptive fitting technique" averages points within a certain range and fits the lines that make-up the surface mesh to this averaged data. In contrast,

"simplification" just removes points within a certain range making the reduction of data more random and less representative of the global shape of the scanned object (Lin and Liang 2002: 294). Typically the meshing process is automated and different software packages will yield varying results (Boehler *et al.* 2002). It is again important to be aware of the differing effects such processing can have on the actual model generation and structure projects around these limitations.

The RP process requires some method of interfacing the virtual model with the RP device. In 1987, 3D systems developed the standard STL (stereolithography) file to allow CAD models to be printed on SLA machines (Kai *et al.* 1997a). All RP systems are equipped to accept the STL format (Kai *et al.* 1997a). The STL format is essentially a triangular surface mesh with defined unit normal vectors (Lin and Liang 2002). Unit normal vectors are directional lines projecting perpendicular to a surface plane. The normal vectors are important because they define the orientation of each triangular surface and allow for the interpretation of their direction. A normal vector facing the wrong way can turn aspects of the model inside out. In order for an STL to be effective, the normal vectors must uniformly face outward for each mesh facet and the coordinates for each vertex (discrete point in the triangle) must correspond with the normal vectors (Lin and Liang 2002). There are two types of STL file, ASCII and binary (Kai *et al.* 1997a). ASCII encoded STL files are written so that they are legible by people familiar with a Cartesian coordinate system. Binary files are a series of one and zeros legible by only computer systems. RP systems can read either file, but the ASCII approach results in files that can be read by the software and in a text editor by a person, meaning that two levels of information processing are available instead of one, as in the binary file.

There are several problems inherent to the STL format. Defining the surface of a model using a polyhedral mesh results in redundant information (Kia *et al.* 1997a). Each triangle representing a given overall surface is defined by three sides, which are in turn shared by triangles defined by one of the same sides on the same given surface. Essentially, the human eye interprets this as one continues surface, but the mathematical representation actually reflects many surfaces. Defects such as holes, cracks and non-manifold surfaces (surfaces that have more than one neighbouring facet), overlapping facets and incorrect normals are common (Kia *et al.* 1997a and Leong *et al.* 1996). These defects result from problems associated with the process of creating the polygon mesh. Since the meshing algorithm is automated, the issues occur when lines are inappropriately connected, or vertices are not joined at all. As mentioned earlier, incorrect normals can cause some surfaces to become inverted. One common problem resulting from the meshing process are overlapping or crossing faces, where the vertices are erroneously connected. The result is a surface with faces that twist and cross over one another. These problems are reduced by simplifying data prior to making a surface mesh (Boehler *et al.* 2002). Holes in the surface mesh occur when areas of significant curvature are incorrectly averaged during tessellation (the process of making a polygon mesh) (Leong *et al.* 1996). Non-manifold conditions can affect edges, vertices and faces when these elements share too many corresponding elements due to "round-off error" (Leong *et al* 1996: 408). For example, a non-manifold edge is one that shares more than one adjacent facet (Leong *et al* 1996). The assignment of the two facets is due to an error in the calculations for the given polygons.

Figure 2.4: Non-Manifold Face

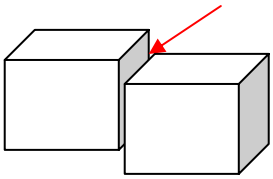

Figure 2.4: The two squares represent 3D triangulated surfaces on a single model. The arrow indicates the point at which two mutually defined surfaces share the same space, causing the non-manifold face. Adapted from Leong *et al* (1996): 409.

Errors such as those mentioned above must be corrected prior to printing, however this is often a very difficult and time consuming task (Leong *et al.* 1996). Software packages such as RapidForm™, Polyworks™ and Geomagic™ are designed to automate the triangulation and geometric repair operations prior to printing. Often errors in the geometric structure of a model are not apparent from the computer screen. Rapid prototyping units require sound geometry for acceptable print jobs. The RP software reslices the virtual object into 2D cross sections and the printing process uses unidirectional lines to generate the 2D cross section (Leong *et al.* 1996). Problems with the geometry result in poorly defined boundaries for the printing lines causing run away features in the build chamber (Leong *et al.* 1996). Run away features are unintentionally printed artifacts caused by problem geometry in the model (Figure 2.5). It is therefore important to correct any problems prior to printing the model.

Figure 2.5: Runaway Feature

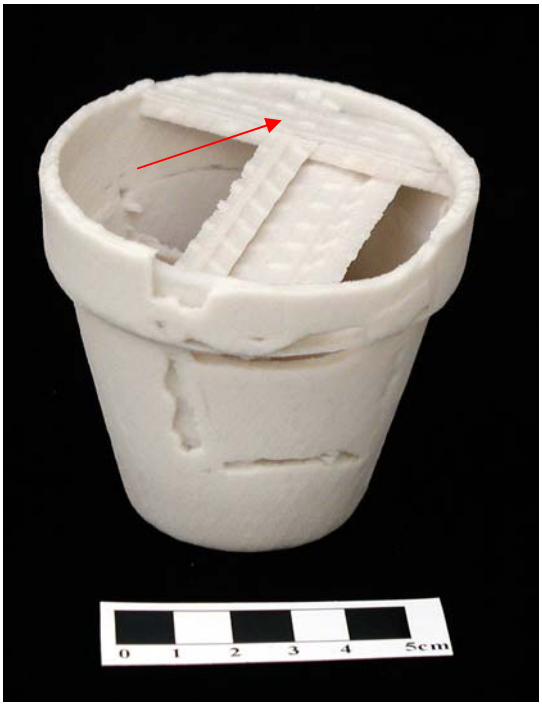

Figure 2.5: Model of a flowerpot, the arrow indicates the runaway feature printed at the top of the pot.

Since STL files contain a great deal of information to describe a relatively simple element such as a surface, they do not contain a "rich" amount of information relative to file size (Kia *et al.* 1997a: 566). In contrast, NURBS surfaces are defined whole surfaces using line equations making them less susceptible to geometric problems and more file size efficient. The NURBS surface is limited to defining smooth surfaces, which makes the line equation approach inappropriate for representing complex biological surfaces. Biological surfaces are often complex and the irregular details are usually of significance to biological researchers. Thus, STLs are still the best choice for printing biological structures.

There are a plethora of 3D file types available today. RP systems primarily utilize the STL file format, however this format is not capable of representing colour. New RP systems such as the Z-Corp 3D printers are capable of printing colour. Typically, a VRML (Virtual Reality Modeling Language) file is used in place of the STL when colour is required. The VRML file used for RP is a polygonal file similar to the STL that can encode various types of multimedia information. For example, VRML files can accommodate colour information within a standard polygon model in the form a regular image file such as a bitmap (BMP). The VRML is still limited by the same problems associated with STL files, but also carries the same advantage of representing complex surfaces.

From the above review of the work on imaging and RP some general trends can be identified. First, RP is likely the most appropriate manufacturing technology to be used to recreate biological objects from digital data. In order for researchers in anthropology to effectively use fabrication technology to create physical replicas of virtual 3D objects, the approach must be easy to use, cost effective and able to reproduce both internal and external structures with accuracy at least relative to data acquisition error. Finally, data acquisition and data processing errors are the most limiting factors in creating 3D models both virtually and physically.

The Role of 3D Printing in Biological Anthropology

Since most uses of RP are limited to case study reports, there is no definitive guide for researchers looking to integrate this technology into existing projects. This is partly due to barriers such as cost and cross-disciplinary communication. A more comprehensive understanding of how RP can be used in biological anthropology is required for this technology to be used in regular research projects. In order for RP to be used more frequently than the odd case study, a more thorough understanding of the role of RP in biological anthropology is also required.

Objectives

The purpose of this work is to explore the role of 3D printing (3DP) in biological anthropology. Understanding how this technology can be used to enhance our understanding of biological anthropology requires first understanding three basic methodological considerations: the types of data acquisition that can be used to create printable virtual models, how the original object, virtual model and printed model compare within the scope of the research project, and how the resulting printed model can enhance our understanding or facilitate the dissemination of research in biological anthropology. Two case studies will be used to identify these basic methodological issues and provide a forum for the larger discussion of the role of 3DP in biological anthropology. These two cases are chosen as a starting point for looking at the potential for the more common use of 3DP.

The first case study will examine the use of 3DP in reconstruction projects using a flowerpot. The choice of a flowerpot is intended to evaluate the basic principals of reconstruction using a simplified object, prior to venturing into more complicated skeletal

material. The ability to successfully create a replica of the broken flowerpot will be evaluated from both the data acquisition and printing perspectives in order to understand the role of 3D printing in this area of biological anthropology.

The second case study will examine the use of 3D printing for the creation of a skeletal replica. This case study will look at the differences in model applications related to methods of data acquisition. Two methods of data acquisition will be used; laser surface scanning and CT scanning. In evaluating the role of 3D printing in biological anthropology, it is important to understand the relationship between data acquisition, processing and printing. The understanding of this relationship is what is lacking in the case study reports of the more general use of RP in biological anthropology.

Cost and accessibility are two barriers to the regular use of RP in biological anthropology to date. Ono and colleagues (2000) have suggested that 3DP has the potential to be effective for anatomical modeling and overcomes the cost barrier reported by other researchers in relation to the more widely accessible approach of SLA (Dolz *et al.* 2000, Hieu *et al.* 2005, Hjalgrim *et al.* 1995, Powers *et al.* 1998). In consideration of this, 3DP was selected as the primary method for both case studies. A project of this scale would have been prohibitively costly using the more commonly used SLA approach.

3D Printing Methods

Z-Corp is the company licensed to manufacture and distribute '3D printers' based on the binder-jet technology developed at the Massachusetts Institute of Technology (MIT). As of December 2005, they market three machines. The Z-310 is a small, economical 3D printer capable of only printing in monochrome. The Z-510 (successor to

the Z-406) is a medium sized unit capable of colour and monochrome printing and the Z-810 is a large format printer also having colour and monochrome capabilities. All of these machines can use either plaster or starch-based materials for the building medium.

The virtual models were printed using a Z-Corp, Z-406 3D printer. Plaster-based material and binder solution was used to recreate the 3D objects. A layer of plaster is first spread onto the build chamber floor. A layer of binding solution is sprayed onto the powder surface in the shape of a 2D cross-sectional slice of the original object. This process is repeated until a 3D object is produced within the build chamber. The maximum build volume for the Z-406 is 203x254x203 millimeters (8x10x8 inches). Figure 2.6 illustrates the building process from 2D cross-section to partially excavated object.

Figure 2.6: Z-406 Build Chamber

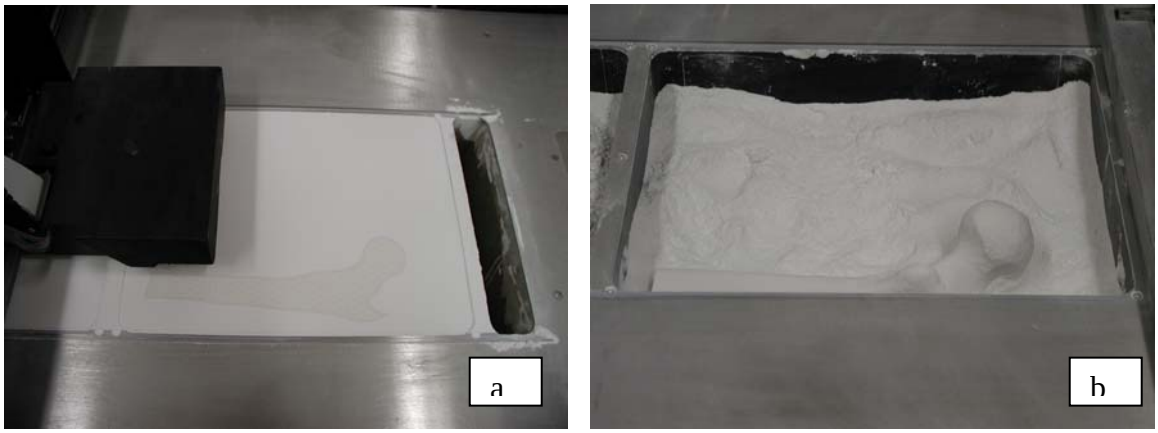

Figure 2.6: Image “a” illustrates the build chamber of the Z-406 during the printing process. A 2D cross-section of the object is printed by depositing a layer of binding solution onto a bed of plaster. Image “b” represents the printed model partially excavated from the build chamber.

Excess powder is cleaned from the model with a conventional brush followed by an airbrush. This research used the zp102/zb56 plaster and binder combination with

corresponding colour binder (donated by Z-Corp). The layer thickness can be custom set using the Z-Print software (0.076mm to 0.254mm); the default setting of 0.2 millimetres was used for this project. Z-Print software version 6.3.28 provided the interface between computer and printer. The models were all infiltrated using a paraffin wax bath to seal and stabilize the plaster models.

Case Studies

Each case study has been organized as a stand-alone chapter. Both case studies use the same 3DP methods described above, but each has a distinct data acquisition and processing methodology. Chapter III will present the first case study on reconstruction. Chapter IV will present the case study on creating the skeletal replica. A discussion of the technical issues of each study is found at the conclusion of both chapters. Chapter V is a more conceptually oriented discussion of the overall role of 3DP in biological anthropology. The discussion chapter synthesizes the overall lessons that can be learned from considering both studies as a representation of the types of applications for 3DP in biological anthropology.

Chapter III: Case Study 1: Virtual Reconstruction

Reconstruction of recovered bone and associated material is an important aspect of some projects in biological anthropology. Reconstructions of fragmented materials allow researchers to assemble the broken pieces of the past to gain a more coherent understanding of form and structure. In biological anthropology reconstructions of the skeleton from ancient peoples can add to the understanding of evolution through morphometric analysis. In a medical-legal context reconstructions of fragmented remains can assist forensic investigations. One of the most significant limitations of such endeavours is the physical manipulation of the remains. Such manipulation can lead to the permanent destruction of unique and precious material. Virtual reconstruction is emerging as a potential tool to overcome the problems associated with the physical manipulation of remains. Virtual reconstruction uses three-dimensional digital technology to capture the form of objects allowing manipulation and study in a three-dimensional computer generated environment. 3D printing offers the potential to move the next step forward and reproduce the virtually reconstructed objects to reflect some aspect of the reconstruction process or model the original object. Zollikofer and Ponce de Leon (2005) term this “real virtuality”, whereby virtual representations are converted back into the form of the original.

Objectives

3D printing technology has the potential to extend the role of virtual reconstructions by offering rapid, low-cost concept modeling and colour layering for enhanced analysis. In order for this technology to be a valuable analytical tool, several conditions must be met. First, there needs to be an effective method of reconstruction that can produce the necessary models for the 3D printing device and the printed objects must be an accurate representation of the original object. Accuracy for this case study is the ability to match the physical dimensions and overall surface topology of the original object within the accuracy limit of the scanning device (1 mm). Finally, the printed model must offer some advantage for the study or dissemination of the results from the original material. This study will also evaluate and identify the methodology for using 3D surface scanning to generate the virtual models. A simple flowerpot is used as a starting point for testing. If a successful reconstruction method can be identified that satisfies the accuracy and usefulness conditions, the concept will be valid and eligible for further study using more complex material (for example, skeletal elements).

Methods

Using laser surface scanning a virtual model of a ceramic flowerpot (Figure 3.1) was created and printed.

Figure 3.1 Original Flowerpot

Figure 3.1: From left to right; side , bottom and top views of original flowerpot.

Following the successful creation of a virtual model, the pot was then broken and reconstructed using surface scan data of the broken pieces. The resulting reconstructed virtual model was compared to the original virtual model for similarity and printed.

Surface Scanning:

A Polhemus Fastscan™ handheld laser scanner was used for surface scanning. This scanner uses a laser, camera and motion-tracking system to record a 3D point set of the original object surface. The laser and range-finding (charge-coupled device or CCD) camera are contained in a portable handheld wand. A fan of laser light is emitted from the wand as the user scans the object's surface using a motion similar to spray painting. The range finding optics calculate the distance from the object to the scanner and record the position as a point in 3-space. The motion tracking system establishes these points relative to a single datum identified as the transmitter 0,0,0. The motion tracking for the Fastscan™ is based on the Fastrak® system marketed by Polhemus. The Fastrak® system tracks the position of a receiver (in the wand) in relation to the transmitter (0,0,0) through a low frequency magnetic field generated by the transmitter. The result is the

ability to scan objects with accurate six degrees of freedom (X,Y,Z, Azimuth, Elevation and Roll). Figure 3.2 illustrates the principals of the Fastscan™ system.

Figure 3.2 Scanning Diagram

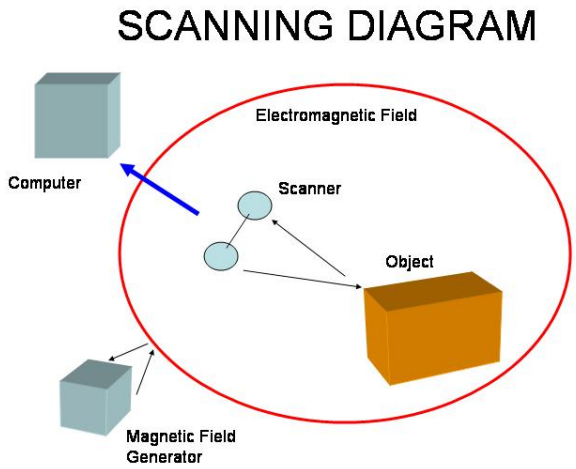

Figure 3.2: The scanner operates within the electromagnetic field and the useful range of the scanner is contained within this area (marketed by red circle). The scanner is identified in relation to the object through the reflection of the laser off the object and recorded by the CCD camera contained within the handheld unit. The resulting data are then processed by a computer.

Resolution of the scanner decreases as the distance between the object and wand increases. Resolution is also affected by the scanning rate (i.e. the speed at which the user passes the wand over the object). Average resolution is 0.5mm at a distance of 200mm from the object, where line-to-line resolution is 1mm at a speed of 50mm per second (pers. comm. Dan Ratta, Polhemus). Since the motion tracking system is based on a field generated from the transmitter, accuracy depends on wand-object range in relation to the transmitter. Accuracy for the Fastscan™ is therefore 1mm at a distance of 200mm (pers. comm. Dan Ratta Polhemus). The limitations of the scanner's resolution are important to consider in the context of the printed object. If the smallest feature that the printer can produce is 0.76 mm (Grimm 2004), then the printer is capable of printing a finer object

than can be imaged using the Polhemus scanner. In this case the limitation on the reproducible amount of detail is with the method of data acquisition.

The pot was scanned upside-down on a black felt cloth. Felt absorbs all the light from the laser, eliminating the capture of background surfaces. It was not possible to accurately scan the inside surface of the pot. The angle of the camera and laser was too wide to capture the detail within the narrow opening of the pot (Figure 3.3).

Figure 3.3: Camera and Laser Angle for Optimum Scanning

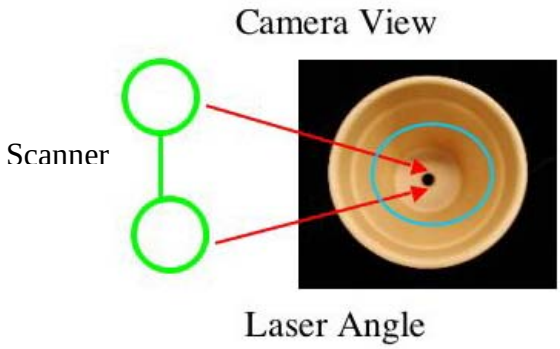

Figure 3.3: Red arrows indicate the triangulation pattern between the camera's line of sight and the light emitted from the laser. The blue circle shows the scanning area possible. Note that the circle is offset, meaning that the scanned area within the pot could be manipulated by changing the angle of the handheld device.

Rather than capturing only some of the surface data inside the pot and filling holes, the outside was scanned and the inside surface was approximated from this data during model post-processing. The scan was exported from the Fastscan™ as an STL file. Post-processing involved two different methods. Each method has advantages and disadvantages. Analyzing these results will provide a better understanding of the most appropriate post-processing methodology for virtual modeling and for 3D printing.

Virtual Modeling of Unbroken Flowerpot

The virtual modeling of the unbroken flowerpot examined two different post-processing methods. Procedure one involved first filling holes using the automatic function in the RapidForm™ software. The hole filling resulted in irregular surfaces, corrected by using the smoothing function. The inside surface of the pot was estimated by giving the shell (surface model) a surface thickness of 3mm using the "volume" function in RapidForm™. Once the model was visually acceptable, an automated cleaning function was executed to find and repair problems in the geometry that were not visually apparent (crossing faces, unstable faces, non-manifold faces and vertices with redundant faces). This automated algorithm for cleaning the problem geometry was not able to remove all the errors in the model, although it did result in a printable model. It actually increased the number of non-manifold faces from 1554 to 1766, redundant vertices from 744 to 870 and crossing faces from 166 to 398; but decreased the number of unstable faces from 1395 to 0. Figure 3.4 below shows the result of post-processing method one.

Figure 3.4: Final Virtual Model of Unbroken Flowerpot

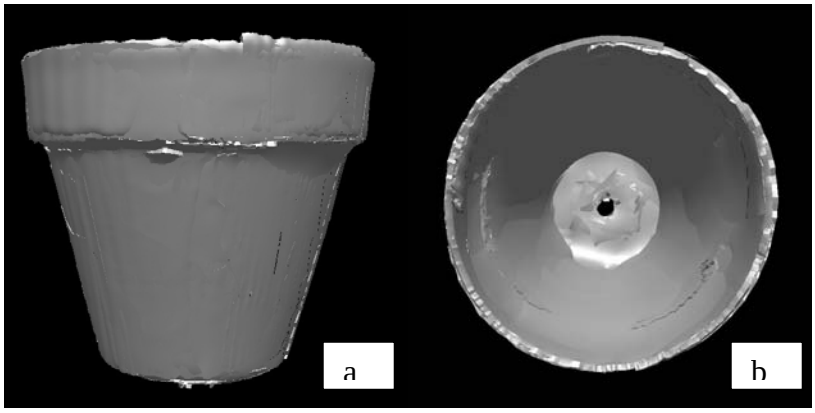

Figure 3.4: Item "a" is a side-view screenshot of the unbroken virtual model using post-processing method one. Item "b" is the inside-view of the same model.

The second post-processing method developed initially for the skeletal reproduction was able to correct all the problem geometry (based also on the procedures outlined in the RapidForm™ user manual). The process requires exporting the point data (x, y, z) of a completed shell prior to giving it the 3millimeter interior surface. This removes the polygon mesh and returns the data to its most basic form (data points without mesh). The data is then imported and copied; the copy is reduced until an accurate hole free shell can be triangulated using the automated triangulation algorithm in RapidForm™. The new shell is fit to the more detailed point-cloud several times. Once the desired amount of detail was obtained, the shell was exported as an STL model and printed using the Z-406. Figure 3.5 below shows the result of post-processing method two. While this method of post-processing created a geometrically sound model, it was not as effective at capturing the shape of the original flowerpot. The most significant example of this is the absence of the drain hole at the bottom of the pot, which appears in

the virtual model using processing method one (Figure 3.4), but not the new procedure (Figure 3.5).

Figure 3.5: Unbroken Flowerpot Post-processing Method 2

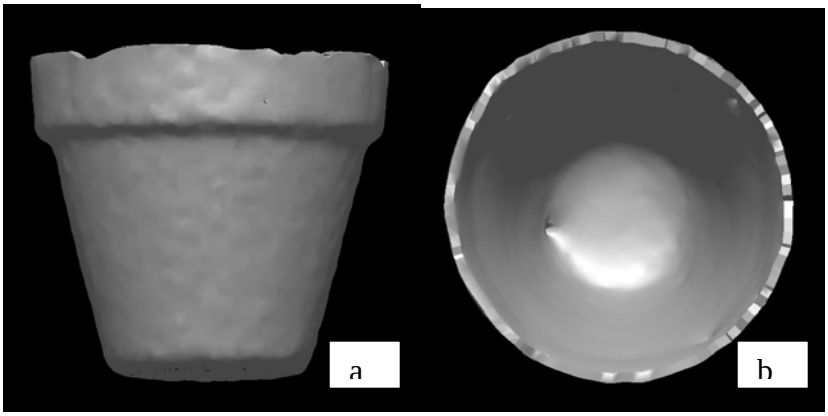

Figure 3.5: Item “a” is a side-view screenshot of the unbroken virtual model using post-processing method two. Item “b” is the inside-view of the same model.

Virtual Reconstruction of Broken Flowerpot

Following the successful virtual modeling of the original unbroken flowerpot, the pot was broken into 5 principal pieces (Figure 3.6).

Figure 3.6 Broken Flowerpot

Figure 3.6: Five broken pieces of the flowerpot. The red circle highlights debris that was too small to be effectively scanned.

The five pieces were individually scanned using the Polhemus laser scanner. All the pieces were scanned on the black felt with the outer surface facing upwards. Each shard was exported directly from the Fastscan™ software in STL format. RapidForm™ was used to put the pieces back into the shape of the original flowerpot.

Figure 3.7: Shard Models

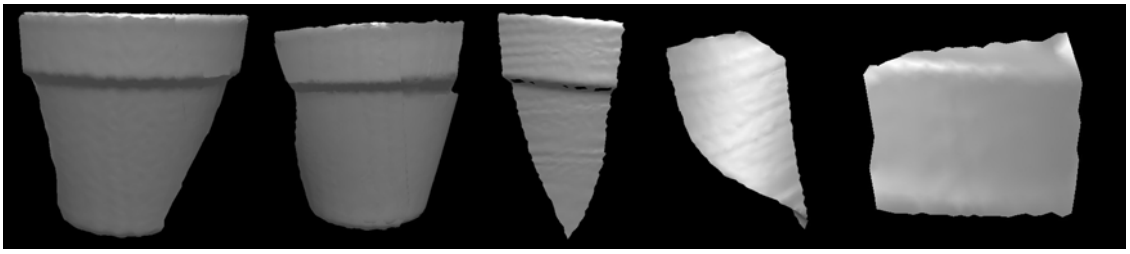

Figure 3.7: Single-sided virtual models of the individual shards organized from smallest to largest (left to right) and magnified for clearer view.

Two approaches to the reconstruction of the flowerpot were evaluated. In order to maintain continuity between the modeling of the unbroken and modeling of the broken pot, only the outside surface was scanned. The inner surface was approximated by thickening the shell by three millimetres as per the making of the unbroken virtual model.

Figure 3.8: Thin Shard to Thick Shard

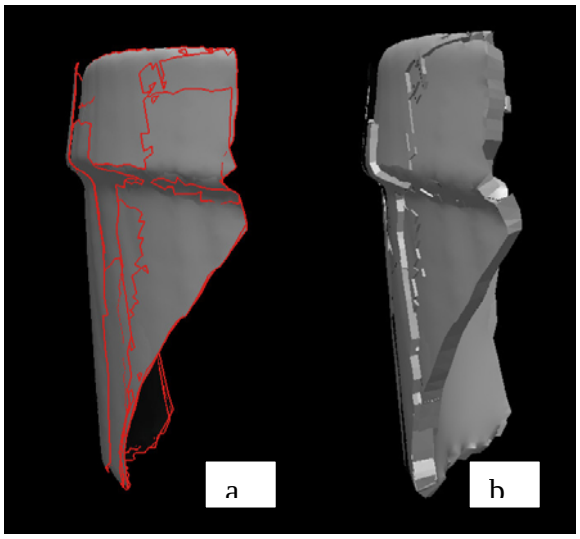

Figure 3.8: Example of shard prior to thickening (a) and after thickening (b). Note the red lines in "a" represent the edges of overlapping scans, an artifact of the scanning process.

The first approach to the reconstruction joined the shards after they were thickened. Adding the other side to the shards increased the amount of irregularity in the attachment surfaces, which made accurate matching very difficult (note the raised edges of 3.8-b). Several large gaps were also present between some of the matched pieces (see Figure 3.9). The hole-filling algorithm in RapidForm™ was not able to fill these gaps. The hole-filling tool is intended to repair gaps defined by boundaries. Boundaries are mathematically defined edges of the polygon shell (red lines depicted in Figure 3.8-a). Since the individual pieces were solid-volumes and the boundaries only defined the edges of the surface model, the software recognized the holes on the surface and not the gaps between the shards. A rough model was created using this method of reconstruction (Figure 3.9).

Figure 3.9: Reconstruction Using Volume Shards

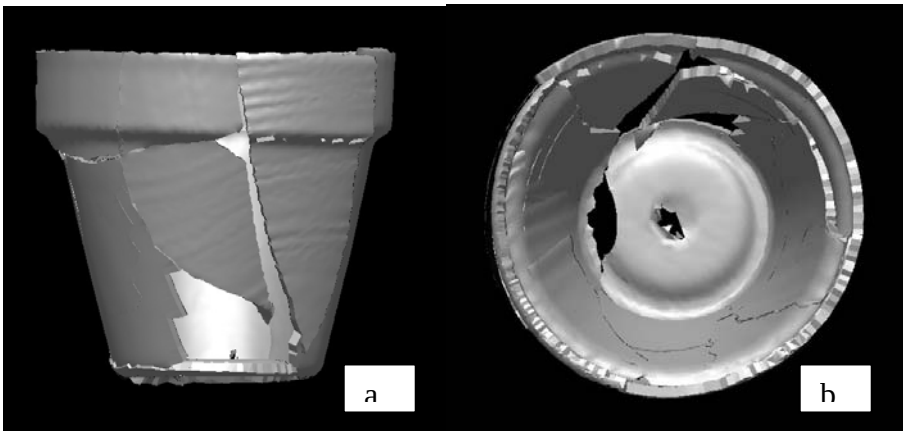

Figure 3.9: Side-view (a) and top view (b) of reconstructed pot using method one.

The second method combined the pieces as single-sided shells and added the inside surface of the model once the pieces were registered together. The second reconstruction method based on the "thin wall registration" function in RapidForm™ was used to produce the most successful reconstructed virtual model. The pieces were fit together prior to making them into volume entities. This function required selecting three points on one shard and another three corresponding points on the adjoining shard as seen in Figure 3.10.

Figure 3.10: Thin-wall Registration

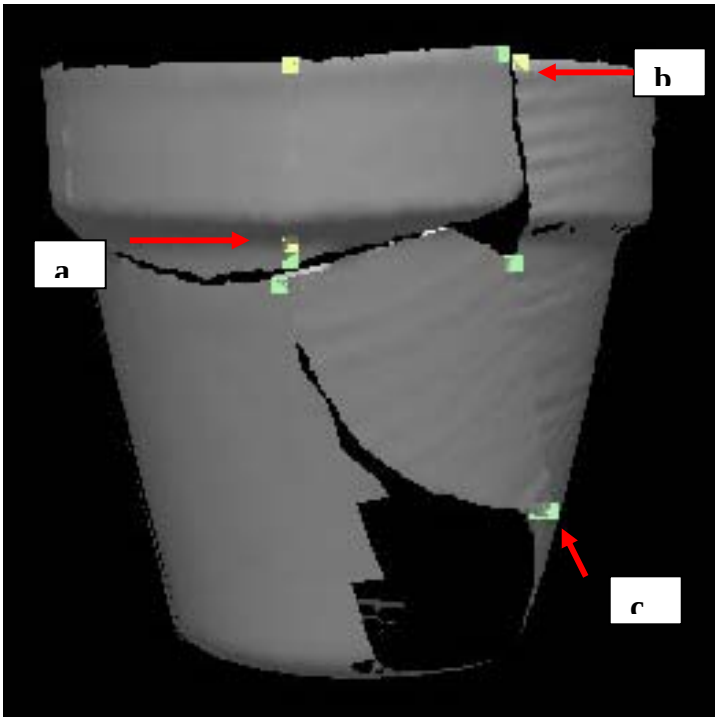

Figure 3.10: Points (yellow) are selected along the edge of one shard model. Analogous points (green) are selected along the corresponding edge of the other shard model. The two sets of points represented by “a” and “b” illustrate successful matching of the two edges. This results in the association of the shard models.

This process uses similarities in the edge shape of the two pieces being combined, this also means that some overlapping geometry is used and may affect dimensional accuracy of this model (note point “c” in Figure 3.10). After each shard was matched, it was added to the total model entity by combining the matched pieces into one shell. The adding of pieces was repeated from largest to smallest until all the shards were integrated into a single shell resulting in a virtual model.

Some of the pieces from the breaking process were too small to scan. As a result, several significant holes remained in the reconstructed model. The holes and other irregularities were corrected by using the RapidForm™ hole-filling tool prior to making

the shell a volume. Since the shell is represented as a single surface, the edges are defined by boundaries. The boundaries therefore defined the holes on the surface of the shell and were filled. Unlike the earlier volume model, in this case, the model consisted of only the outer surface. Following the hole-filling procedure, extensive smoothing was required. Automatic filling of the largest hole resulted in a major deformity from the surface, which was necessary but difficult to correct. The top of the pot was also very irregular and required cropping and smoothing. Figure 3.11 illustrates the before and after result of smoothing and cropping the model.

Figure 3.11: After Hole Filling and Smoothing

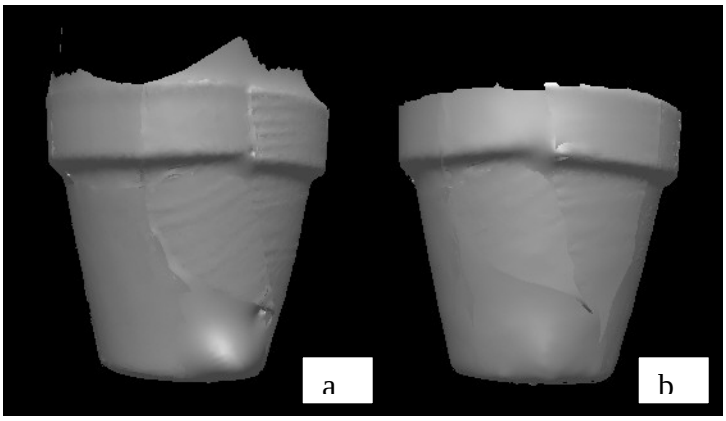

Figure 3.11: Image “a” depicts the pot with bulging deformity on the bottom and extended brim. Image “c” shows the result of the smoothing and cropping process.

After the above-mentioned processing was completed, the model was then thickened by 3 mm to approximate the inner surface. This resulted in the final model that was exported to he printer as an STL file (Figure 3.12).

Figure 3.12: Final Virtual Model Using Reconstruction Method Two

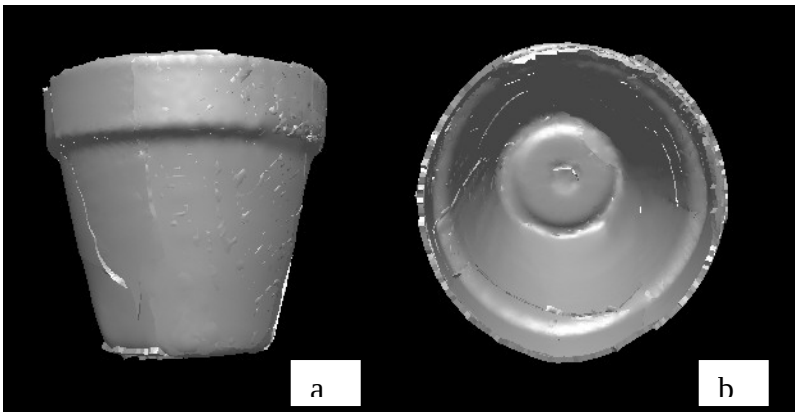

Figure 3.12: Side-view (a) and top-view (b) of virtual flowerpot model based on reconstruction method two.

A third model was also created, which synthesized method two with post-processing method two used for the unbroken pot (simplification, detailing and cleaning). This last model was created in order to overcome problems with the geometry of the reconstructed pot models. The process of combining models together to make a single entity causes the development of many crossing faces, redundant faces and inappropriate boundaries. The result of using post-processing method two produced a smoother more refined surface finish for both the unbroken (a) and reconstructed (b) pots, as seen in Figure 3.13.

Figure 3.13: Virtual Models of Unbroken and Reconstructed Flowerpots

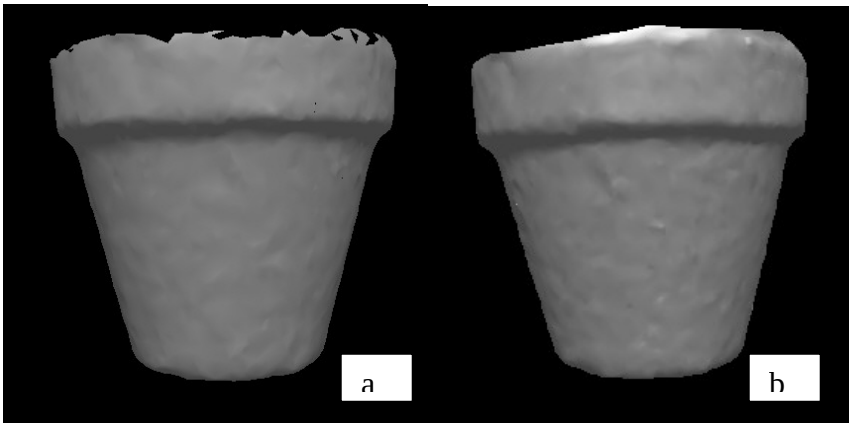

Figure 3.13: Side-views of both the unbroken virtual model (a) and the model created using reconstruction method two (b), using post-processing method two.

Once the virtual models were ready, they were imported into the Z-Print software that interfaces with the Z-406 printer. The first models were printed at 70 percent of their original size to reduce overall material cost. The model from reconstruction method one was not printed due to the poor quality of the virtual model. The following figures (3.14 to 3.18) depict the results of the printed models by each method.

Figure 3.14: Unbroken Model Using Post-Processing Method One

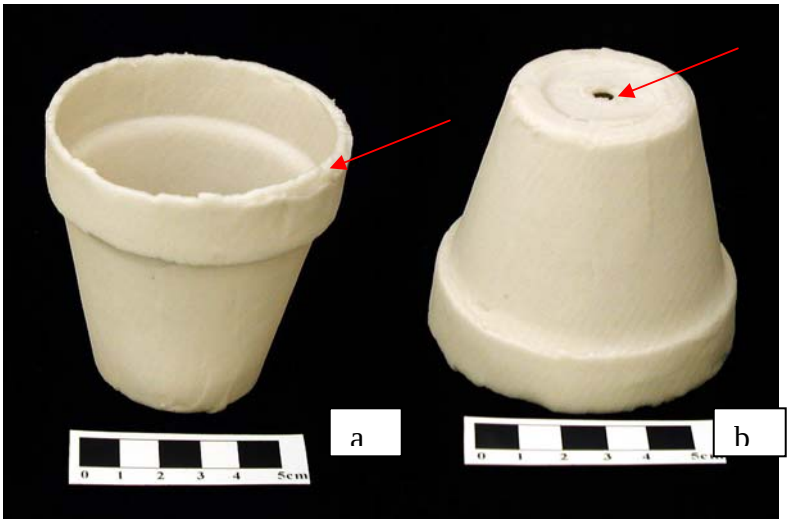

Figure 3.14: Images “a” and “b” show top facing side-view and bottom facing side view respectively. Red arrows mark imperfections in the rim of the pot and the detail of the drain hole.

Figure 3.15: Unbroken Model Using Post-Processing Method Two

Figure 3.15: Image “a” illustrates the top facing side view and image “b” shows the bottom facing side view. Note the red arrow marks the absence of the drain hole detail in this model, but the surface is smoother.

Figure 3.16: Reconstructed Model Using Method Two

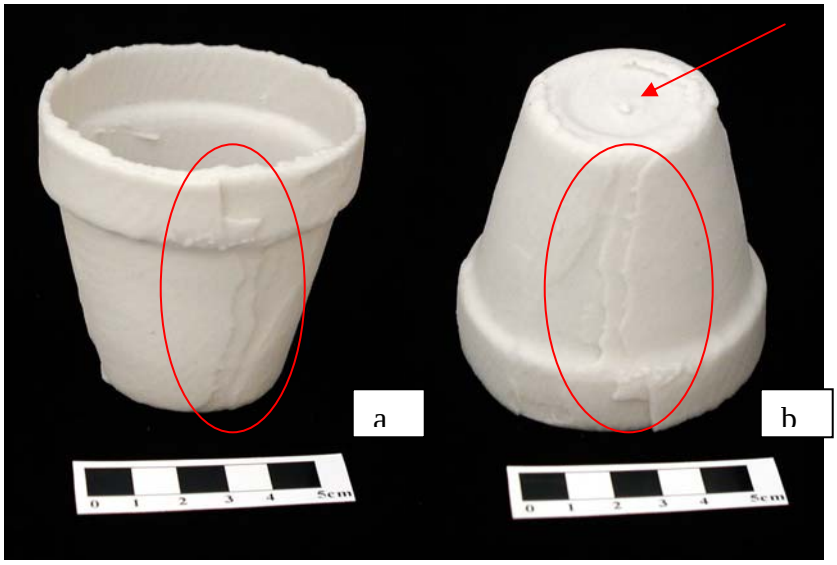

Figure 3.16: Images “a” and “b” depict the top facing and bottom facing side views respectively. Areas of surface imperfection are circled in red. The arrow points out the absence of the drain hole detail.

Figure 3.17: Reconstructed Model Three (Combined Methods)

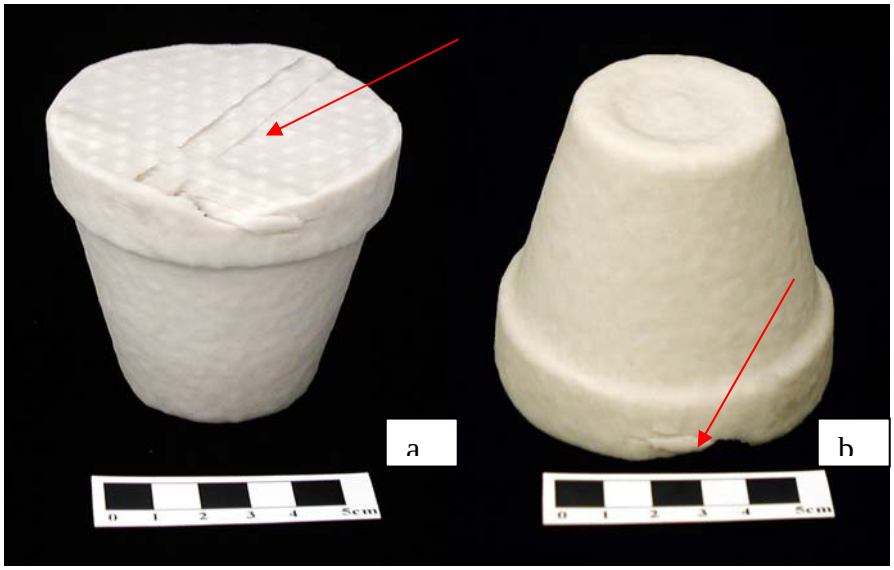

Figure 3.17: Images “a” and “b” depict the top facing and bottom facing side views respectively. The red arrow in image “a” highlights the thin plate that formed inside the top of the pot. The arrow in image “b” illustrates a geometry imperfection (crossing face) likely related to formation of the unwanted structure in image “a”.

Results

The intention of this work is to move beyond testing just the linear accuracy of the printer. Therefore, the following analysis examines the dimensional and topographical accuracy of the overall process from original to printed object. It is however, necessary to establish a base-line understanding of where to expect the greatest amount of dimensional error in the overall process. In order to do this, a 1:1 scale model of the unbroken flowerpot (using post-processing method two) was printed and compared to the original and virtual models from each of the processing and reconstruction methods. Height was measured from the base of the pot to the top of the rim, parallel to the side . Maximum external width was measured from the top rim of the pot. The virtual models were all measured in RapidForm™. The results of these measurements are summarized in Table 3.1.

Table 3.1: Original and Printed Pot Comparison

	Pot Version					
Measurement	Original	Virtual Unbroken Method One	Virtual Reconstruction Method One	Virtual Unbroken Method Two	Virtual Reconstruction Method Two	Printed Unbroken
Height (cm)	9.75	10.00	10.12	10.00	10.00	10.50
Width (cm)	14.50	11.01	10.07	11.14	11.34	11.20

The above measurements provide a quick overview of where the largest challenge exists for recreating a dimensionally accurate model. Height is the most accurate distance between all the models, with the printed model showing the greatest difference (+0.75 cm). Some of this difference is seen in the move from the original to the virtual model by an inflation of 0.25 cm (held by three of the four virtual models). The remaining 0.5cm difference appears to be the result of accuracy between the virtual

model and printing process. The pot was printed upside down in the build chamber to prevent excess pressure from the loose plaster within the walls of the pot, when being excavated. This also means that the dimension of height corresponds to the z-axis during the printing process. The z-axis has the most significant amount of error during the printing process due to the layering of the cross-sections in 0.2-millimeter thicknesses. If the pot were printed with a different orientation inside the build chamber, the height dimension would likely be affected.

The greatest amount of overall difference is seen in the width measurements, with the majority of the discrepancy being between the original and virtual models. The difference between the original and four virtual models is around three centimetres. The difference in width between the original and the virtual model that the printed version is based on is 3.16 cm. In contrast, and with the exception of virtual reconstruction method one, the virtual models are all within a few millimetres in width. The difference in width between the virtual and printed model is 0.14 cm (or 14 mm). This clearly illustrates that the problems in the width dimension originate in the virtual modeling process and not the printing process. This is consistent with what is expected of the printer given that the width of the printed pot is determined on the x and y axes, which are known to be the most accurate.

This simple and relatively quick assessment of dimensional accuracy in the modeling process from original to printed model has pointed out two important issues. First, the orientation of the printed object within the build chamber is a significant determinant of dimensional accuracy. Every effort should be made to limit the amount of printing on the z-axis. Secondly, a greater amount of error is seen between the original

pot than amongst the virtual models. This confirms an earlier assumption that the method of data acquisition (in this case laser scanning) contributes the most to accuracy problems. This may be due to the actual limitations of the scanner, but is also likely due to the extent of post-processing required to generate a 3D model from point data. The accuracy of the scanner is based on the ability to record individual coordinate data from the surface of the object in the form of a point-cloud. The virtual model results from a complicated algorithm and editing process to generate a meshed surface from this coordinate data.

An analysis of the overall surface shape differences between the complete and reconstructed virtual pots was performed using RapidForm™. This process involved first registering the two virtual models to a common set of coordinates and datum. This allows the software to measure the distance between the models by each coordinate (x,y and z) in relation to the common datum point. The results of this analysis can be displayed graphically with colour coding to illustrate areas of difference, or by exporting the actual displacement values to a spreadsheet program for further analysis. This inspection process was tested for validity by performing the inspection on the same model. The result was a deviation value of zero, suggesting that real differences can be observed using this method.

Only the unbroken and reconstructed virtual models that were post-processed using method two could be registered using the RapidForm™ inspection process. The other models had far too many geometry problems to be accurately registered. Twisted geometry is a particular problem as registration is only effective if all the vertices are

oriented to the same plane of reference. Table 3.2 summarizes the displacement of common vertices between these models based on 11,328 coordinates.

Table 3.2: Unbroken and Reconstructed Differences (mm)

	Variable			
	X	Y	Z	Total
MEAN	0.02	0.00	0.05	-0.19
ST. DEV.	0.31	0.30	0.23	0.45
MIN.	-1.34	-1.96	-3.55	-1.93
MAX.	2.61	1.52	1.27	3.64

Coordinates on the X-plane show the greatest amount of difference and variation. The total variation for all points ranges between -1.9mm and +3.6mm. The range of variation can be limited to a specific set of values with a colour map displaying the variation over the 3D shape of the object. Figure 3.18 and 3.19 show the deviation of the reconstruction as compared to the unbroken virtual model between the values of –1 and +1 millimetres.

Figure 3.18: Side View of Flowerpot Inspection Results

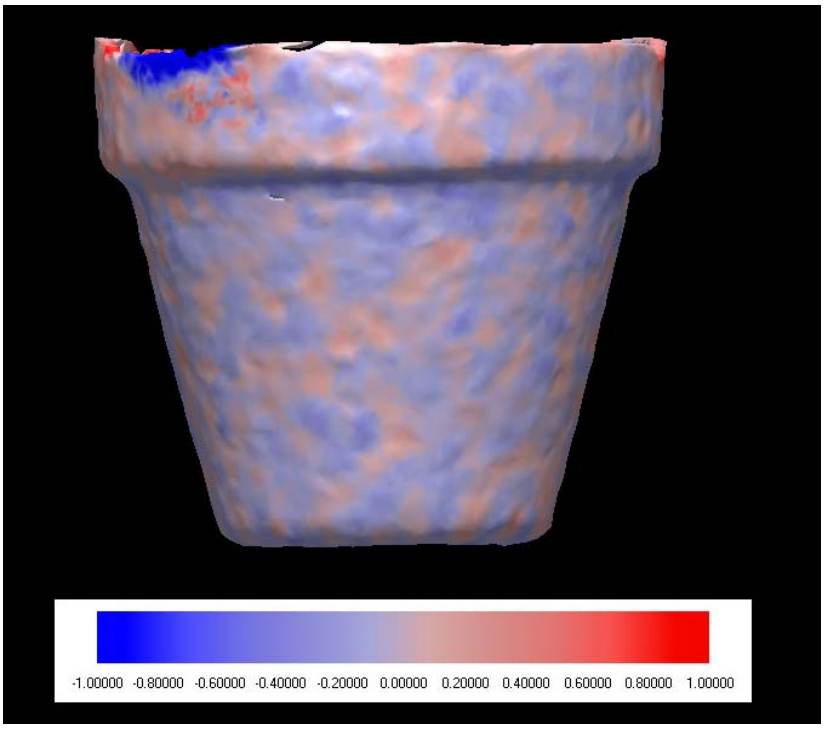

Figure 3.18: This image represents a colour-coded model of the deviation in coordinate values between the unbroken and reconstructed models. The values are expressed as a relationship between the deviation of the reconstruction from the unbroken model. The blue represents negative values to a limit of –1-mm (see scale) and positive values to a limit of +1-mm (see scale). The dominance of the blue colour indicates that the reconstruction is primarily smaller than the unbroken model.

Figure 3.19: Top/Inside View of Flowerpot Inspection Results

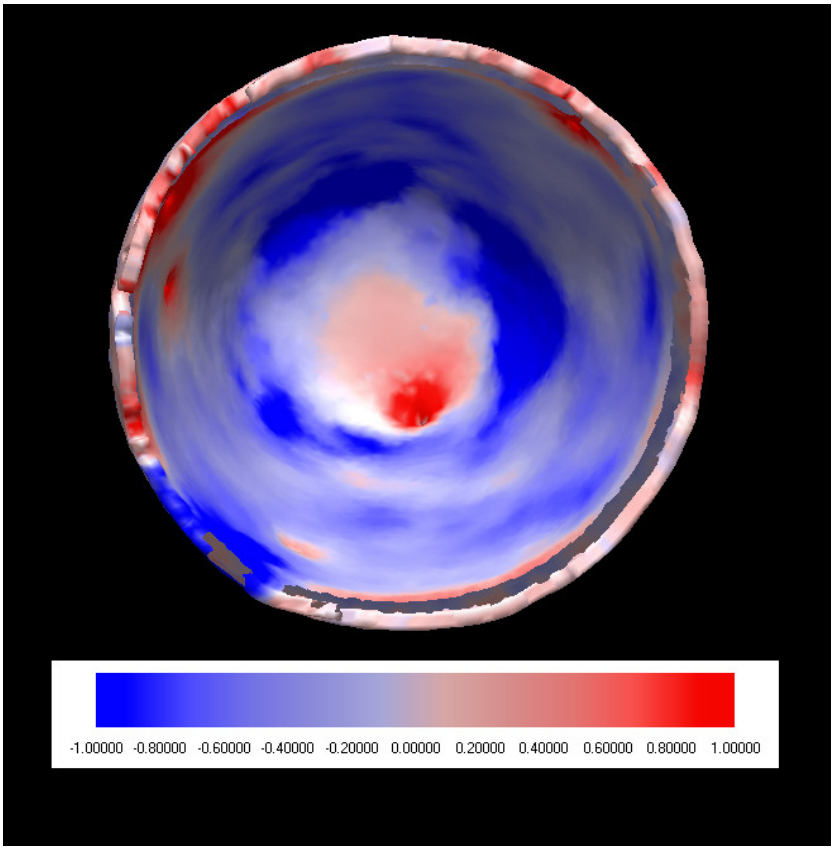

Figure 3.19: Same model and display values as Figure 3.19. This view shows the extent of variation on the inside surface. From this image it is possible to understand the variation in the topology between the models. The rim is particularly variable, differing by both positive and negative values. As well, there seems to be several localized and random areas of variation. Again, the dominance of the colour blue indicates that the reconstruction is smaller than the unbroken model.

Larger values failed to show shape differences and displayed the model in a solid blue colour, which corresponded to an overall negative dimensional relationship between the unbroken and reconstructed models. This makes sense since Table 3.1 shows that the

unbroken virtual model in this case is smaller than the reconstructed model. Tightening the limits allows for the display of the variation in surface topology.

Discussion

The result of this inspection process indicates that despite some heavy variation around the rim of the pot, the topological difference between the models is relatively minor. Figure 3.18 shows some regular variation along the outer surface that corresponds to a pattern of surface dimpling. While somewhat uniform, this variation could disqualify the reconstruction as an accurate representation of the shape of the unbroken model in a strict sense. In this case, the purpose of the reconstruction really should dictate the decision to accept or reject the validity of the reconstruction.

It is important to frame the decision of whether or not the reconstruction of the flowerpot was successful within the context of the end goal. The issue with any reconstruction, especially of the past, is that it is difficult to know how exact the reconstruction is to the original. If a general likeness in size and shape is the only requirement, then the above reconstruction was successful. If more detail is required to understand changes in shape of the surface (as would be required for evolutionary studies or forensic applications), then this reconstruction effort was not successful. A particularly problematic issue is the absence of the drain hole, which was only reproduced in the virtual model of the unbroken pot using post-processing method one. Post-processing method two yielded a geometrically sound model, but destroyed much of the individualizing elements of the original flowerpot. Also important to note is that width changed more than height between the original and virtual models (particularly the reconstructions). This means that overall shape also changed.

There is an alternative usefulness for the 3D printer to reproduce virtual reconstructions. The colour capabilities of the Z-406 allow for the communication of differences in design and reconstruction iterations, through a tangible object that can be directly compared to the original. The unbroken and reconstructed models where given opposite colours (red for the unbroken and blue for the reconstruction), and registered using the same approach as the inspection process. The models were then saved as a single model and exported to the printer for printing. The result was a printed colour model of the absolute differences between the models that could be handled and examined in association with the original or other material. Figure 3.20 illustrates the resulting model.

Figure 3.20: Colour Model of Flowerpot Differences

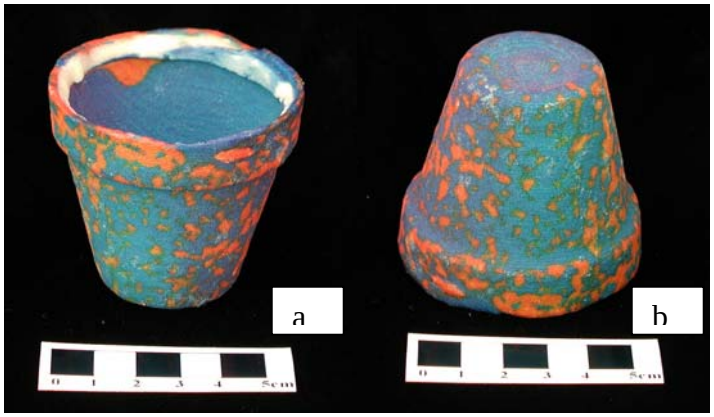

Figure 3.20: Image “a” and “b” illustrate the top facing side view and bottom facing side view of the colour differences model respectively.

The above colour model illustrates the beginning of a new level of communication possible using colour 3D printing. This type of colour modeling may also help museums disseminate the limitations of reconstructions and be used to highlight differences in

interpretations of the past, and could apply to either biological specimens or material culture.

Conclusion

The sum of the results in this section indicates some clear issues that need to be considered for the reconstruction project. First, despite the problems associated with accuracy of printing on the z-axis, there is good agreement between the virtual and printed models. The problem lies with the post-processing of the original data and the overall reconstruction approach. As seen in the elimination of the drain hole in the unbroken virtual model using post-processing method two, extensive editing erodes a great deal of the surface detail. Not processing enough introduces other quality issues relating to geometry problems that translate into surface quality issues in the final printed object. A more accurate method of reconstruction is required for future studies as well, especially those involving more complex material. It is conceivable that an acceptable reconstruction could be printed using a more accurate reconstruction method and data that requires less manipulation than the surface scan data. A possible way to mitigate these problems would be to use CT data, which may require less manipulation to create clean models. A test of this hypothesis is carried out in case study two using skeletal material.

Chapter IV: Case Study 2: Skeletal Reproduction

Objectives

The focus of this case study is to build upon and test the methodological concepts developed in Case Study One on actual skeletal material. Case study one showed that extensive post-processing of scan data is required for the creation of printable virtual models of a flowerpot (unbroken and reconstructed). This led to the conclusion that extensive post-processing of the raw data reduces the degree of analysis possible with the virtual models or printed objects. CT scanning was proposed as an alternative method of data acquisition, which may provide a solution to the limitations identified for the surface scans. This proposal is evaluated using case study two by attempting to reproduce an entire skeleton using both laser surface and CT scanning methods of data acquisition. Case study two has two components: first, an evaluation of the use of laser surface scanning and 3D printing to create a replica of an entire skeleton, and second an evaluation of the use of CT scanning as an alternative method to laser surface scanning of skeletal material. As well as illustrating the technical limitations of each data acquisition method, a procedure for developing printable models of skeletal material will be highlighted for future use by other researchers.

Each approach to data acquisition will be compared in relation to the degree of usefulness of the resulting physical models. Usefulness is contextualized through three specific applications relating to research in biological anthropology:

1. Application of the physical models for general education.
2. Application of the physical models for the dissemination of research.

3. Potential for using physical models in traditional osteological analysis.

Usefulness of the resulting models relates to the overall goal of this work, which is to discuss the role of 3D printing in biological anthropology. Part of understanding this role is knowing what methods of data acquisition should be used to accomplish the specific goals of any given project in biological anthropology.

Materials

The Mennonite Heritage Village Museum (MHV) wanted to incorporate a replica of an early Mennonite skeleton as part of a larger exhibit entitled "New Life", describing funerary practices of Mennonite settlers in Manitoba, Canada. Myra Sitchon, a doctoral student at the University of Manitoba originally proposed using laser surface scanning to make 3D virtual models of a skeleton for this exhibit (Sitchon et al 2004). The skeleton of interest to the MHV is thought to be a woman who lived during the 1800's and early 1900's from the former Schoenfeld village in southeastern Manitoba. The remains were archaeologically recovered in 1995 and have been analyzed by Dr. Deborah C. Merrett and Dr. Chris Meiklejohn at the Department of Anthropology, University of Winnipeg. This skeleton is complete but very fragile with some broken elements. In some areas, patches of cortical bone have flaked off exposing the trabecular bone underneath. Heavy soil staining is also found on most bone surfaces. Myra Sitchon introduced the idea of using a non-invasive means of reproduction, such as 3D surface scanning, to overcome the difficulties of reproducing the fragile skeleton using traditional means (such as casting, which was totally unacceptable due to the fragility of the material).

Methods

Laser Surface Scanning

The laser surface scanning was accomplished using the Polhemus Fastscan™ and took place at the University of Winnipeg, Anthropology Laboratory where the skeleton is curated. A laptop computer was used to run the Polhemus software and all the scan files were saved in STL format. In order to capture all the surfaces of each bone, a specific scanning procedure was used. Each bone was scanned multiple times: one scan covered the distal or inferior aspect, another covered the proximal or superior side. In some cases a third or fourth scan was required from an alternate perspective. The goal of this scanning procedure was to generate multiple scans that could be stitched together using the post-processing software. This also meant that all the scans of a given bone required sharing some geometry in common. This gave the software a reference point for merging, or registering the scans to make a complete model. Figure 4.1 illustrates the concept of multiple scans.

Figure 4.1: General Scanning for Bones

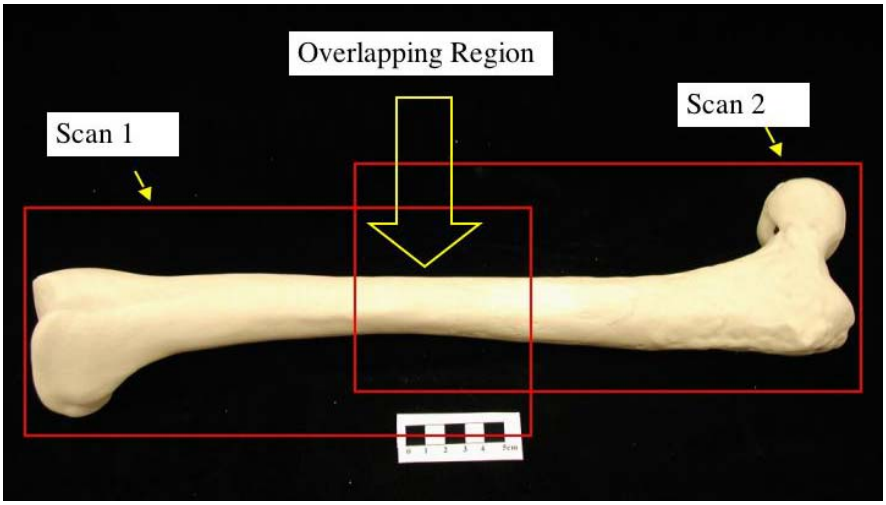

Figure 4.1: Scan one covers the distal epiphysis to the metaphysis of the long bone. Scan two covers the proximal epiphysis and metaphysis. Note the critical overlapping scan region that yields the common geometry necessary for the registration of the two scans to make a complete bone model.

A total of fifty-seven skeletal elements were surface scanned. Soil staining and erosion of the cortical bone leading to the exposure of the underlying trabeculae made scanning some items challenging or impossible. Problems associated with soil staining could be partially compensated for by adjusting laser intensity, since the darkly stained areas absorbed more light than non-stained areas. Higher intensity values were used for stained areas; the laser could then be turned down on the fly after passing over the stained areas. Several vertebrae could not be scanned due to a combination of feature size, staining and cortical bone erosion (cervical 1 through 7, thoracic 1 through 7 and lumbar 1 through 3). The three cuneiforms for both the left and right feet were also too small and too stained to yield effective scans. The ribs were significantly stained with extensive cortical erosion making their structure weak and difficult to handle. Any elements too fragile to handle were not scanned. Only 10 of the 24 ribs were preserved well enough to be handled without damage during the scanning process. The time constraint placed on the skeletal reproduction necessitated reducing the number of scans when possible, therefore only the right metatarsals and right metacarpals were scanned. The most significant limitations to successful scanning were size of the bone (too small) and fragility. Table 4.1 summarizes the scanned elements along with the number of scans and their orientation, required to complete the model.

Table 4.1: Surface Scan Summary

Element	*Number of Scans*	*Scan Orientation*
Sacrum	4	Proximal, Distal, Superior, Inferior
Mandible	2	Anterior/Superior, Posterior/Inferior
Skull	4	Proximal, Distal, Superior, Inferior
Sternum	4	Proximal, Distal, Superior, Inferior
Vertebrae T8 to T12	2	Superior, Inferior
Vertebrae L4 & L5	2	Superior, Inferior
Calcaneus (L & R)	2	Proximal, Distal
Talus (L & R)	2	Proximal, Distal
Tarsals (2)	2	Proximal, Distal
Metatarsals (5)	2	Proximal, Distal
Femur (L & R)	2	Proximal, Distal
Fibula (L & R)	2	Proximal, Distal
Patella (L & R)	2	Proximal, Distal
Tibia (L & R)	3	Proximal, Distal, Inferior Diaphysis
Pelvis (L & R)	2	Superior, Inferior
Clavicle (L & R)	2	Proximal, Distal
Metacarpals (5)	2	Proximal, Distal
Humerus (L & R)	2	Proximal, Distal
Radius (L & R)	2	Proximal, Distal
Scapula (L & R)	4	Proximal, Distal, Superior, Inferior
Ulna (L & R)	2	Proximal, Distal
Ribs (10 scanned)	3	Proximal, Distal, Shaft
Total: 57		

Image processing of the surface scan data was undertaken using the RapidForm™ software. The editing process followed a series of steps: registration, simplification, detailing and cleaning (a method suggested in the RapidForm™ user manual). This method was required to overcome the problems associated with generating models of skeletal material, which have a complex surface morphology. Surface scans collect a series of points representing the object; these points are then made into a surface mesh using an automated algorithm. Object complexity increases the chance that the algorithm

will make errors in the calculation of the surface mesh. The above-mentioned procedure overcomes this difficulty by reducing the complexity of the data prior to generating the surface mesh and then adding the detail back to the simpler surface.

In order to cover all surfaces of each bone, multiple scans were taken. The first step in processing the scan data to make a model was to register the multiple scans of each bone together. The software uses common geometry between two scans to estimate the best fit. The identification of the common geometry is user directed by selecting four points that corresponded to common areas between two scans of a single element and executing a registration function (note the overlapping scans in Figure 4.1). The registration function aligns the two scans together based on this input and combines the scans into one. The result is a model file of the entire bone. The matching requires the user to visually judge areas of similarity between the two scans. Working with meshed surfaces such as the STL files exported from the scanner makes this process a great deal easier. It is possible to use the unmeshed point cloud data, but that makes identifying areas along the surface very difficult since there is no visual reference for the surface, only a series of points. The registration process is explained graphically in Figures 4.2 and 4.3.

Figure 4.2: Registration Process Step One

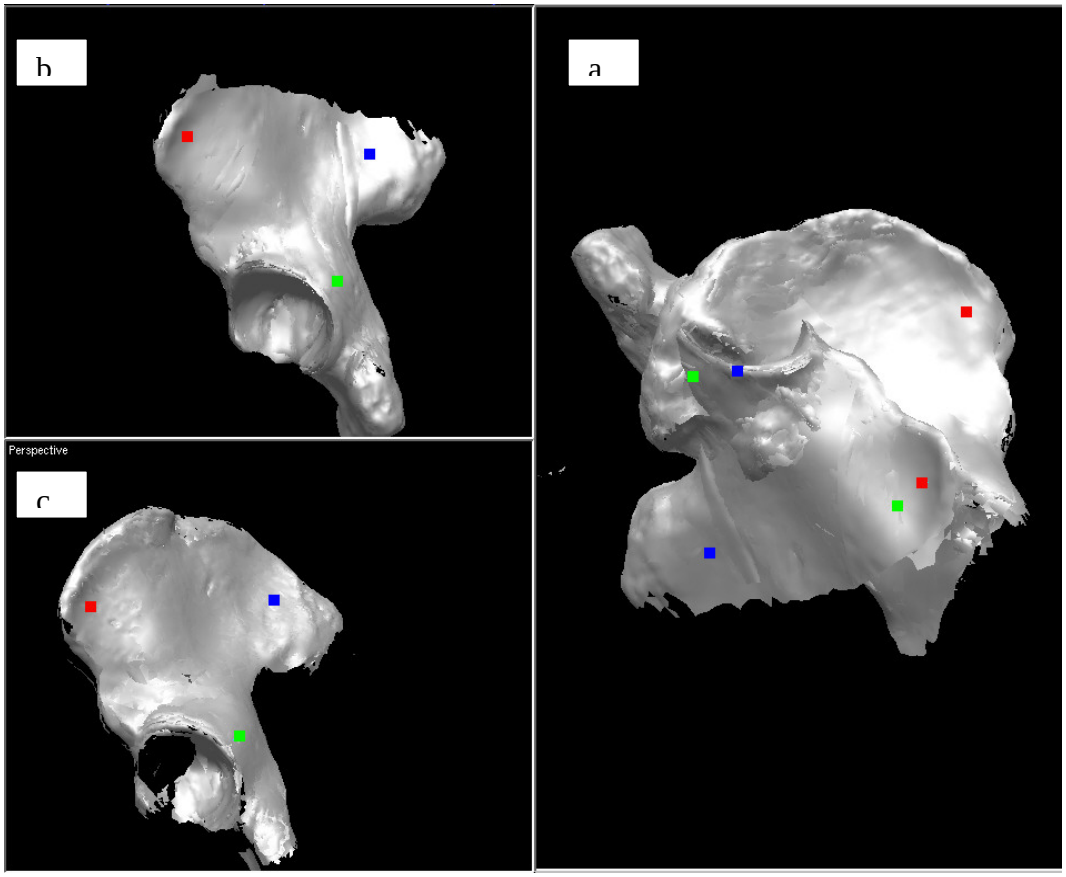

Figure 4.2: Image “a” shows the unregistered view of the inferior scan and the superior scan of the right innominateinnominate. The scans are separated into viewing windows “b” and “c”. Red, blue and green dots represent the user specified common areas of geometry. These do not need to be exact, as the software uses the curvature of the model’s surface in that area to more accurately match the scans.

Figure 4.3: Result of Registration

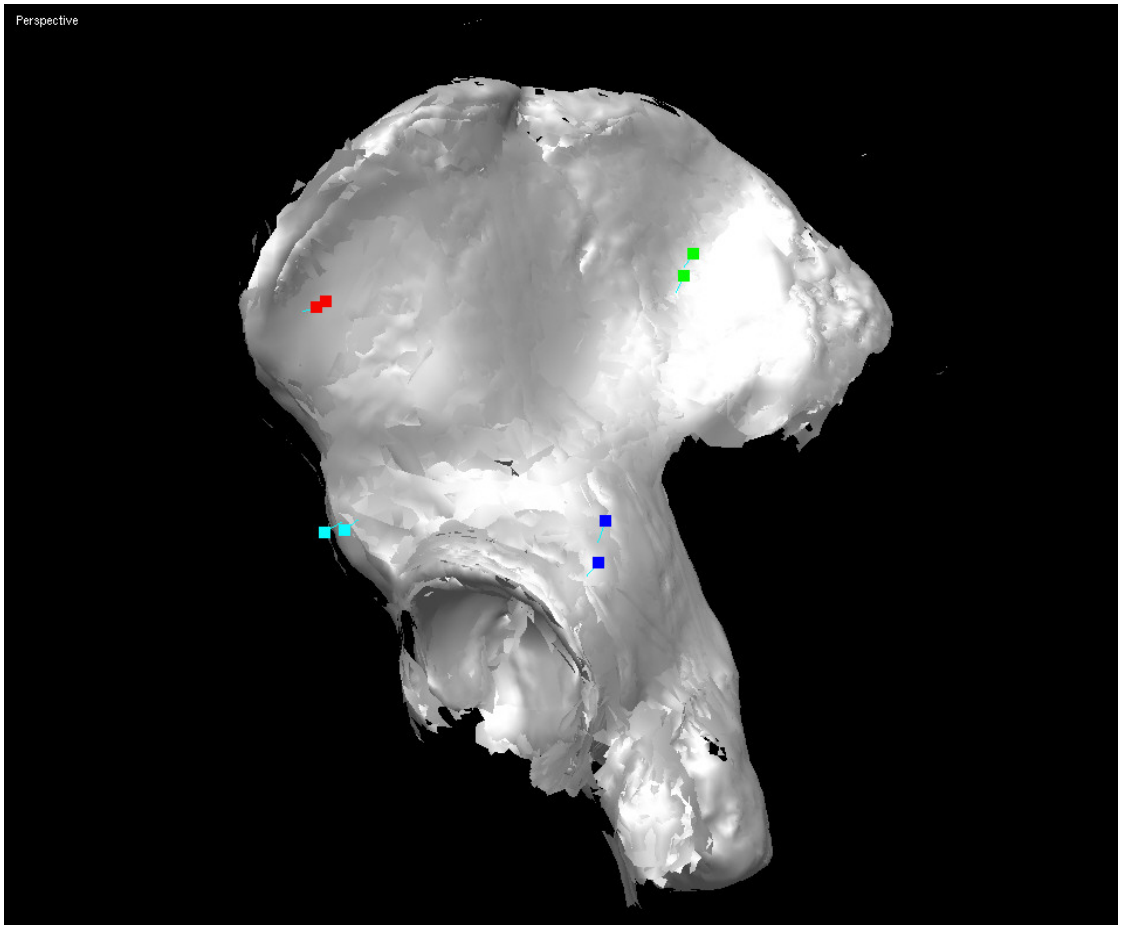

Figure 4.3: Illustrates the result of the registration process. The colour-coded dots are arranged in groups corresponding to similar geometry between the two scans. The scans are thus oriented correctly, yielding a whole model of the right innominate.

The model file resulting from the registration process is exported as a point cloud file for the simplification process. This removes the polygon mesh from the shell. The file is then reloaded under a new project window as a point set. An exact copy of this point cloud is made and the object is reduced in complexity from the copied point-cloud. This reduced point-cloud is then re-triangulated using the automatic algorithm in RapidForm™. Figure 4.4 illustrates the simplification process.

Figure 4.4: Simplification

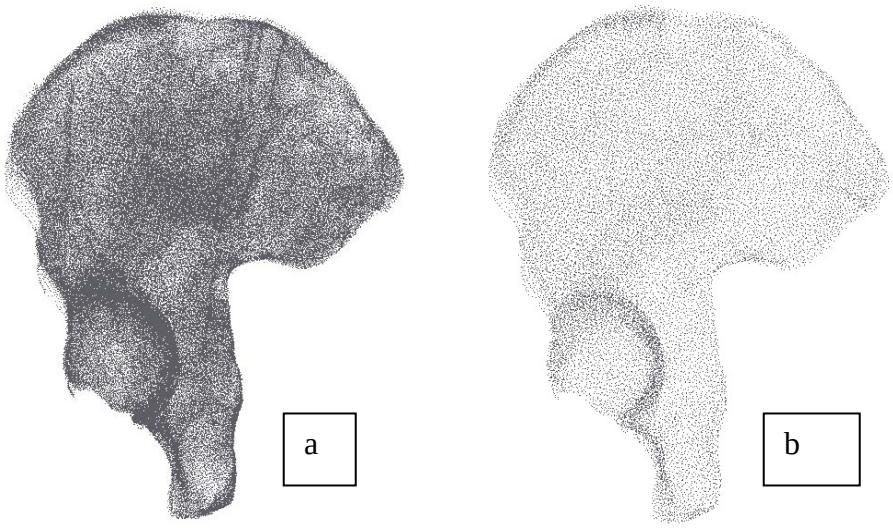

Figure 4.4: Image “a” shows the result of removing the polygon mesh from the model file generated in Figure 4.3. Note the density of the points giving the model an almost solid appearance. Image “b” shows the result of reducing the point-cloud several times until the points represent the basic outline of the shape of the original model.

The simpler model is then re-triangulated using the automated algorithm in the software. Any resulting holes are filled at this stage of the process to ensure the model is completely sealed and has no boundaries. Once this is achieved, the detail is added to the simple shell by fitting the original point-cloud to the surface over several iterations. This replaces some of the lost detail while maintaining the geometric soundness of the simpler model. Unfortunately, this also adds a great number of polygons to the surface mesh increasing the overall file size of the model. A decimation algorithm was then used to reduce the number of polygons without noticeably affecting surface quality. Figure 4.5 illustrates the process of adding detail to the simplified shell.

Figure 4.5: Model Detailing

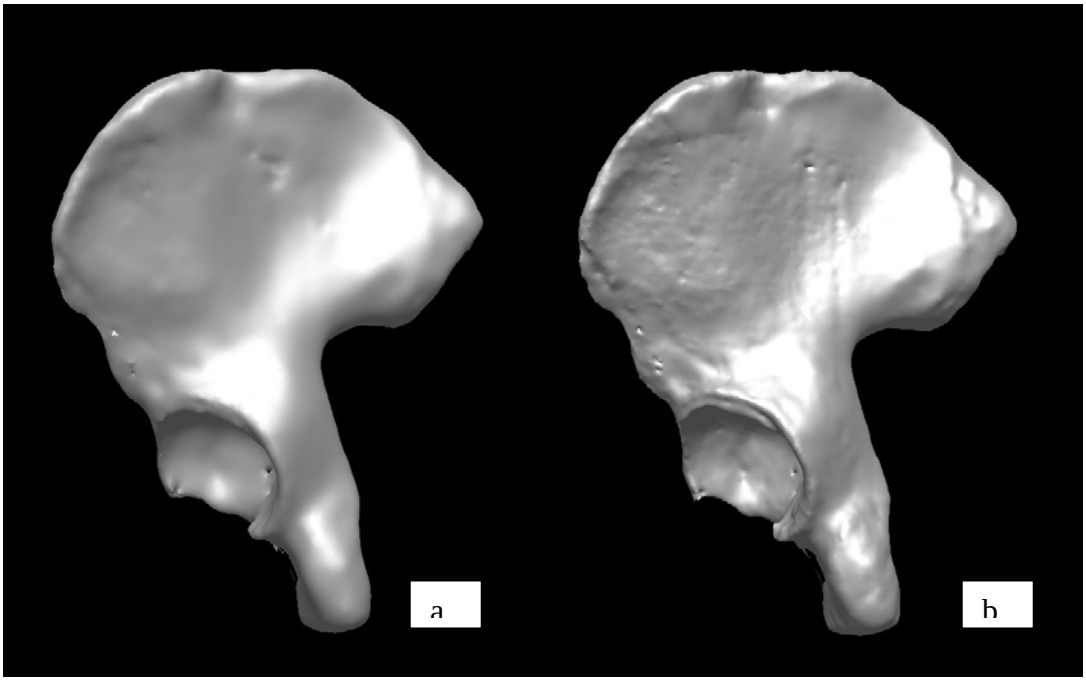

Figure 4.5: Image “a” is the simplified surface model. Image “b” illustrates the result of several iterations of the detailing process.

Once the re-detailed model is decimated to reduce the file size while maintaining surface quality, it is exported as an STL. The STL file is imported into the Z-Print software and printed. All the skeletal elements were oriented so that the least amount of printing was done on the z-axis of the build chamber. For example, the length of a humerus would be oriented along the x or y axes, and the width was oriented along the z-axis.

CT Scanning

CT scanning was undertaken at the Department of Radiology, Winnipeg Sick Children's Hospital. The material was scanned using a Toshiba Asteion™ multi-slice CT scanner at 1-millimeter slices, with 0.5-millimeter convolution. A board was placed on the surface of the scanning table and the skeletal material was grouped into a series of five scans.

Figure 4.6: Series One

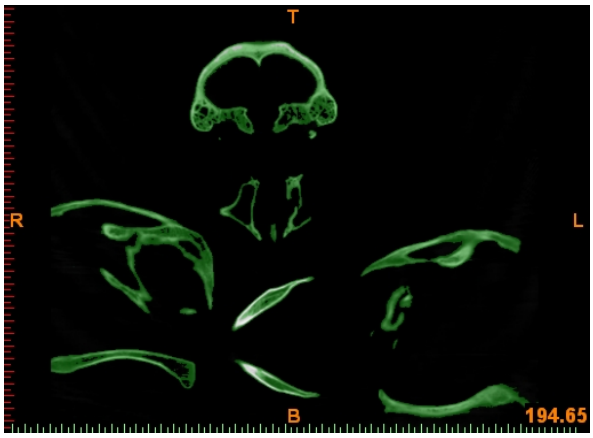

Figure 4.6: Mimics screen-grab of the layout of scan one: cranium, mandible, left and right scapulae, left and right clavicle.

Figure 4.7: Series Two

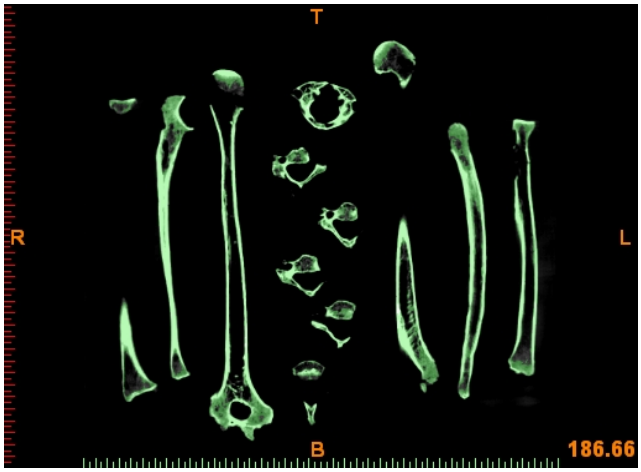

Figure 4.7: Mimics screen-grab of scan two: cervicel vertebrae (1 through 7), left and right humerus, left and right radii, left and right ulnae.

Figure 4.8: Series Three

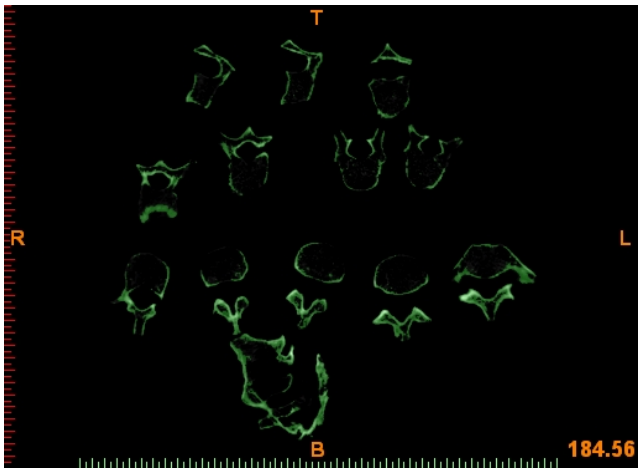

Figure 4.8: Mimics screen-grab of scan series three: thoracic vertebrae (1 through 12) and sacrum.

Figure 4.9: Series Four

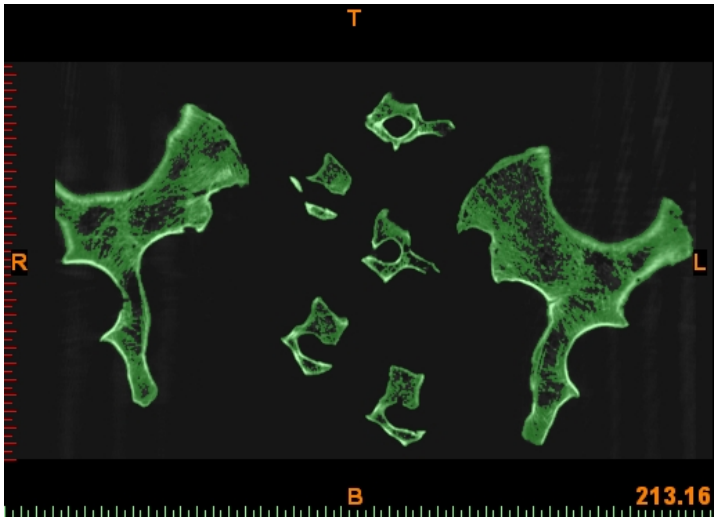

Figure 4.9: Mimics screen-grab of scan series four: left and right innominates, lumbar vertebrae (1 through 5).

Figure 4.10: Series Five

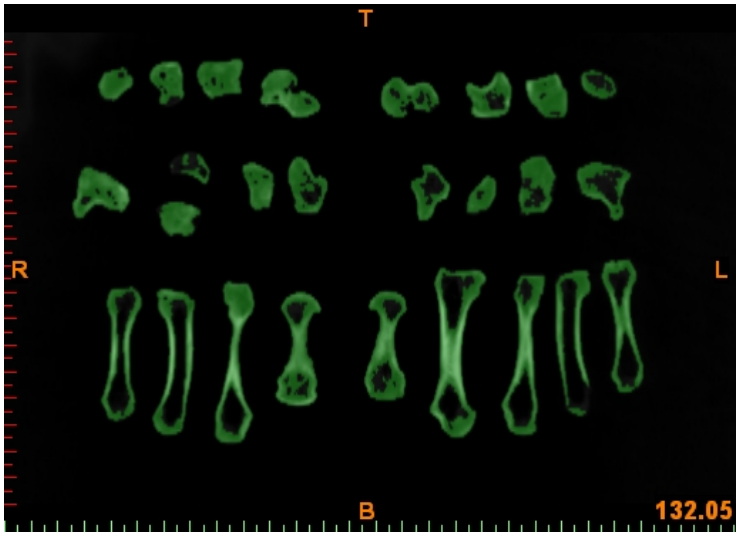

Figure 4.10: Mimics screen-grab of scan series five: left and right carpals and metacarpals.

During the scanning process, the left clavicle and right innominate were incorrectly positioned. This resulted in a portion of these two elements being cut off and not completely recorded. Unfortunately this error was noticed only after the images were processed from raw files into DICOM and delivered to the researcher. This problem is illustrated in Figure 4.11.

Figure 4.11: CT Position Error

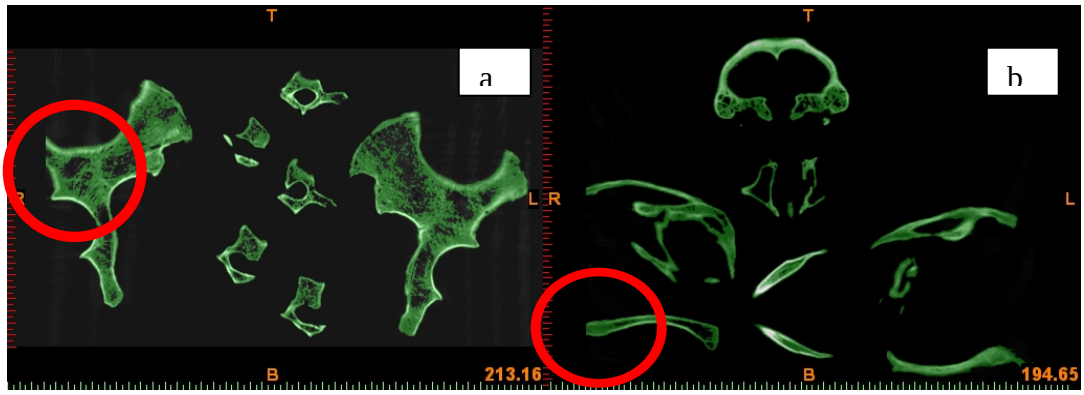

Figure 4.11: Images "a" and "b" are not related by scale. The red circles in both images "a" and "b" mark the positional error where the bone has not been completely imaged due to being positioned outside of the field of view of the CT scanner.

A total of 65 elements were successfully CT scanned for this project. The scanning took approximately 3 hours. During the scanning process, the CT equipment needed to be cooled periodically. This added to the total scanning time.

The CT images were processed using the medical imaging software Mimics. Mimics converts the DICOM images into a proprietary format and displays three different views of the subject material (axial, coronal and sagital). This gives the researcher the ability to edit structures while relating the process conceptually to the overall 3D perspective of the subject. A project management window uses a system of

"masks" (colour coded projects) to organize the editing process. The colour coding between the mask and object in the three image planes is coordinated.

Figure 4.12: Working in Mimics

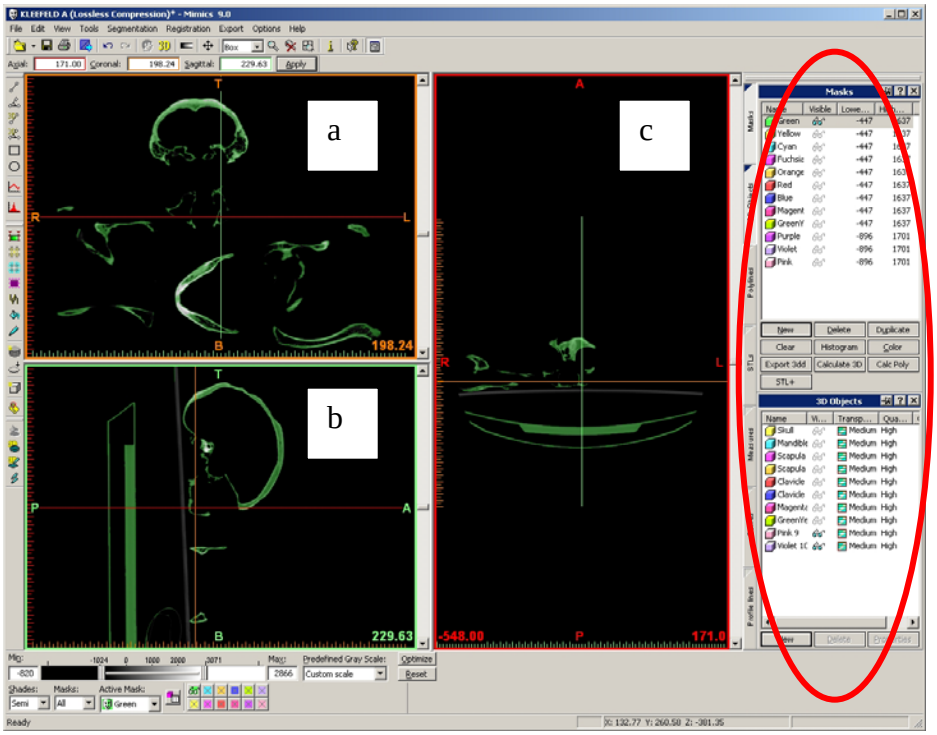

Figure 4.12: Provides an overview of the work process in Mimics. The different views (axial, coronal and sagatal) are marked "a", "b" and "c" respectively. The project management window is marked with a red circle.

The skeletal elements were made into virtual models by first selecting an average threshold of Hounsefield values between –450 and +1637 for the material used in this project. In general, this range captured the detail of each element in each scan series. The skeletal elements were then separated from the board by deleting several slices of the board holding the elements and applying the "region-growing" function to the undeleted slices. This tool classifies all the connected pixels within the identified threshold value as a single region of interest over the entire stack of images. The board and the skeletal

material are then classed as separate entities and are given distinguishing identities in the project management window, and corresponding colour coding in the image-plane windows. Since no soft-tissue was present, the remaining elements were individually isolated using the same region-growing function and were assigned their own colour coded identities (Figure 4.13). The individual elements were then exported as STL files and loaded into the Z-406 for printing.

Figure 4.13: Segmented Elements

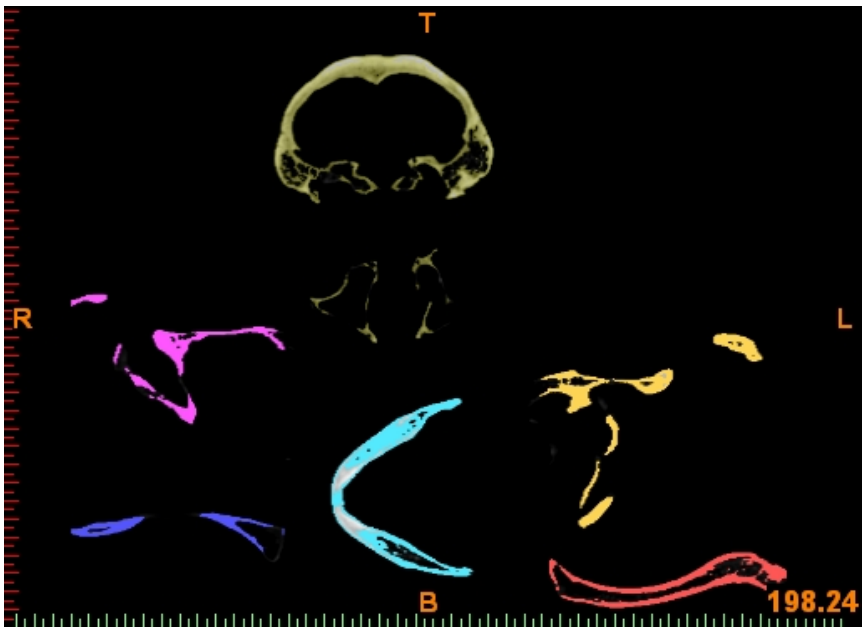

Figure 4.13: Different coloured entities depict the result of the region growing process to isolate the individual skeletal elements. From this stage, each bone can be exported as a separate 3D model.

3D Printing Whole Bones

The orientation of bones was a significant point of consideration in the printing process (as per Case Study One), since the z-axis is where the greatest amount of printing error and the lowest amount of part strength occurs. Therefore, it is important to orient long thin bones to maximize the x-y plane. To save time multiple bones were loaded into a single build series since the speed of the printer is mainly limited by the number of times the gantry can move across the build chamber (six layers per minute in monochrome and two in colour mode), the most efficient use of time and space involves limiting the z-axis depth of items as much as possible in the build chamber. The printed object needed to be left for several hours before removing. This allowed the binding solution to dry and cure. While in theory, objects can be removed immediately, for this project objects were left for at least 5-6 hours.

Large bones, such as the Femora and Tibiae, were printed as two segments due to the limited size of the build chamber in the Z-406 (8 inches wide and 10 inches long). This meant that these elements also needed to be glued together. The best technique for this involved beveling the circumference of the adjoining shaft surfaces to provide a channel for the cyanoacrylate (CA) when the two portions are held together. The CA was first applied to both adjoining surfaces, and held together until slightly firm (Figure 4.14). Additional glue was applied through the beveled channel to increase the seal between the surfaces.

Figure 4.14: Joining the Proximal and Distal Femurs

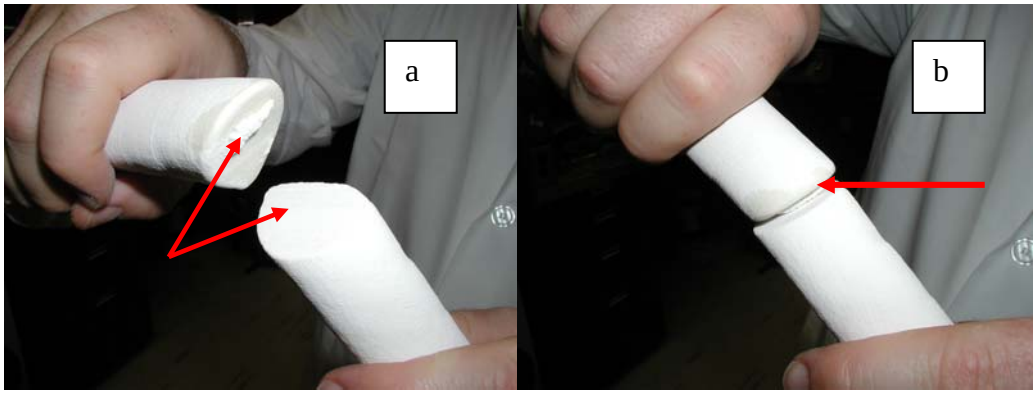

Figure 4.16: Image “a” shows the metaphysial surfaces of the proximal and distal femur. The red arrows indicate where the CA was placed prior to putting the ends together. Image “b” illustrates the joined surfaces; the red arrow marks the beveled edge. CA is placed along this channel as well and later sealed with the powder and binder putty.

The original virtual models were bisected on an angle to increase the surface area for gluing. Excess CA changes the surface colour of the model and must be covered appropriately to hide the gluing process. To fix this problem a putty was made with the plaster and binder solution and applied to the beveled channel. The rough edges were sanded. This process was repeated until the seam was barely visible. Figure 4.15 illustrates the result of this process.

Figure 4.15: Completed Long Bone

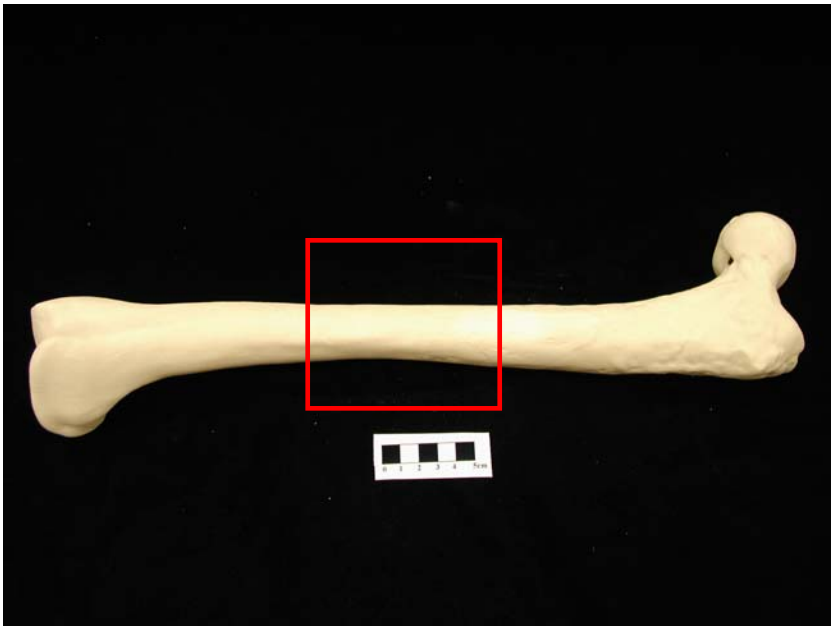

Figure 4.15: This femur illustrates an example of the joined procedure used for long bones that did not fit in the build chamber. The red box highlights the area that was filled with the putty and sanded for smoothness. Note: the seams are only visible upon very close inspection of the actual printed object.

The final stage for the entire model collection involved submersion into a paraffin wax bath.

Results

The principal reason for printing models created using both laser surface scanning and CT scanning is to evaluate the degree of difference in virtual models between each acquisition method. This will add to the understanding of the differences and limitations of surface laser and CT scanning. Eleven of the surface and CT scan models were compared for differences in shape using RapidForm™. The inspection process was similar to the one used to compare the unbroken and reconstructed pots in the first case study. The surface and CT scans of each bone were first registered together using the

registration function in the Inspection workbench of RapidForm™. This method compares both models as if they are the same, by registering them to a common datum point in three-space. The total number of vertices (and thus polygons) was reduced equally for both the surface and CT scans after registration using the decimation algorithm in the software. The two models contained too many points of data for the software to operate. There was no change in the overall appearance of any of the models following the decimation procedure, as this algorithm is designed to remove redundant data points without significantly affecting the overall surface quality of either model.

Following the decimation procedure, RapidForm™ was used to calculate the displacement between vertices (x, y, z coordinates) and the results were exported to an Excel spreadsheet for analysis. The surface scan data was compared to the CT data as though the CT data was the standard; therefore, results reflect the difference of the surface scan data in relation to the CT data.

Table 4.2: Total Deviation Between Surface and CT Scan Data (mm)

	TOTAL VALUES				
ELEMENT	MEAN	ST DEV	MIN	MAX	Total Range
Left Innominate	-0.63	0.78	-5.35	4.06	9.41
Left Scapula	-1.44	0.51	-4.48	4.15	8.63
Left Humerus	-0.24	1.00	-3.40	3.36	6.76
Right Clavicle	-0.26	0.83	-2.02	5.01	7.03
Right Humerus	-0.98	1.05	-5.24	7.12	12.36
Right Radius	-0.71	0.78	-2.49	2.85	5.34
Right Ulna	-0.96	0.87	-5.45	2.33	7.78
Right Scapula	-1.01	1.44	-7.31	4.35	11.66
Skull	-0.74	1.15	-4.96	7.62	12.58

While the linear statistical analysis (in Table 4.2) of the comparison between acquisition methods is limited, it does identify basic trends in the differences between the models resulting from the two methods. All but two of the means for total variation are negative values. This suggests that overall the CT data is larger than the surface scan data. The two outliers for this trend are the left clavicle and right innominate. Both of these CT scanned items are missing portions due to improper placement on the CT table during the scanning process and they were removed from the inspection analysis. Figure 4.16 depicts the missing portion of the left clavicle from the CT scan (blue), versus the surface scan (red).

Figure 4.16: CT vs. Surface Scan for Left Clavicle

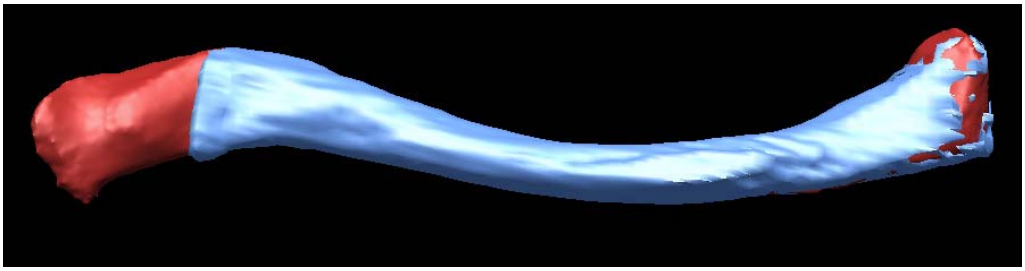

Figure 4.16: Red represents the laser surface scan and blue represents the CT scan. Note that the CT scan model is noticeably larger than the surface scan model.

The head of the right humerus was held to the shaft by tape. The discontinuous junction between the affixed humeral head and diaphysis created significant problems during triangulation of the surface scan data that necessitated removing that portion. The CT scan of the skull contained a great deal more inferior and endo-cranial data (from internal boney structures such as the sinuses) than the surface scans (Figure 4.17). This likely contributed to the range in differences between the CT and surface scans for the skull.

Figure 4.17: Registered CT and Surface Scans of the Skull

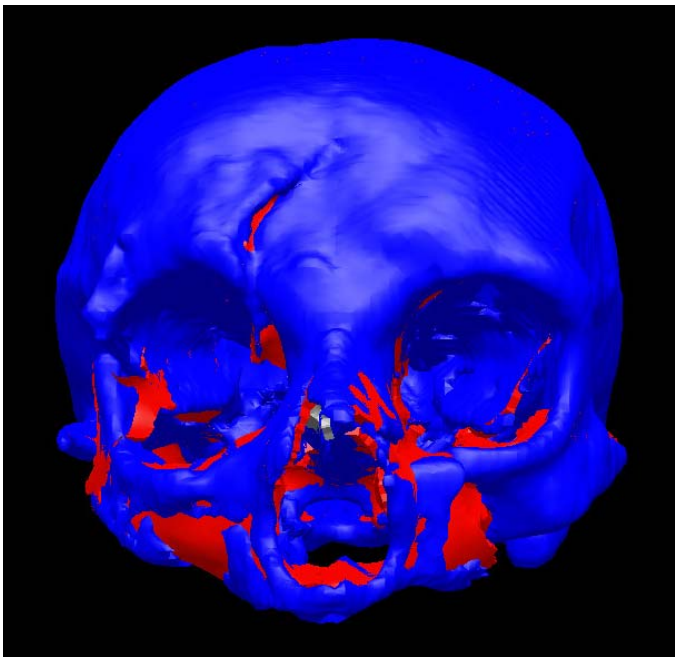

Figure 4.17: The red represents the surface scan model and the blue represents the CT scan model. Note the areas of difference are located in the regions most difficult to surface scan, such as the irregularity of the bones of the face.

The average deviation and range values from Table 4.2 were effective for understanding general trends in the differences between the two acquisition methods. As discussed in case one the inspection module of RapidForm™ offers a graphical representation of differences between models based on a threshold of values. The 3D models from CT and surface scanning were also compared graphically based on two different scales. This was effective for understanding basic differences in shape between models from the two different acquisition methods. A control scale capturing variation between +1 and –1 millimeters of displacement was used for this comparison. Table 4.2 was used to calculate the threshold for the other scale based on the range data for each element. The results of this graphical analysis are reported in figures 4.18 to 4.26 for each

model. In each comparison, the blue end of the scale corresponds to the negative difference values; where as the red end of the scale corresponds to positive difference values.

Figure 4.18: Innominate Inspection

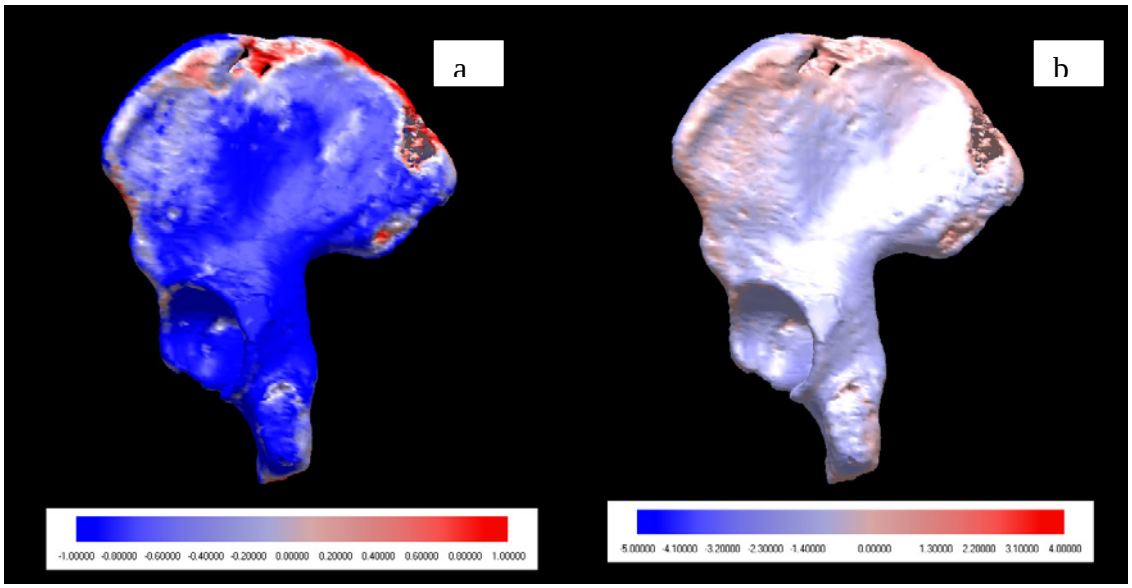

Figure 4.18: The control threshold (a) shows that the positive value differences are concentrated along the iliac crest and auricular surface. The same pattern is seen in (b) where the values illustrated represent the minimum and maximum deviation, taken from Table 4.2.

Figure 4.19: Left Humerus Inspection

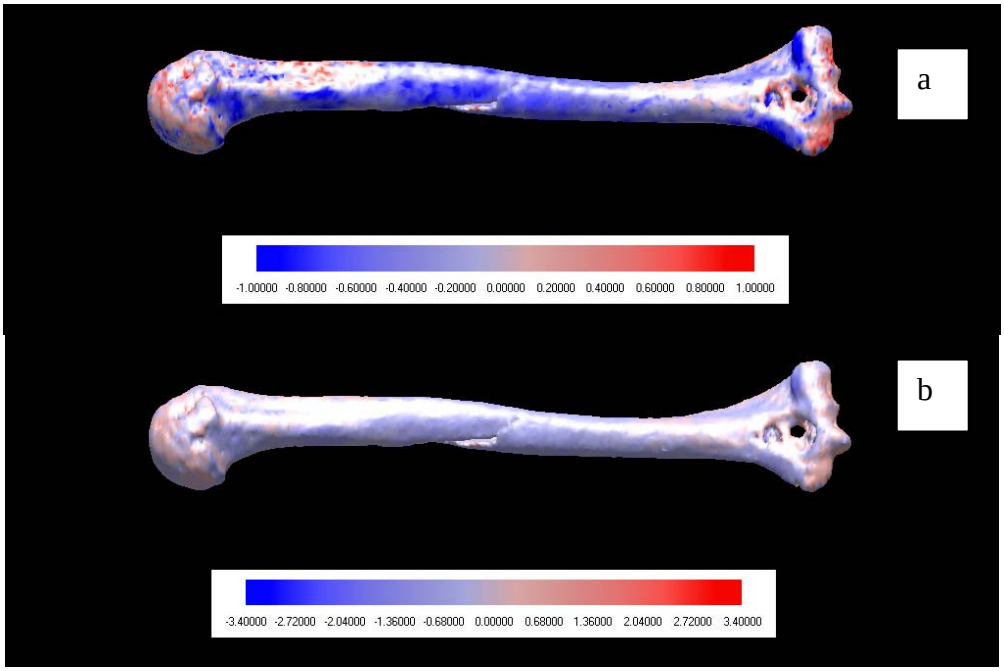

Figure 4.19: The left humerus inspection shows that the surface scan data is larger toward the proximal and distal ends, with the smaller differences concentrated along the diaphysis. The control values are represented in image “a” and the values based on range data are presented in image “b”.

Figure 4.20 Left Scapula Inspection

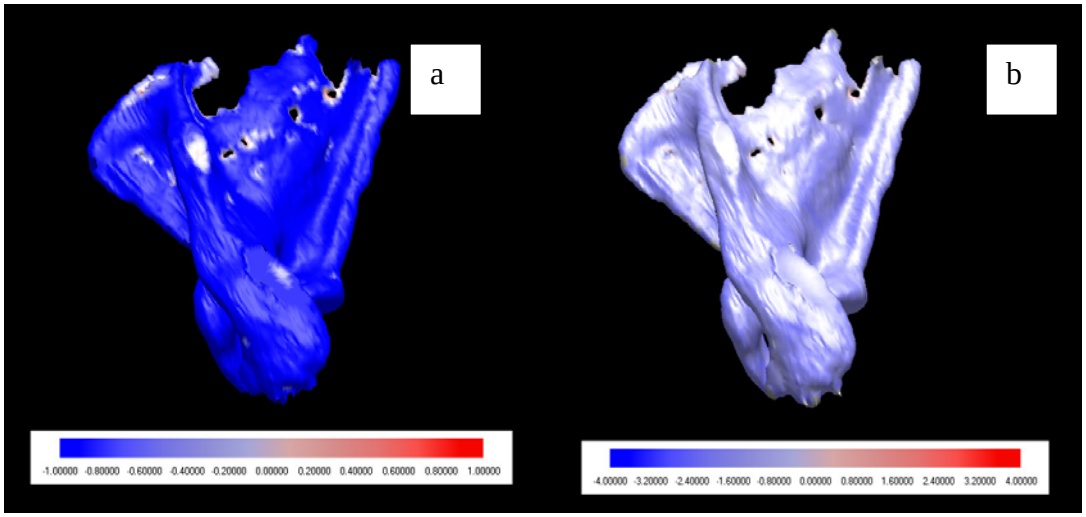

Figure 4.20: The control values (a) illustrate the negative size difference of the surface scan data to the CT scan data. The range values (b) maintain the same size pattern difference, but also suggest similarity in shape between the scans by not having a great deal of colour variation.

Figure 4.21: Right Clavicle Inspection

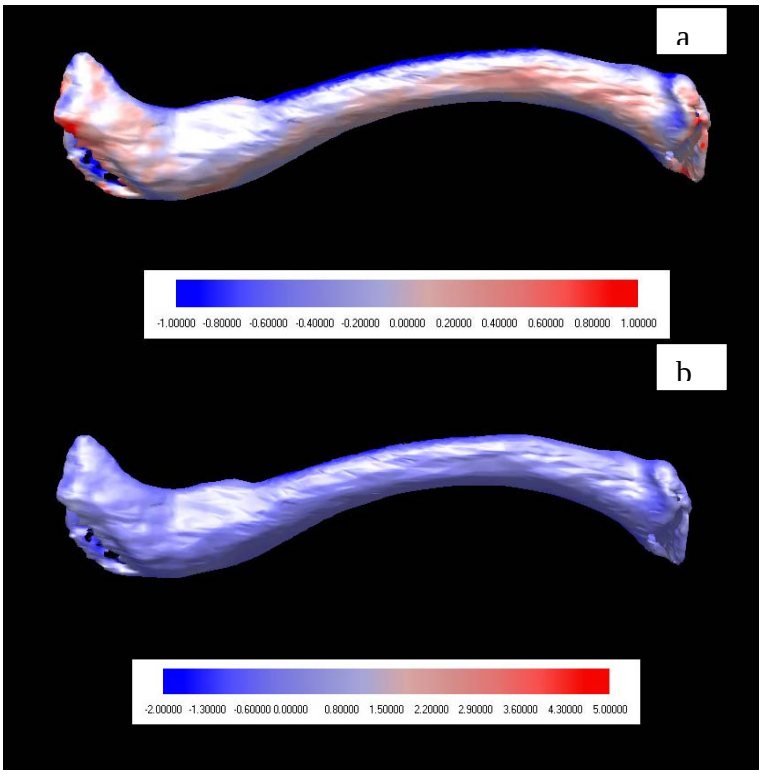

Figure 4.21: The control (a) shows an intermittent colour pattern suggesting greater variability. The range data (b) indicates that the surface scan data is smaller overall than the CT scan data, obscuring the differences with a solid colour.

Figure 4.22: Right Humerus Inspection

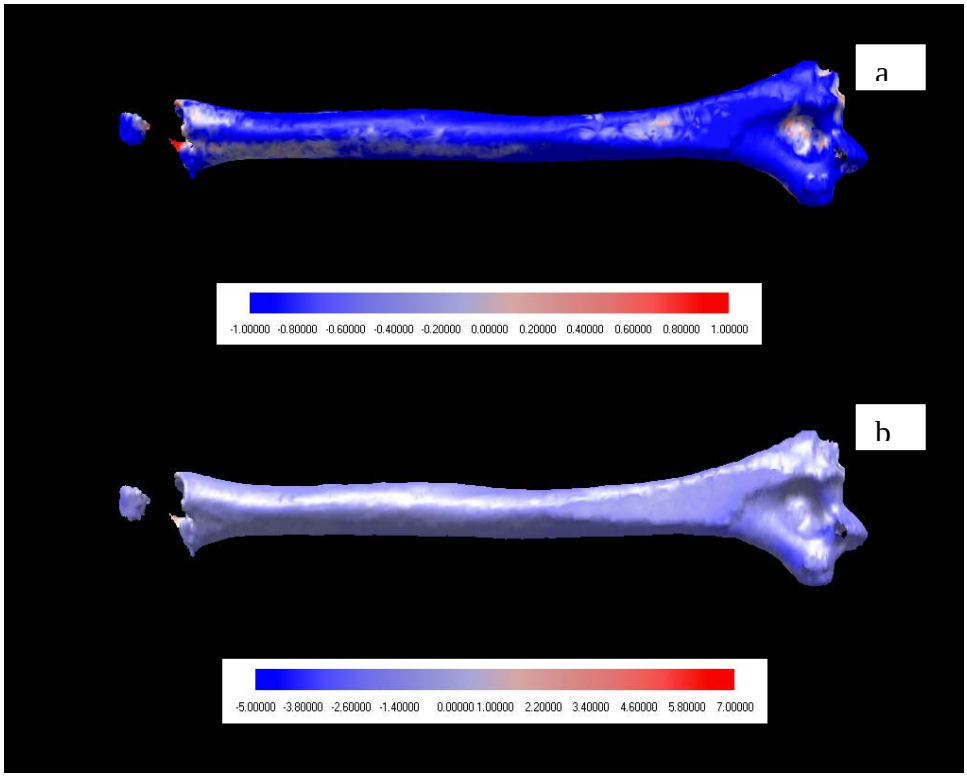

Figure 4.22: Both the control (a) and range (b) values indicate shape similarity between the models. The surface scan data is generally smaller except at the proximal end around the broken epiphysis.

Figure 4.23: Left Ulna Inspection

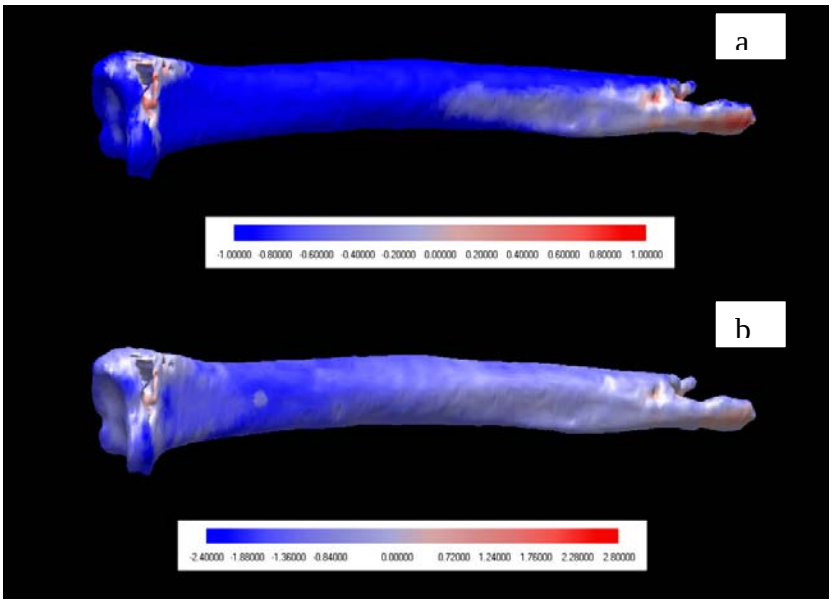

Figure 4.23: Both the control (a) and range (b) values indicate similar results. The surface scan model is smaller toward the distal diaphysis and parts of the epiphysis.

Figure 4.24: Right Ulna Inspection

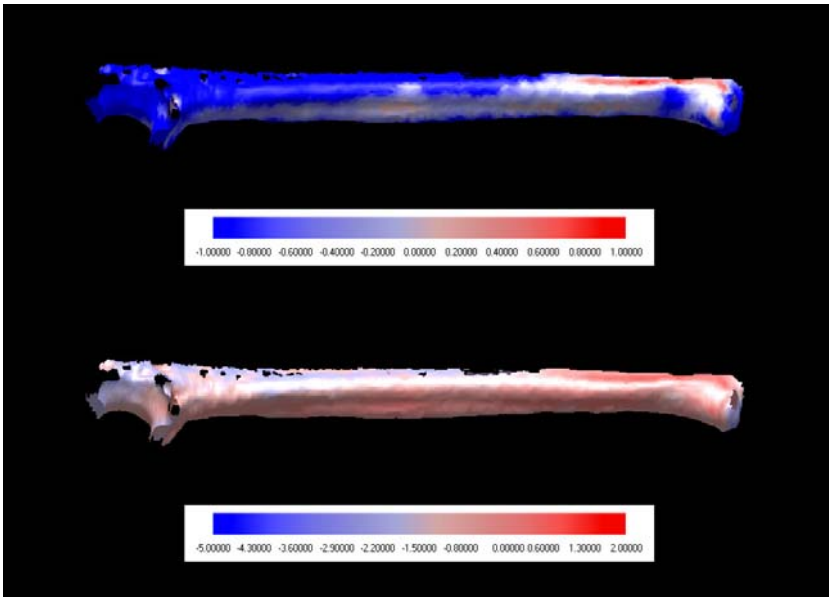

Figure 4.24: The control (a) and range (b) results indicate different patterns. The control suggests the surface scan model is mostly smaller than the CT model, but the range data suggests the opposite. This may indicate that there is considerable difference between the shape of both models.

Figure 4.25: Skull Inspection

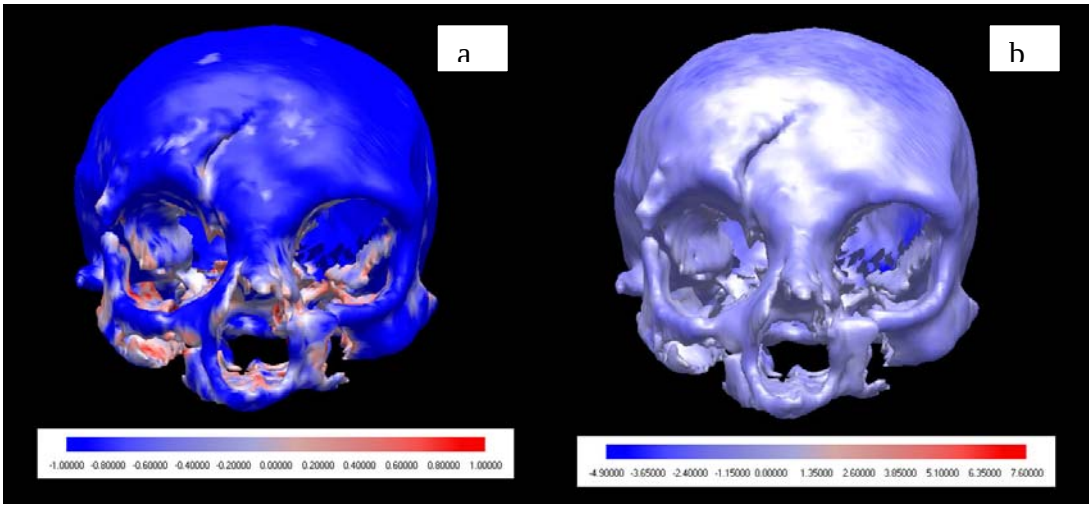

Figure 4.25: The control (a) shows significant positive-value variability around the maxilla, orbital and zygomatic areas. The range scale (b) indicates that overall the surface scan model is smaller than the CT model.

While not quantitative, the graphical comparisons between the CT and surface scan models offer a level of understanding not possible from the numerical comparisons in Table 4.2. The colour-coded differences allow the researcher to understand where the patterns of variation are in relation to the overall 3D structure of the skeletal elements. From this, general trends in the differences between data acquisition modes can be understood. First, these results confirm that the CT models are generally larger than the surface scan models. More importantly however, the trends in the graphical analysis confirm that the more complex areas of surface morphology differ the most between the CT and surface scan models.

Some linear dimensional measurements were taken for comparison of the CT virtual models and printed skull and sacrum models. The skull measurements assessed maximum length (glabella to opisthocranion), width (euryon to euryon) and height (basion to bregma). The sacrum measurements assessed maximum length from the most distal point of the coccyx to the body of S1 and maximum width between the widest parts of the left and right auricular surfaces. The results of these comparisons are reported in Table 4.3.

Table 4.3: Skull and Sacrum Comparison of Virtual and Printed Models

Measurement (cm)			
Element	Max Length	Max Width	Max Height
Virtual Skull (CT)	15.75	14.15	13.15
Printed Skull	16.10	14.10	13.90
Percent Difference	2.22%	-0.35%	5.70%
Virtual Sacrum (CT)	8.99	12.08	NA
Printed Sacrum	9.30	11.60	NA
Percent Difference	3.45%	-3.97%	NA

Table 4.3 shows good agreement in dimensional accuracy between the virtual and printed models. The largest difference is 0.75 centimeters (5.70 %), between the height of the virtual and printed skull models. The height also corresponds with the z-axis in the build chamber. This observation is consistent with the results of case study one that suggested the z-axis error contributed to the largest differences in the printing of the pot.

The initial purpose of this case study was to reproduce an entire skeleton for the MHV. This was accomplished using the 3D surface scan models identified in Table 4.1.

A total of 57 skeletal elements were produced using the 3D surface scanning and printing methods described earlier. The model skeleton was placed into a display case lined with sand to give the skeleton a semi-excavated appearance. Educational material was organized around the outside of the display case. The result of the skeletal model in the "New Life" exhibit is illustrated in Figure 4.26.

Figure 4.26: New Life Exhibit

Figure 4.26: Skeletal replica in the "New Life" exhibit at the MHV. Note the educational material about Mennonite ways of life at the turn of the 19th Century (marked with arrow).

Despite not being a scientifically accurate representation of the skeletal morphology, the replica skeleton was adequate for the public educational display in this context. As shown in Figure 4.27, numbered cards were paired with specific areas of interest on the skeletal replica. This provided a platform for communicating basic ideas about the biological anthropology of the skeleton to the community of visitors.

Figure 4.27: Skeletal Reproduction

Figure 4.27: Images “a” through “d” illustrate the placement of number cards next to skeletal elements. These cards associate information along the educational panel and the skeletal morphology being highlighted.

Discussion

The use of CT scanning allowed for the imaging of structures that needed to be omitted from the surface scan modeling. All the vertebrae, carpal and metacarpal bones could be imaged and made into virtual models with relatively little post-processing. The post-processing required for the vertebrae using the surface scan method was extensive (approximately 10 hours in total). The segmentation of the vertebrae from the CT data required less than an hour and was more effective for the smaller more intricate structures. Post-processing is a limitation for generating surface scan models, particularly for the irregular shape of biological material. There has been a great amount of success with surface scanning for monuments and buildings (Ahmon 2004, Fontana *et al.* 2002, Fowles 2000, Godin *et al* 2002, Taylor *et al* 2002 and 2003, Willems 2005 etc). However, buildings and monuments are far larger and more uniform in shape than biological material.

A special processing method was used to overcome the problems associated with generating models of complex surfaces (Allard *et al* 2005). Early trials for creating surface models of the skeletal material resulted in a significant amount of triangulation error, including non-manifold conditions, holes and improperly defined object boundaries. These problems needed to be corrected prior to printing the models since the Z-406 only recognizes the models as geometrically defined mathematical representations. A great deal of time was spent trying to clean models using the RapidForm™ automated algorithms. These tools are effective for fixing minor problems, but not effective for most of the issues that resulted from creating surface models of the skeletal material with irregular surface morphology. Starting with a shell without holes makes fixing geometric

problems easier. Holes in the shell are a symptom of problems encountered during the triangulation process. The detail of the object is then "carved" out of the simple shell by adding points from the original, data rich point-cloud. The downside to this approach is that the surface is the result of averaging the detail from the original point-cloud with the simplified shell. This causes a level of dimensional inaccuracy due to the size difference between the shell and original point cloud. This downside for this method is out-weighed by the advantage of being able to create morphologically complex surface models without geometric errors.

The other problem with the above-mentioned post-processing method is the potential to create very large files. Each time an averaging sequence is performed triangles are added to the surface mesh as a means of defining the surface with more detail. After several iterations the model can become too cumbersome to work with (for example, the skull model was originally larger than 1.5 gigabytes). Models of that size are completely impractical to work with and require downsizing. Fortunately, RapidForm™ does have an automated algorithm that will reduce the size of the file while maintaining an acceptable level of detail. In many situations the result of using this algorithm has little effect on the overall quality of the model.

Figures 4.18 to 4.25 highlight an interesting concept concerning the evaluation of shape differences. While quantitative data will always be the principal component of most scientific studies, a great deal of understanding can be communicated using a visual interface. Quantitative data combined with an analytical procedure is capable of proving or disproving a hypothesis about the subject material; for example, the numerical values prove (in a measurable way) that the surface scan models are not the same as the CT scan

models. Sets of comparative coordinate data however, add little to the understanding of that information in relation to the overall distribution of the deviation. Knowing what differences exist only indicates that the two scanning methods result in differently shaped models. Understanding shape differences between the models adds a great deal to the complexity of the understanding of the differences between the two acquisition methods. Thus, the 3D colour model provides a readily identifiable reference for understanding these differences, which can be communicated to a general audience without prior training in understanding numerical analysis.

In keeping with the above argument, two additional colour models were produced virtually and then printed. The surface scan and CT scan models of the skull were registered together and given opposite colours. The same procedure was performed for the right humerus. The skull was also bisected sagittally in order to view the endocranial differences between the scans. The resulting virtual models were then printed in 3D (Figure 4.28).

Figure 4.28: CT and Surface Scan Comparison Models

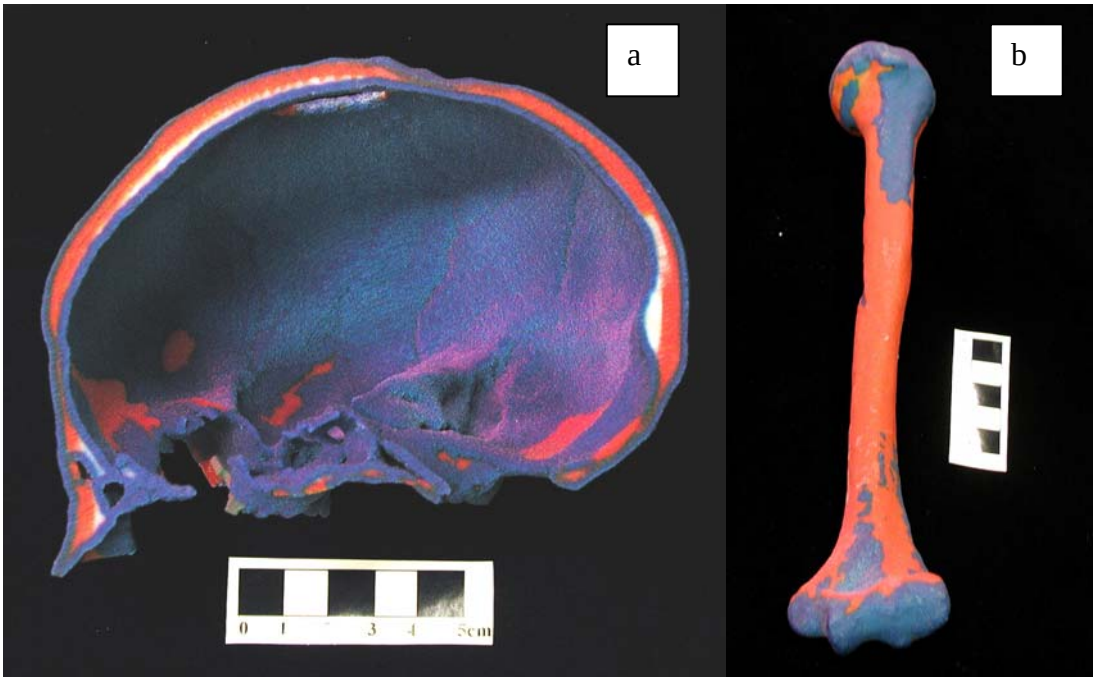

Figure 4.28: The sagittally-bisected view of the skull (a) shows the degree of size difference between the surface (red) and CT (blue) scans. In this case the endocranial and exo-cranial surfaces of the CT model exceed the dimensions of the surface scan. For the humerus (b), the surface scan model (red) is larger along the humeral diaphysis than the CT scan (blue). However, the CT scan model is longer overall as evidenced by the blue epiphyses.

The size differences in the models depicted in Figure 4.28 may be due to errors in generating the models from the surface scan data, but may also be due to the segmentation of the structures from the CT data. As described noted by Choi and colleagues (2002) in Chapter Two, it is difficult to identify actual tissue boarders in CT images. Identifying tissue boarders is further complicated by the lack of soft tissue surrounding the bone that can act as a marker for distinguishing tissue boundaries. The archaeological skeleton imaged was very fragile due to the extent of tissue decomposition. The very thin areas of cortical bone may have further complicated this, especially in regions with complex morphology. In these areas, partial volume averaging can cause structures to look larger than what they actually are since the attenuation

coefficient for the pixels along the boarder of these structures is averaged with the air surrounding it. The colour modeling in Figure 4.28 assisted in examining the differences between the surface scan and CT models more critically, by adding a level of understanding related to the shape differences.

Colour modeling is an area that requires further investigation with a variety of case studies. As seen in Figure 4.28, a great deal of information can be communicated about an object beyond recreating a photorealistic model. In this case, the superimposition of two similar models provides a new and robust method of understanding the shape differences between the two models. This may lead to one of the most useful aspects of the 3DP technology.

Conclusions

The most appropriate method of data acquisition is dependant upon the end goal of the project. As discovered in this case study, both surface scanning and CT scanning have their own issues relating to the post-processing of the data into virtual models. While CT scanning may be the most accurate representation of shape, it may not be dimensionally perfect and is limited by the resolution and accessibility of the CT scanner. The laser surface scanner is more accessible, but the post-processing of the data for complex objects such as skeletal elements introduces a great deal of morphological error. The laser surface scan models were effectively used for the MHV exhibit “New Life”, which provided an educational outlet for the public. The skeletal models printed for this project were not of the standard required for traditional anthropological analysis due to the degree of post-processing and resulting loss of detail required to make printable models. The colour modeling of the differences between laser surface and CT scan

models opens another door for the use of 3DP for scientific understanding that goes beyond just accurate or photorealistic replicas.

Chapter V: The Role of 3D Printing in Biological Anthropology

Consider the statement "the medium is the message" from Marshall McLuhan's Understanding Media: The Extensions of Man. From this phrase, McLuhan (1966: 23) discusses two mutual processes in the creation of media: media carries a deliberate message from the creator, and more importantly, the use of the medium to carry the message becomes a component of cultural significance shaping the way in which we interact with the world. The photograph shaped the way in which we approached the visualization of items, through the desire to capture what our own visual system perceived at a given moment and freezing that in time and space. Naturally, our first instinct is to model this same approach in our pursuit of the creation of 3D virtual objects. This is a testament to the hegemony of photography in the culture of technology. Once this barrier in thinking is overcome, we can begin to realize that we are not constrained by the confines of reproducing physical reality, but that we can actually create a new and truly virtual reality that extends our understanding beyond what is apparent on the surface. Thus, as new technologies replace older ones, they acquire new positions in the hegemonic structure of a culture.

The goal of this research is to explore the role of 3D printing in biological anthropology. Consider the 3D model as a medium of information exchange as defined by McLuhan. The question that should really be asked is how 3DP will change the way in which we approach research in anthropology and how we perceive what we study. There is already an overarching paradigm in anthropology today to be minimally invasive with our research methodology. Fortunately virtual technology is making this goal a

reality, and is possibly adding insight into material not possible with conventional methods.

Methodology is a key subject in each case study. Unlike conventional methods of investigation, such as taking measurements, there are many different ways to create a 3D virtual model for printing. The source data is the single most limiting factor. The methods of data acquisition used in this work were not capable of capturing the form of objects as accurately as the printer. In addition to this, the data must be handled and processed to create the model. This introduces a significant amount of subjectivity into the reproduction. The best method of data acquisition is directly linked to the purpose of the model. This is the point at which the medium begins to shape the message. The planning and preparation that goes into producing the model is as important and informative as the model itself. The model actually preserves the researchers' bias by storing a record of the acquisition process.

The first case study used a pot for examining the role of 3D printing for virtual reconstruction projects. Reconstruction is a very active field of research in anthropology (e.g., Kampel and Sablatnig 2003, Thompson and Illerhaus 1998, Zollikofer and Ponce de Leon 2005, Zollikofer *et al* 2005). Virtual approaches to reconstruction offer the advantage of being non-destructive and adhere to the paradigm of non-invasive research. Zollikofer (2002) provides an excellent example of the importance of virtual reconstruction by showing how adherents from earlier reconstructions and matrix can be removed in the virtual environment and the specimen (in this case a skull) can be recreated seamlessly in three-space. Ponce de Leon (2002) also shows how the virtual reconstruction of that same skull can be used to reverse the effects of taphonomic

distortion. This level of manipulation changes the types of questions we can ask of the material. In this case, it can be used to challenge our understanding of phylogeny or evolutionary processes. As shown by case study one, the results of the reconstruction can be printed and used to verify the assumptions of the reconstruction. This allows repeatability of results not possible when reconstructing the original specimen, since the original is left untouched and subsequent versions use the digital data. It also provides for a comparative collection of the various results, which can be held directly to each other or other similar specimens for comparison. The focus can shift slightly from the information gained about the reconstruction itself to include a greater discussion of the methodology as it relates to the reconstruction. Figure 3.20 illustrates how colour modeling can also be used to show differences between reconstructions. The colour modeling of the superimposed unbroken and reconstructed pots gave the researcher the ability to effectively communicate the absolute differences between the models using the more universal language of visualization to communicate results to a broader audience.

Items concealed in matrix can be extracted efficiently and accurately using virtual modeling without secondary damage due to the extraction process (Zollikofer and Ponce de Leon 2005). In other research, Gill-Robinson and colleagues (2006) have used CT imaging to extract the skull of an ancient Egyptian mummy without damaging or unwrapping the original body. This type of non-invasive data acquisition is very important to the future success of anthropology as researchers and students become more aware of the sensitive nature of historical resources. The 3D printing of human remains allows researchers to handle and interpret the original item and pass this information on to others in a way that is tangible and easy to use. For the work by Gill-Robinson and

colleagues, the skull that was printed was used for facial reconstruction and allowed the researchers to accomplish this task without harming or even making physical contact with the original skull. Access to previously inaccessible material affects the questions that are asked. Further to this, the researcher does not even need to be in the same city, country or continent to examine the skeleton. By giving researchers and students access to material from around the world, it inspires collaboration and facilitates discussion that can lead to successful partnerships and the sharing of knowledge.

The skeletal replica from case study two was created for the Mennonite Heritage Village exhibit entitled New Life. This exhibit describes the beliefs about death and funerary practices of early Mennonite settlers. The replica of a skeleton was created to show how people were buried and describe how researchers can glean information about ancient ways of life through the skeleton. The display of human remains in Canada is typically frowned upon and can offend communities. From an ethical and research perspective, human remains should be properly curated in a responsible manor. These conditions may limit the use of human remains for museum exhibits. It has been suggested that a way around these limitations is to create a replica of the skeleton in question, which will satisfy all parties' interests and present the material in a socially responsible fashion (Brownlee *et al* 2005, Sitchon *et al* 2005).

The initial approach to producing this skeletal replica involved using surface scanning to acquire the surface geometry. This approach was completely non-invasive and only required handling the bones. Although limited to some extent in the amount of detail and size of items the result was adequate. The skeletal elements were set into the sand in a mock semi-exhumed state. The creation of this exhibit provided members of

the public with the resource of the skeleton in manner never before possible with such delicate remains. This is the first known example of the replication of an entire skeleton from laser scan data and 3DP technology, however, it is similar to the approach used by Hjalgrim and colleagues (1995) in their production of the skull of the Iceman. In the case of the Iceman, the skull was completely inaccessible, but the model provided access for both the researchers and for the dissemination of the findings. As projects like this and the New Life exhibit become more commonplace, the nature of public dissemination of research will also change.

McLuhan (1966) uses the example of photography to explain how a medium can become ingrained into the fabric of a culture. Omitted from this example are the practical reasons for the widespread adoption of the technology. Any self-respecting anthropologist knows that the use of technology in culture is governed by the practical implications of the item in question. For example, fire would not have been used by early humans and incorporated into human culture if there was no advantage to it. RP as a medium in general is constrained by a number of factors. As discussed in Chapter II, most of the anatomical modeling has been done with SLA technology. There are a number of differences between the 3DP technology and the more widely used SLA approach, which make 3DP more appealing to research in biological anthropology.

The off-white plaster material provided an excellent proxy to the skeletal material. Even though actual bone is not white and is usually stained by the soil, the off-white colour of the plaster is more similar to what people associate with the colour of bone than the semi translucent yellow resin of traditional SLA technology. The plaster used is actually mostly calcium carbonate, the same compound found in bone. This gives the

material a more similar “feel” to bone than the SLA resin. Another advantage to the Z-Print materials is the workability prior to infiltration with wax. Grimm (2004) is noted in Chapter II as commenting about the lack of stability of items from the Z-Print machine prior to infiltration. This was discussed by Grimm in the context of being a limitation of the Z-Print technology since the parts require additional finishing and are not stable right out of the build chamber. The long bones of the skeleton were too large to fit into the build chamber and needed to be printed in sections. The sections were then joined together prior to infiltration with wax. The simplicity of the plaster and binding solution allowed for the creation of putty, similar to drywall compound that was used to hide the seams. The excess was sanded down to yield a perfectly smooth surface that, at a distance, makes the long bones look like a continuous structure (Figure 5.1). This is not possible to do using the SLA materials that are stable right out of the build chamber.

Figure 5.1: Seamless Long Bones

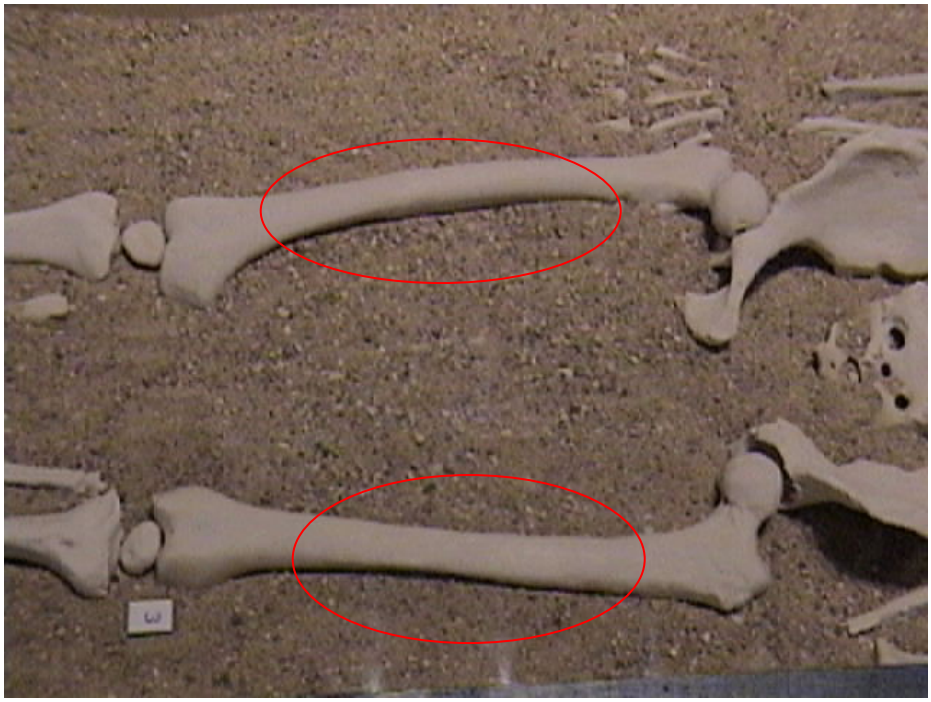

Figure 5.1: The red circles highlight the seamless femur bones printed originally in two sections.

A major barrier to making replicas the size of an entire skeleton using RP technology is cost. In Chapter II several researchers reported that the high cost of production using SLA technology limited widespread use in a variety of projects (Dolz *et al.* 2000, Hieu *et al.* 2005, Hjalgrim *et al.* 1995, Powers 1998). It is difficult to isolate material cost from overall cost, however, Hjlagrim and colleagues (1995) reported a research cost of $2500 U.S. for one skull replica using the SLA technology. According to verbal communication with other researchers this number is not unrealistic as the cost of photosensitive resin for SLA machines is very high. The consumable cost for the entire skeletal reproduction for the MHV was approximately $500. This value made the skeletal replica possible. In order for RP technology to be used regularly in the research environment the cost of production needs to be more accessible to researchers.

The creative process that was involved for both case studies in this work and the other work done in the Bioanthropology Digital Image Analysis Laboratory (BDIAL) at the University of Manitoba requires equipment that can produce concept models affordably. A significant advantage to the Z-Corporation equipment is the relatively low cost of operation, which allows for large-scale projects such as the skeletal replica. It also promotes accessing creativity that comes from free association with tangible objects, such as that suggested by Rountree and colleagues (2002). The speed of production for the Z-406 also increases accessibility to concept models. A small-scale replica of an edited CT project can be produced in a matter of hours and used to evaluate project progress. This is not possible using the more costly SLA production method. The speed and cost effectiveness of the 3D printing approach make it a more appropriate choice for the research environment and can provide access to methods of reproduction not previously possible. For the MHV, this means being able to give the community a very enriching and positive experience using the skeletal replica.

From Real to Virtual and Real Again

As stated in Chapter II, Zollikofer and Ponce de Leon (2005) are noted as writing that RP is not an analytical tool, but simply a tool used to share information. This reasoning assumes that the printed model is a passive element in the investigative process, drawing a parallel between a page of text and the printed object. An analytical tool on the other hand is a method of organizing and interpreting data. Examples of this are statistical functions, where data are imported into a spreadsheet, organized and interpreted based upon various formulae (average, standard deviation etc.). Similarly, the focus of this thesis research is to identify methodological approaches to producing 3D

models using a 3D printer. The process has involved the acquisition of data, processing and the production of a result. Zollikofer and Ponce de Leon (2005) maintain that the physical object produced by this process has no interpretative value beyond what can be gathered from the virtual model. This is what is meant by their use of the term 'real virtuality', which hinges on this assumption that RP is not an analytical tool.

Traditional concepts of data analysis encompass numerical values analyzed in some measurable and standardized way, such as with statistical analysis. Often the goal is a measurable value of how much one object differs to another, or is similar to another. The ability to acquire and generate very large and complex numerical data sets is becoming a very common theme in many research areas (van Dam *et al.* 2002). Such large data sets can be difficult to interpret mathematically, and often require first-hand knowledge of the methods of analysis to be understood at any level. The visual medium has the potential to play a role in the analysis of large datasets (van Dam *et al.* 2002). The visual medium has the potential to transcend discourse and offer researchers from different fields the ability to interpret data without complex mathematical analysis. In some circumstances mathematical analysis can impede the learning process by requiring extensive knowledge of the analytical techniques and overshadowing the point of the comparison being made. For example, Fischer and colleagues (2003) identified a visual method for understanding the complicated architecture of Gaudi's *Sagrada Familia*. In this work, the superimposition of geometric shapes arranged continuously along the z-axis and colour coded, added insight for students into the way in which Gaudi used simple geometry to create complicated architectural shapes. This is also an example of Occam's razor, which states that entities should not be multiplied beyond necessity.

Table 5.1 shows the results of only 15 lines of the several thousands of lines of comparative numerical data for the shape differences between the laser surface and CT scanned humerus from case study two.

Table 5.1: Numerical Results of Acquisition Method Comparison

	Measured Point			Model Point			Displacement			Distance
	X	Y	Z	X	Y	Z	X	Y	Z	
1	-47.75	-6.95	1.60	-47.81	-8.65	1.01	-0.06	-1.70	-0.59	-1.80
2	-156.88	0.63	25.99	-156.99	0.06	26.16	-0.11	-0.56	0.17	-0.60
3	95.08	0.24	-16.36	94.72	0.64	-17.10	-0.36	0.41	-0.74	-0.92
4	-165.77	16.63	23.03	-165.79	16.62	23.00	-0.02	-0.01	-0.03	-0.04
5	-168.33	1.41	20.43	-169.01	0.32	21.73	-0.69	-1.10	1.30	-1.83
6	-55.57	-1.77	13.10	-55.53	-0.65	11.75	0.05	1.13	-1.35	-1.76
7	-157.91	-0.50	28.38	-157.93	-0.51	28.38	-0.02	-0.01	0.00	0.02
8	88.03	-5.72	-15.25	87.71	-5.66	-16.43	-0.32	0.06	-1.19	-1.23
9	-165.13	17.32	24.64	-165.44	17.52	25.01	-0.31	0.19	0.37	-0.52
10	-128.70	6.69	-7.78	-128.18	6.44	-9.17	0.52	-0.25	-1.39	-1.50
11	-52.36	-0.32	13.93	-52.16	-0.34	12.29	0.20	-0.03	-1.64	-1.65
12	-158.47	0.57	26.52	-158.42	0.67	26.88	0.05	0.09	0.36	-0.37
13	83.15	-8.83	-12.78	82.47	-9.31	-14.01	-0.68	-0.48	-1.23	-1.48
14	-164.21	17.37	23.23	-164.13	17.55	23.13	0.08	0.18	-0.10	0.22
15	7.59	-7.61	-0.66	7.55	-8.22	-0.66	-0.04	-0.61	0.00	-0.61

Alternatively the same data can be represented in the 3D model as a visual-spatial data set (Figure 5.2).

Figure 5.2: Visual-Spatial Data Analysis Using 3D Object

Figure 5.2: The red portion corresponds to the surface scan data and the blue corresponds to the CT data.

The visual-spatial context provided by the 3D colour model of the aligned data sets yields a more readily understandable representation of the differences between the models. Admittedly, the model does not give a measurable account of the differences, however, that is not required in all circumstances. In cases where presentation to the public or to a group of non-specialists, colour modeling such as in Figure 5.2 can facilitate discussion and understanding of relatively complex data quickly and easily. This in no way replaces the need for quantitative analyses; it merely facilitates the sharing of such results to a broader audience using a simpler but powerful medium.

A common question for most in a variety of industries is how RP can be used (Carrion 1997, Grimm 2004, Kochan 2000). This is also a question that arises whenever

anyone first encounters an RP device or 3D printer. Drawing from the above-mentioned examples, 3D printing changes our accessibility to information. In doing so, the data is transformed into objects of analytical value. Researchers are beginning to recognize that scientific methods are now able to generate large volumes of information, but that humans are not able to interpret this data without some form of visual reference (Gaither *et al.* 2004, van Dam *et al* 2002). This is the case for the humerus scan comparison, where the numerical data comparing the morphology of the two models is unintelligible without the statistical analysis. The 3D model of the two models registered together in Figure 5.2 overcomes this barrier and provides the user with a direct interpretation of the data. The colour modeling can provide visual insight into how the differences manifest throughout the 3D structure of the object. When combined with the appropriate quantitative analysis the researcher can gain a more comprehensive understanding by not only providing quantifiable verification of difference but also visually displaying how the differences are presented. This can lead to new questions by guiding the researcher to query why variation occurs in one area versus another. Visual data can be presented in a number of ways. The computer screen has become a popular interface, but it is limited by only being able to present 2D images of 3D objects. Virtual reality is becoming another popular area of research for presenting visual-spatial concepts. Researchers use virtual reality to model objects in 3D space and provide the user with an immersive interaction within the field of data. This does have potential for overcoming the barriers imposed by numerical analysis alone by providing a more intimate relationship with the data. The limitation however, concerns the point at which a virtual object is experienced in a real sense (Luciani *et al.* 2004). A degree of physical coherence is required for

people to perceive objects in a virtual environment as real (Luciani *et al.* 2004). This has inspired researchers to focus on such things as photorealism. An alternative approach to this pursuit involves the use of 3D printing. Real objects are produced, bridging the perceptual barrier of virtual reality. However, instead of trying to hold onto the hegemony of photorealism, the model can be used to express ideas not possible in the original object.

Rountree and colleagues (2002) investigated the use of 2D images, 3D images and physical replicas in teaching students about ancient art forms. Although their study did not result in a difference in test results between methods of visualization, students did report a more poignant experience with the physical replicas. This study illuminated a very interesting point to be investigated further. The 2D images guided the students' experience in a particular and predictive direction. The 2D images were more commonly associated with the students' assumption that the particular image chosen had a deliberate purpose and depicted the item in some fashion of directed importance (Rountree *et al* 2002). A similar theme is inferred from Grimm (2004) noting that the advantage of RP is the production of items that require little explanation for the user to understand. Further to this end, Rountree and colleagues note that students reported being able to visualize using the objects better when they were holding the replica versus the images. Thus, holding an object gives the beholder a more intuitive experience. Regular images tend to guide the users perception based on the producers' intentions, whereas a free-form object allows the user to form their own ideas independent of the producer of the item.

To date, most visualization projects in anthropology have been focused on making photorealistic replicas of heritage items, overlooking the other potential tools for virtual

exhibits (Roussou and Drettakis 2003). This idea can extent to the 3D printing world as well and represents a general bias of most researchers to want to recreate what we perceive to be the real world. In the case of the MHV exhibit, a condition of the display was that it could not be overly gratuitous (pers.com. Roland Sawatzky). This meant that the natural white colour of the 3DP models was appropriate, but representing the staining on the bones would not be acceptable. Virtual technologies offer insight into the world we cannot perceive naturally. This is the real advantage of these technologies that needs to be realized and put to use. Printing a 3D model of a bone that is indistinguishable from the original is interesting, but printing the model so that it shows information of analytical value that cannot be seen by the human eye is interesting and useful. Now that 3D models can be produced quickly and inexpensively using colour, it is necessary to explore the different analytical results that can be displayed on these models for the real potential of this technology to be realized.

CT scans contain information about the internal structure of bones, including the variation in density throughout the different structures. A pilot project stemming from case study two successfully implemented a method of representing Hounsefield values as a proxy for bone density on the 3D model of the mandible. This involved attaching a colour texture map of the Hounsefield value variation to each slice of CT data. A 3D model was then created from the CT slices and made into a polygon model. The colour information was incorporated into this model generation as a texture map and the result was exported as a VRML file for printing. This proof of concept was performed using a demonstration version of the Amira™ software and the help of the Amira™ technical support staff. Amira™ has the ability to attach arithmetic functions to the image data,

and can include formulas for calculating and displaying true density information. This project simply used the Hounsefield values as a proxy of bone density. The printed model for this study is illustrated in Figure 5.3 below.

Figure 5.3: Colour Bone Density Model of Mandible

Figure 5.3: Colour-coded 3D model of the mandible from Case Study Two.

While it was possible to generate a bone density model of the above mandible, some problems can be noted. The surface of the model is not as smooth as the other prints of the same element. Since the density information was calculated on individual CT slices, the combination of this and the lack of model smoothing produced over-extended slice ridges. These ridges show density information that is likely supposed to be under the cortical bone surface, but appear along the surface of the model. This problem makes the surface information confusing.

The colour density map used for this case study was not a true depiction of density. Variations in the Hounsefield units were used as a proxy for changes in bone mineral density using the assumption that density changes will affect the attenuation coefficients and result in changes in Hounsefield units. This assumption is more acceptable in this situation where only the skeletal material is CT scanned. Adding soft tissue may complicate this for other studies. Further more, a calibration equation was not used to identify the actual density values for human bone. It is possible to attach an arithmetic module to the data set in the Amira™ software, however this was not done in this case. The goal of this exercise was to simply illustrate the use of a colour density map with the printed 3D model as a means to illustrate that the models can be used to display information not apparent in a photorealistic depiction of the original.

The idea that inspired this project was encountered at a Z-Corp User Group Meeting in 2004, where Dr. Urrutia presented a series of 3D models that depicted bone density changes on the 3D structures of skulls and mandibles. Dr. Urrutia used these models for planning his surgical procedures on a case-by-case basis. Yao and Taylor (2001) also recognize the usefulness of understanding bone density changes for surgical procedures and started to create a bone density atlas of the human skeleton for these purposes. They note that their approach does not fully account for the extent of human variation possible in the average population. The approach used by Dr. Urrutia overcomes this obstacle by printing 3D models of individual patients' bone density from CT scans. The time and expertise required to create a graphical visualization described by Yao and Taylor is more cumbersome than using software that can calculate density

values based on CT images and printing a 3D model. This is a major advantage to using 3D printing for custom, on-demand models of unique anatomical manifestations.

This same principal can be extended to archaeological material to understand taphonomy, trauma and other pathological conditions. Lam and Pearson (2005) note that bone density is a common measure of a bone's resistance to damage and that this can apply to understanding taphonomic forces in the archaeological record. For example, one would expect changes in bone density around pre-mortem wounds and less change in density around peri-mortem and ante-mortem wounds. Density changes can be represented in 3D replicas of bones and used as proxies for measuring osteogenic response. The 3D model provides the observer with the ability to examine the actual bone with the data mapped to the surface for a better understanding of the relationships.

One other new use of 3DP technology that bears mentioning briefly is the printing of live tissue. Some researchers have begun to explore the possibility of using the binder-jet 3D printing approach to building whole live organs layer by layer (Jakab *et al.* 2004a and 2004b, Markwald 2003 Mironov *et al.* 2003). This research uses a bioactive substrate deposited onto a holding medium in the build chamber to grow tissues layer by layer. It is limited in the size that can be built, since the technology itself is limited to dots per inch. In order to be really effective the technology will need to adapt to be able to print microscopic structures.

While printing live structures is an extreme example of where the 3DP technology could progress to in the future, it is given in this work as support for the idea that the role of 3DP has not been fully realized. In returning to McLuhan's (1966) idea the medium is the message, it is possible to see how 3DP has the potential to shape the questions we ask

in future studies. By affecting the questions we ask, it moves from being simply a method of communication as Zollikofer and Ponce de Leon (2005) have suggested and becomes an interpretive tool within the broader context of scientific discovery. If the photograph influenced the development of modern human culture by allowing people to capture and preserve moments in time and space, then 3DP has the potential to do the same. Instead of capturing objects in a moment at a given point in time and space, 3DP may very well allow us to recreate the entire object so that it may be perpetuated in time and space, releasing human discovery from the bonds of temporality.

3DP changes the access to the remains we study in biological anthropology. It provides researchers with the ability to make replicas of skeletal remains quickly, simply and cost effectively. The colour capabilities allow researchers to represent data in a visual-spatial capacity that is tangible and easy to understand. It also challenges our imagination and capacity to think creatively about the representation of the people we study. In these ways, 3DP has the potential to change and enhance the dissemination of results and also facilitate the asking of new questions.

Chapter VI: Conclusion

3D printing has the potential to overcome the barriers to the widespread use of RP in biological anthropology. The 3DP technology is easy to use, fast and economical to operate making it well suited to supporting projects in biological anthropology. The main limitation of the use of 3DP is the level of awareness of how it can be used to enhance or facilitate projects in biological anthropology. This work has shown and discussed ways in which researchers in biological anthropology can take advantage of 3DP. Two case studies are presented in order to provide a forum for discussion and explore the methodological considerations of 3DP projects. In general, both case studies proved that data acquisition and post-processing procedures were the most limiting factor in 3DP projects. The 3D printer is capable of far greater accuracy than the most common data acquisition methods available today. The most important lesson to be gained from the sum of the case study experiences is the need to identify an appropriate data acquisition methodology for the project of interest. For example, case study two shows that while surface laser scanning is not as accurate as CT scanning, it can be acceptable for the production of models for public dissemination and museum exhibits.

The most exciting discovery and potential use for 3DP in anthropology is the production of colour models. The 3D printer is not capable of producing photorealistic replicas of bones, however colour models that depict some other analytical concept can be created. If we can release ourselves from the confines of wanting to reproduce what we can only see with our eyes, we can find a hidden power in the ability to represent more conceptually complex ideas in the readily intelligible form of the 3D model. The

3D model has the potential to transcend barriers of discourse between disciplines to communicate in the visual medium more effectively than words or photographs.

Finally and most importantly, 3DP has the potential to change our access to information in a way that can inform the research questions we ask. Replicas of skeletal elements that are hidden from direct inspection for various reasons (for example encased in matrix or a wrapped mummy), offer researchers the chance to study and explore remains without damaging the original. Researchers can now handle the skeletal elements of individuals without actually needing to be with the body. Fragile skeletal elements can be reproduced and handled for study, education or dissemination. These are just a few ways in which less accessible material can become more accessible to a broader group of people. Access to information and study material naturally increases the richness of the types of questions and level of understanding that can be gained from the human skeleton.

This work describes only the beginning of the use of 3DP in biological anthropology. It is intended to provide a platform for understanding how researchers can incorporate 3DP in anthropology projects by discussing the issues of data acquisition and methodology. Future work should examine the many potential uses for colour modeling to enhance research projects. The bone density colour map of the mandible presented in Chapter V is an example of where more work is needed. A great deal of information is contained in a CT scan and can be displayed in an innovative way using 3D models. More work is also clearly needed on virtual reconstruction so that models of fragmented remains can be presented with confidence. This is already an important are of study in anthropology that would benefit greatly from the use of 3D printing. These suggestions

are merely the beginning, as McLuhan (1966: 23) argues, “the medium is the message”. In time 3DP will change the way in which we approach some projects in biological anthropology as making physical replicas of objects becomes more common.

Work Cited

Ahmon J (2004) The application of short-range 3D laser scanning for archaeological replica production: The Egyptian tomb of Seti I. Photogrammetric Record *19:*111-124.

Allard TT, Sitchon ML, Sawatzky R, and Hoppa RD (2005) Use of Hand-held Laser Scanning and 3D Printing for Creation of a Museum Exhibit. The 6th International Symposium on Virtual Reality, Archaeology and Cultural Heritage (VAST 2005), pp. 97-101.

Anderl H, Zur Nedden D, Muhlbauer W, Twerdy K, Zanon E, Wicke K, and Knapp R (1994) CT-guided stereolithography as a new tool in craniofacial surgery. Br J Plast Surg *47:*60-4.

Azouz ZB, Shu C, Lepage R, and Rioux M (2005) Extracting Main Modes of Human Body Shape Variation from 3-D Anthropometric Data. 5th International Conference on 3-D Digital Imaging and Modeling (3DIM 2005).

Barker TM, Earwaker WJ, and Lisle DA (1994) Accuracy of stereolithographic models of human anatomy. Australas Radiol *38:*106-11.

Bibb R, and Sisias G (2002) Bone structure models using stereolithography: a technical note. Rapid Prototyping Journal *8:*25-29.

Boehler W, Heinz G, Marbs A, and Siebold M (2002) 3D Scanning Software: An Introduction. Mainz, Germany: i3mainz, Institute for Spatial Information and Surveying Technology.

Borah B, Gross GJ, Dufresne TE, Smith TS, Cockman MD, Chmielewski PA, Lundy MW, Hartke JR, and Sod EW (2001) Three-dimensional microimaging (MRmicroI and microCT), finite element modeling, and rapid prototyping provide unique insights into bone architecture in osteoporosis. Anat Rec *265:*101-10.

Bouyssie JF, Bouyssie S, Sharrock P, and Duran D (1997) Stereolithographic models derived from x-ray computed tomography. Reproduction accuracy. Surg Radiol Anat *19:*193-9.

Brown GA, Firoozbakhsh K, and Gehlert RJ (2001) Three-dimensional CT modeling versus traditional radiology techniques in treatment of acetabular fractures. Iowa Orthop J *21:*20-4.

Brown KR, and Wood H (1999) The utility of minimal CT scanning in the study of two egyptian mummy heads. International Journal of Osteoarchaeology *9:*199-204.

Brownlee K, Sitchon ML, and Hoppa RD (2005) Planning for the future: Developing strategies for post-repatriation analysis of archaeological materials. Annual Meeting of the Canadian Archaeological Association.

Calhoun PS, Kuszyk BS, Heath DG, Carley JC, and Fishman EK (1999) Three-dimensional volume rendering of spiral CT data: theory and method. Radiographics *19:*745-64.

Carrion A (1997) Technology Forecast on Ink-Jet Head Technology Applications in Rapid Prototyping. Rapid Prototyping Journal *3(3):*99-115.

Choi JY, Choi JH, Kim NK, Kim Y, Lee JK, Kim MK, Lee JH, and Kim MJ (2002) Analysis of errors in medical rapid prototyping models. Int J Oral Maxillofac Surg *31:*23-32.

Clark NDL, Adams C, Lawton T, Cruickshank ARI, and Woods K (2004) The Elgin marvel: using magnetic resonance imaging to look at a mouldic fossil from the Permian of Elgin, Scotland, UK. Magnetic Resonance Imaging *22:*269-273.

D'Urso PS, Earwaker WJ, Barker TM, Redmond MJ, Thompson RG, Effeney DJ, and Tomlinson FH (2000) Custom cranioplasty using stereolithography and acrylic. British Journal of Plastic Surgery *53:*200-204.

Dolz MS, Cina SJ, and Smith R (2000) Stereolithography - A potential new tool in forensic medicine. American Journal of Forensic Medicine and Pathology *21:*119-123.

El-Hakim SF, Beraldin JA, Gonzo L, Whiting E, Jemtrud M, and Valzano V (2005) A Heirarchical 3D Reconstruction Approach for Documenting Complex Heritage Sites. The XX CIPA International Symposium.

Faber J, Berto PM, and Quaresma M (2006) Rapid prototyping as a tool for diagnosis and treatment planning for maxillary canine impaction. American Journal of Orthodontics and Dentofacial Orthopedics *129:*583-589.

Fajardo RJ, Ryan TM, and Kappelman J (2002) Assessing the Accuracy of High-Resolution X-Ray Computed Tomography of Primate Trabecular Bone by Comparisons With Histiological Sections. American Journal of Physical Anthropology *118:*1-10.

Feng HY, Liu YX, and Xi FF (2001) Analysis of digitizing errors of a laser scanning system. Precision Engineering-Journal of the International Societies for Precision Engineering and Nanotechnology *25:*185-191.

Fischer T, Herr CM, Burry MC, and Frazer JH (2003) Tangible interfaces to explain Gaudi's use of ruled-surface geometries - Interactive systems design for haptic, nonverbal learning. Automation in Construction *12:*467-471.

Fontana R, Greco M, Materazzi M, Pampaloni E, Pezzati L, Rocchini C, and Scopigno R (2002) Three-dimensional modelling of statues: the Minerva of Arezzo. Journal of Cultural Heritage *3:*325-331.

Fowles PS (2000) The Garden Temple at Ince Blundell: a case study in the recording and non-contact replication of decayed sculpture. Journal of Cultural Heritage *1:*S89-S91.

Gaither K, Ebert D, Geisler B, and Laidlaw D (2004) Panel 2: In the Eye of the Beholder: The Role of Perception in Scientific Visualization. IEEE Visualization, pp. 567-568.

Gateno J, Xia J, Teichgraeber JF, and Rosen A (2003) A new technique for the creation of a computerized composite skull model. J. of Oral Maxillofacial Surgery *61:*222-227.

Gibbons A (2005) Paleoanthropology - Facelift supports skull's status as oldest member of the human family. Science *308:*179-+.

Gibson I, and Ming LW (2001) Colour RP. Rapid Prototyping Journal *7:*212-216.

Harrison JA, Nixon MA, Fright WR, and Snape L (2004) Use of hand-held laser scanning in the assesment of facial swelling: a preliminary report. British Journal of Oral and Maxillofacial Surgery *42:*8-17.

Hieu LC, Zlatov N, Sloten JV, Bohez E, Khanh L, Binh PH, Oris P, and Toshev Y (2005) Medical rapid prototyping applications and methods. Assembly Automation *25:*284-292.

Hjalgrim H, Lynnerup N, Liversage M, and Rosenklint A (1995) Stereolithography: potential applications in anthropological studies. Am J Phys Anthropol *97:*329-33.

Hoffman H, Torres WE, and Ernst RD (2002) Paleoradiology: advanced CT in the evaluation of nine Egyptian mummies. Radiographics *22:*377-85.

Jakab K, Neagu A, Mironov V, and Forgacs G (2004a) Organ printing: fiction or science. Biorheology *41:*371-5.

Jakab K, Neagu A, Mironov V, Markwald RR, and Forgacs G (2004b) Engineering biological structures of prescribed shape using self-assembling multicellular systems. Proc Natl Acad Sci U S A *101:*2864-9.

Jung H, Kim H-J, Kim D-O, Hong S-i, Jeong H-K, Kim K-D, Kim YO, Yoo SK, and Yoo HS (2002) Quantitative analysis of three-dimensional rendered imaging of the human skull acquired from multi-detector row computed tomography. Journal of Digital Imaging *15:*232-239.

Kai CC, Jacob GGK, and Mei T (1997) Interface between CAD and Rapid Prototyping systems. Part 1: A study of existing interfaces. The International Journal of Advanced Manufacturing Technology *13:*566-570.

Kim D-O, Kim H-J, Jung H, Jeong H-K, Hong S-i, and Kim K-D (2002) Quantitative evaluation of aquisition parameters in three-dimensional imaging with multidetector computed tomography using human skull phantom. Journal of Digital Imaging *15:*254-257.

Knopf GK, and Kofman J (2002) Surface reconstruction using neural network mapping of range-sensor images to object space. Journal of Electronic Imaging *11:*187-194.

Kochan A (2000) Rapid prototyping gains speed, volume and precision. Assembly Automation *20:*295-299.

Kofman J, and Knopf GK (2003) Continuous unconstrained range sensing of free-form surfaces without sensor-head pose measurement. Optical Engineering *42:*1496-1510.

Lam YM, and Pearson OM (2005) Bone density studies and the interpretation of the faunal record. Evolutionary Anthropology *14:*99-108.

Lee SJJ, Sachs E, and Cima M (1995) Layer Position Accuracy in Powder-Based Rapid Prototyping. Rapid Prototyping Journal *1(4):*24-37.

Leong KF, Chua CK, and Ng YM (1996) A study of stereolithography file errors and repair .1. Generic solution. International Journal of Advanced Manufacturing Technology *12:*407-414.

Lester DS, and Olds JL (2001) Biomedical imaging: 2001 and beyond. Anat Rec *265:*35-6.

Lin AC, and Liang SR (2002) Rapid prototyping through scanned point data. International Journal of Production Research *40:*293-310.

Luciani A, Urma D, Marliere S, and Chevrier J (2004) PRESENCE: the sense of believability of inaccessible worlds. Computers & Graphics-Uk *28:*509-517.

Lynnerup N, Hjalgrim H, Nielsen LR, Gregersen H, and Thuesen I (1997) Non-invasive Archaeology of Skeletal Material by CT Scanning and Three-dimensional Reconstruction. International Journal of Osteoarchaeology *7:*91-94.

Marcia S. Ponce De LeÛn (2002) Computerized paleoanthropology and Neanderthals: The case of Le Moustier 1. Evolutionary Anthropology: Issues, News, and Reviews *11:*68-72.
Markwald R (2003) Desktop organ printing. Anat Rec B New Anat *273:*120-1.
McLuhan M (1966) Understanding media : the extensions of man. New York ; Toronto: McGraw-Hill.
Mehta BV, Rajani S, and Sinha G (1997) Comparison of image processing techniques (magnetic resonance imaging, computed tomography scan and ultrasound) for 3D modeling and analysis of the human bones. J Digit Imaging *10:*203-6.
Mironov V, Boland T, Trusk T, Forgacs G, and Markwald RR (2003) Organ printing: computer-aided jet-based 3D tissue engineering. Trends Biotechnol *21:*157-61.
Ono I, Abe K, Shiotani S, and Hirayama Y (2000) Producing a full-scale model from computed tomographic data with the rapid prototyping technique using the binder jet method: a comparison with the laser lithography method using a dry skull. J Craniofac Surg *11:*527-37.
Pasquier E, De Saint Martin Pernot L, Burdin V, Mounayer C, Le Rest C, Colin D, Mottier D, Roux C, and Baccino E (1999) Determination of age at death: assessment of an algorithm of age prediction using numerical three-dimensional CT data from pubic bones. Am J Phys Anthropol *108:*261-8.
Perez-Arjona E, Dujovny M, Park H, Kulyanov D, Galaniuk A, Agner C, Michael D, and Diaz FG (2003) Stereolithography: neurosurgical and medical implications. Neurol Res *25:*227-36.
Ponce-De-Leon MS, and Zollikofer CPE (1999) New evidence from Le Moustier 1: Computer-assisted reconstruction and morphometry of the skull. The Anatomical Record (Part B: New Anat.) *254:*474-489.
Powers DB, Edgin WA, and Tabatchnick L (1998) Stereolithography: a historical review and indications for use in the management of trauma. J Craniomaxillofac Trauma *4:*16-23.
Rountree J, and Wong W (2002) Learning to Look: Real and Virtual Artifacts. Educational Technology & Society *5(1).*
Roussou M, and Drettakis G (2003) Photorealism and Non-Photorealism in Virtual Heritage Representation. VAST: 4th International Symposium on Virtual Reality, Archaeology, and Intelligent Cultural Heritage.
Ruhli FJ, Hodler J, and Boni T (2002b) Technical note: CT-guided biopsy: A new diagnostic method for paleopathological research. Am J Phys Anthropol *117:*272-5.
Ruhli FJ, Lanz C, Ulrich-Bochsler S, and Alt KW (2002a) State-of-the-art Imaging in Palaeopathology: the Value of Multislice Computed Tomography in Visualizing Doubtful Cranial Lesions. International Journal of Osteoarchaeology *12:*372-379.
Seely JC (2004) Digital Fabrication in the Architectural Design Process. Master of Science, Massachusetts Institute of Technology.
Shapiro D, and Richtsmeier JT (1997) Brief communication: A sample of pediatric skulls available for study. American Journal of Physical Anthropology *103:*415-416.
Sitchon ML, Sawatzky R, Finch D, and Meiklejohn C (2005) Second time around: Mennonite repatriation efforts in Manitoba. Annual Meeting of the Canadian Archaeological Association.

Souza A, Udupa JK, and Saha PK (2005) Volume rendering in the presence of partial volume effects. IEEE Trans Med Imaging *24:*223-35.
Spoor F, Jeffery N, and Zonneveld F (2000) Using diagnostic radiology in human evolutionary studies. Journal of Anatomy *197:*61-76.
Taylor J, Beraldin JA, Godin G, Baribeau R, Cournoyer L, Blais F, El-Hakim S, Picard M, Rioux M, and Domey J (2002) Culture as a Driving Force for Research and Technology Development: A Decade's Experience of Canada's NRC 3D Technology. Electronic Imaging and the Visual Arts (EVA2002), pp. 4.1-4.13.
Upcraft S, and Fletcher R (2003) The rapid prototyping technologies. Assembly Automation *23:*318-330.
van Dam A, Laidlaw DH, and Simpson RM (2002) Experiments in immersive virtual reality for scientific visualization. Computers & Graphics-Uk *26:*535-555.
Vialet A, Li TY, Grimaud-Herve D, de Lumley MA, Liao MY, and Feng XB (2005) A proposal of reconstruction of the second Homo erectus skull from Yunxian (China). Comptes Rendus Palevol *4:*265-274.
Wang GJ, Wang CC, and Chuang SHF (1999) Reverse engineering of sculptured surfaces by four-axis non-contacting scanning. International Journal of Advanced Manufacturing Technology *15:*800-809.
Weber GW (2001) Virtual anthropology (VA): A call for Glasnost in paleoanthropology. The Anatomical Record (Part B: New Anat.) *265:*193-201.
Weber GW, Schafer K, Prossinger H, Gunz P, Mitterocker P, and Seidler H (2001) Virtual anthropology: the digital evolution in anthropological sciences. J Physiol Anthropol Appl Human Sci *20:*69-80.
Willems G, Verbiest F, Moreau W, Hameeuw H, Lerberghe KV, and Gool LV (2005) Easy and Cost-effective Cuneiform Digitizing. The 6th International Symposium on Virtual Reality, Archaeology and Cultural Heritage (VAST), pp. 73-80.
Williams FLE, and Richtsmeier JT (2003) Comparison of mandibular landmarks from computed tomography and 3D digitizer data. Clinical Anatomy *16:*494-500.
Wood B (2000) Investigating human evolutionary history. Journal of Anatomy *197:*3-17.
Yao J, and Taylor R (2000) Tetrahedral Mesh Modeling of Density Data for Anatomical Atlases and Intensity-Based Registration.
Zollikofer CPE (2002) A computational approach to paleoanthropology. Evolutionary Anthropology *11:*64-67.
Zollikofer CPE, de Leon MSP, Lieberman DE, Guy F, Pilbeam D, Likius A, Mackaye HT, Vignaud P, and Brunet M (2005) Virtual cranial reconstruction of Sahelanthropus tchadensis. Nature *434:*755-759.
Zollikofer CPE, and Ponce de Leâon MS (2005) Virtual reconstruction : a primer in computer-assisted paleontology and biomedicine. Hoboken, N.J.: Wiley-Liss.
zur Nedden D, Knapp R, Wicke K, Judmaier W, Murphy WA, Jr., Seidler H, and Platzer W (1994) Skull of a 5,300-year-old mummy: reproduction and investigation with CT-guided stereolithography. Radiology *193:*269-72.

Appendix I: List of Abbreviations

3DP: Three-Dimensional Printing

ASCII: American Standard Code for Information Interchange

BMP: Bitmap (image file format)

CA: Cyanoacrylate

CAD: Computer-Aided Design (or drawing)

CCD: Charge-Coupled Device

CMM: Coordinate Measuring Machine

CNC: Computer Numerical Control

CT: Computed Tomography (X-Ray)

DICOM: Digital Imaging and Communications in Medicine

FDM: Fused Deposition Modeling

LOM: Laminated Object Manufacturing

NURBS: Non-Uniform Rational B-Spline

MR(I): Magnetic Resonance (Imaging)

PVE: Partial Volume Effect

RP: Rapid Prototyping

SLA: Stereolithography (process)

SLS: Selective Laser Sintering

STL: Stereolithography (file format)

VRML: Virtual Reality Modeling Language